Interfacial behavior of lignin containing cellulose nanofibrils (LCNFs) and their impact on composite materials

by

María Celeste Iglesias

A thesis submitted to the Graduate Faculty of
Auburn University
in partial fulfillment of the
requirements for the Degree of
Doctor of Philosophy

Auburn, Alabama
December 11, 2021

Key words:

lignin-containing cellulose nanofibrils, LCNF, rheology, residual lignin, composite materials, lignocellulosic materials

Approved by

Dr. Maria Soledad Peresin, Associate Professor of Forest Biomaterials, School of Forestry and Wildlife Science
Dr. Virginia A. Davis, Dr. Daniel F. and Josephine Breeden Professor, Chemical Engineering
Dr. Brian K. Via, Regions Bank Professor, Forest Products, School of Forestry and Wildlife Science
Dr. Zhihua Jiang, Auburn Pulp and Paper Foundation Assistant Professor, Chemical Engineering
Dr. Burak Aksoy, Assistant Research Professor, Chemical Engineering

Abstract

Over the last decade, the utilization of nanocellulose for novel applications has positioned this renewable source as a promising alternative substitution for petroleum-based materials. In an attempt to utilize and incorporate lignocellulosic materials from different raw materials and varying chemical compositions into composite materials, it is crucial to understand the interfacial interactions between the different chemical components of such composites. These interactions will dictate the behavior of the nanocellulosic suspensions, and they will directly impact the intrinsic properties of the resulting materials. Thus, understanding the fundamental physico-chemistry of the raw material and how they influence properties such as morphology, chemical composition, thermal degradation, and surface charge will offer a better understanding of the performance of the products. Through this dissertation, specific emphasis was made on the rheological behavior of the nanocellulosic suspensions. Rheology provides insight into interfacial interactions and knowing the flow characteristic of the materials might help during the handling and processing. Chapter 1 of the dissertation is a literature review focused on the interfacial interactions between different chemical components in lignocellulosic materials. Chapter 2 states the objectives and hypotheses consider in each chapter. The nature of the raw material and the processes used to produce the nanofibers and how those affect the viscoelastic behavior of the samples is presented in Chapter 3. Furthermore, focusing on a single raw material, Chapter 4 is centered on the rheological study of four different softwood LCNFs samples with lignin contents from <1.0 to 16.8%. Particularly in Chapter 5, the analysis of the interfacial interactions between wood adhesives and LCNF suspensions was emphasized. After investigating the fundamental properties of those nanocellulosic suspensions, their incorporation into a composite material to improve properties such as adhesion, wettability, and mechanical performance was studied. Along

this dissertation, the interfacial interactions using a quartz crystal microbalance with dissipation monitoring (QCM-D) and surface free energy analyzed by contact angle (CA) measurements were studied. These techniques were supported with the fundamental study of the samples in terms of morphology, using atomic force microscopy (AFM) and scanning electron microscopy (SEM); viscoelastic behavior; chemical composition, using Fourier transform infrared spectroscopy (FT-IR); thermal behavior by thermal gravimetric analysis (TGA), crystallinity by X-ray powder diffraction (XRD), surface charge density, and zeta potential by dynamic light scattering (DLS). Together these results highlight the importance of understanding the atomic and molecular interactions in the nanocellulosic systems to take full advantage of the biomass. The use of the explained phenomena within this dissertation opens a wide range of possible materials and applications that can be targeted with these renewable and sustainable materials. As a result, the use of forest and agricultural by-products can be enhanced, increasing its potential value, and providing a more environmentally friendly alternative to displace fossil-based polymers.

Dedication

"In one of those stars I shall be living. In one of them I shall be laughing. And so it will be as if all the stars were laughing, when you look at the sky at night. And when your sorrow is comforted (time soothes all sorrows) you will be content that you have known me. You will always be my friend... I shall not leave you." - *Antoine de Saint-Exupéry, "The Little Prince"* -

To my dear dad, words will never be enough to describe how much I miss you. Thank you for your unconditional love and support.

I will always love you. Your little one, Cele.

Dedicatoria

"En una de esas estrellas estaré viviendo. En una de ellas me reiré. Y así será como si todas las estrellas se rieran, cuando mires al cielo en la noche. Y cuando tu dolor se consuele (el tiempo calma todos los dolores) estarás contento de haberme conocido. Siempre serás mi amigo... nunca te dejaré" - *Antoine de Saint-Exupéry, "El Principito"* -

Para mi querido papá, las palabras nunca serán suficientes para describir cuánto te extraño. Gracias por tu amor y apoyo incondicional.

Siempre te voy a amar. Tu chiquita, Cele.

Acknowledgements

The author would like to thank her major professor, Dr. Maria Soledad Peresin, for the opportunity of pursuing a Ph.D. degree under her supervision, which has been invaluable. Thank you for all these years of constant support, guidance, and encouragement at every moment of this path, I feel so grateful of having the opportunity to work by your side. Thank you for being part not only of my professional but also personal development. Thank you for being supportive in the most challenging times I have had to go through during the past year.

Special thanks to my Ph.D. committee members. Thank you, Dr. Virginia Davis, Dr. Zhihua Jiang, Dr. Brian Via, for your support and guidance during these years. Thank you for helping me grow academically and for your invaluable help and knowledge. I have learned so much from all of you. Thank you to my university reader, Dr. Burak Aksoy. Your help and patience during all these years have been invaluable for me. Thank you for always being willing to help me.

The author wants to thank Dr. Charles Frazier and Dr. Ann Norris for XRD measurements, Dr. Evert Duin for EPR analysis, Dr. Michael Miller for SEM and confocal microscopies training, and Dr. Byron Fardum for XRD training.

The author would like to thank her working partners for their hard and competitive work. Thank you for always inspiring me to give the best and for your constant help and support, Dr. Diego Gomez Maldonado, Dr. Osei Asafu-Adjaye, Javier Hernandez Diaz, Yufei Nan, and Sydney Brake. Thank you to the undergrads working in our group. Being able to work with you has been an excellent experience for me. Special thanks to Philip McMichael for all your help during the years you worked with us and to Dr. Yurany Villada and Tina Ciaramitaro; thank you, thank you, thank you, for everything.

Special thanks to all the people working in the Forest Products Laboratory, thank you for all the good times and the memories. It has been my pleasure to work by your side and learn from all of you. Thank you to all the staff, faculty members, colleagues, and friends of the School of Forestry and Wildlife Science.

In giving appreciation, the author would like to thank her family; her mother Vivi, siblings Flori, Lu, and Anibal, and her niece and nephew Justina and Santiago. Thank you for your constant and unconditional support in the distance. Thank you for your love, this would not be the same if without you. I want to express my deep gratitude to my best friend, the best partner I could have asked for, Nick; thank you for your constant support, patience, and love, for making my life better, and giving me the best family ever with Trigger and Artemis. I love you, thank you.

Finally, the author would like to thank her Argentinian friends and the Auburn friends that have become family during these years. Thank you for your friendship and support. This experience would not have been the same without all of you.

Table of content

List of tables

List of figures

List of Equations

List of publications and contributions

Peer-reviewed (N = 2) and articles under preparation (N = 2) derived from this dissertation:

PAPER I: **Iglesias, M. C.,** Gomez-Maldonado D., and Peresin, M. S. The importance of interfacial interactions in nanocellulosic-based systems and its impacts for the development of applications and substitution of fossil-based polymers: a Review. *(Under preparation).*

PAPER II: **Iglesias, M. C.,** Hamade, F., Aksoy, B., Jiang, Z., Davis, V. A., and Peresin, M. S. Correlations between Rheological Behavior and Intrinsic Properties of Nanofibrillated Cellulose from Wood and Soybean Hulls with Varying Lignin Content. *BioResources*, 16(3): 4831-4845 (**2021**). DOI: 10.15376/biores.16.3.4831-4845

PAPER III: **Iglesias, M. C.,** Davis, V. A., and Peresin, M. S. Correlation of the chemical composition of CNF aqueous suspensions from softwood sources with their microstructure and flow behavior trough rheological measurements. *(Under preparation).*

PAPER IV: **Iglesias, M. C.,** McMichael, P. S., Asafu-Adjaye, O. A., Via, B., and Peresin, M. S. Interfacial interactions between urea formaldehyde and cellulose nanofibrils (CNFs) of varying chemical composition and their impact on particle board (PB) manufacture. *Cellulose*, 28, 7969–7979 (**2021**). DOI: 10.1007/s10570-021-04007-1

Peer-reviewed manuscripts in archival literature not included in this document (N = 6):

1. Villada Y., **Iglesias M. C.**, Casis N., Zhu, J., Peresin M. S., Erdmann E., and Estenoz D. Cellulose nanofibrils obtained from organic processes as additive in water-based muds

(WBMs) for a shale formation. *Cellulose* 28, 417–436 (**2021**). https://doi.org/10.1007/s10570-020-03502-1.

2. **Iglesias M. C.,** Shivyari N., Norris, A., Martin Sampedro R., Eugenio, M. E., Auad, M. L., Elder, Thomas, Jiang, Z., Frazier, C. E., and Peresin, M. S. (**2020**) Residual lignin and its effect on the rheological properties cellulose nanofibrils suspensions. *Journal of Wood Chemistry and Technology*, 40:6, 370-381. https://doi.org/10.1080/02773813.2020.1828472

3. Solala I., **Iglesias M. C**., and Peresin M. S. (**2020**) On the potential of lignin-containing cellulose nanofibrils (LCNFs): a review on properties and applications. *Cellulose* 27, 1853–1877 https://doi.org/10.1007/s10570-019-02899-8

4. **Iglesias M. C.,** Gomez-Maldonado D., Via B. K., Jiang Z., and Peresin M. S. (**2019**). Comparison of kraft and sulfite pulping processes and their effects on cellulose fibers and nanofibrillated cellulose properties: a review. *Forest Products Journal*, 70(10):10-21 https://doi.org/10.13073/FPJ-D-19-00038

5. Villada Y., **Iglesias M. C.**, Casis N., Peresin M. S., Erdmann E., and Estenoz D. (**2018**) Cellulose nanofibrils as a replacement additive of xanthan gum (XGD) in water-based muds (WBMs) for a shale formation. *Cellulose* 25, 7091–7112. https://doi.org/10.1007/s10570-018-2081-z.

6. De Assis, C.A., **Iglesias, M.C.**, Bilodeau, M., Johnson, D., Phillips, R., Peresin, M.S., Bilek, E.M., Rojas, O.J, Venditti, R., Gonzalez, R. (**2018**). Cellulose micro-and nanofibrils (CMNF) manufacturing-financial and risk assessment. *Biofuels, Bioprod. Bioref.* 12: 251–264. https://doi.org/10.1002/bbb.1835

Additional projects related to the dissertation submitted or under preparation (N = 3):

1. Hernández, J. A., Soni B., **Iglesias M. C.,** Vega Erramuspe I. B., Frazier C. E., and

Peresin M. S. Pectin and nanocellulose from soybean hull as interfacial agents for increasing tack properties in emulsions of polymeric diphenylmethane diisocyanate. Submitted to ***Journal of Material Science***.

2. Arango Sanchez, M. C., **Iglesias, M. C**., Peresin, M. S., and Alvarez Lopez, C. Evaluation of sericin/cellulose mixtures for the development of porous scaffolds for future application in cell regeneration. Submitted to ***Journal of Applied Polymer Science***.

3. Ehman Nanci, **Iglesias, M. C.,** Peresin, M. S, and Area, M. C. **2021** Microfibrillated cellulose production as alternative of eucalyptus sawdust valorization in a biorefinery scheme *(Under preparation).*

1. The importance of interfacial interactions in nanocellulosic-based systems and their impact on sustainable products development

1.1.Introduction

The United Nations has estimated that the global population will rise to around 9.7 billion in 2050 (Department of Economic and Social Affairs 2019) resulting in a projected production of over 25 billion metric tons of plastic waste by the same year (Geyer et al. 2017; Meereboer et al. 2020). This overproduction of material shall not only impact the environment and ecosystems with the pollution linked to the manufacture steps, but most likely a significant impact will be related to the disposal and end-of-life management (Meereboer et al. 2020). Traditional synthetic fossil-based plastics such as poly(ethylene terephthalate) (PET) and polypropylene (PP) have four disposal routes; (i) incineration for energy; (ii) recycling for new materials; (iii) landfill disposal for containment; or the less desirable (iv) leakage/littering (Hestin et al. 2017). Recycling is the most convenient from an environmentally standpoint. However, in 2017 it was reported that less than 10 % of the plastics were recycled in the United States (US) (Patel and Tullo 2020) with an added an important challenge presented by a common social behavior of improper disposal and disinterest (Roy et al. 2021).

Due to the elevated amount of plastic waste, the pressing need to reduce the consumption of traditional petroleum-based materials for biodegradable and compostable options is imminent. Moreover, by merging the utilization of these materials, the energy requirements and the gas emissions during production would also be decreased (Harding et al. 2007; Gironi and Piemonte 2011; Meereboer et al. 2020). A bio-based material is defined as all of it or a portion is intentionally proceeding form a living or once living organism (Plackett 2011; Filpponen et al. 2020). Thus, all

lipids, proteins, carbohydrates, and even smaller molecules such as toxins could be used to develop a so-called bio-based material. It is worth mentioning that there is controversy on the definitions depending on the field of study, where the term “bio-based material” is used as an umbrella term, this could variate depending on their end-use such as biomaterials when related to biomedical applications or bioplastics when used for packaging, textiles or automotive (Gumpert and Material Connexion 2021). In this review, we utilized the term biomaterial as a general definition without differentiating among the final applications.

Understanding the main interactions between the elements of a composite material, such as natural occurring biomass, is essential for its use in applications. This review aims to make a comprehensive overview of the interactions forming the polysaccharides of the lignocellulosic materials in a molecular level, as well as the interactions between their different macromolecules, and the biocolloidal systems they can form. Finally, an search into different applications where these lignocellulosic materials have been applied was done, as the fundamental understanding could help elucidate improvements to the fields and a more funded application of these materials to solve day-to-day problems could be developed.

1.2. Current state of agro-forest bioproducts as lignocellulosic sources

To accomplish the development of more sustainable and green pathways in the materials science field, the biorefinery concept has emerged during the last years as a viable alternative. The International Energy Agency (IEA) defined biorefinery as “the sustainable processing of biomass into a spectrum of marketable products and energy”, meaning that value is added to the entire supply chain during the lifetime of that biomass (IEA Bioenergy 2009).

The main advantage of using biomass as raw material is the possibility of obtaining it from environmental, economical, and socially responsible pathways, such as well-established renewable industries such as forestry, agriculture, fisheries, cattle, or sericulture. As a result, many are the raw materials alternatives to be utilized as sources for bio-based products, such as the derivatives generated after crops harvesting or the wood residues caused by the timber industry.

Regarding the forestry industry, only in 2019, the US production of sawlogs and veneer logs was 187 m^3 generating a as result, 15.3 m^3 of wood residues, also known as sawdust (FAOSTAT 2019). The large volume of such residues, open new alternatives for its recovery and utilization in the nanotechnology areas and in new markets focused on high value-added products. In the case of agriculture harvest, most of the crops are utilized for alimentary ends, as food security is still of public concern (Philp 2015). The most produced agricultural commodities in the US are soybean, corn, wheat, and cotton, which account for approximately 70% of the total harvested area (Yang and Suh 2015). Additionally, farmers are increasingly interested in growing hemp due to its versatility to extract the oil and the fiber portion for different applications (Alabama Farmers Federation 2021). Therefore, there is an enormous potential on utilizing lignocellulosic bioproducts acquired from agricultural sources to produce biopolymers and develop biomaterials (Oksman et al. 2014; Filpponen et al. 2020).

Although the commodity types mentioned above are different regarding their properties, uses, and chemical characteristics, they share similarities at the most fundamental level of their structure. The main component of these raw materials are polysaccharides; biomacromolecules composed of sugar monomers (Cox and Nelson 2021; Tardy et al. 2021). These sugar monomers can be arranged in a rigid linear chain to give rise to the cellulose chain (Azizi Samir et al. 2005) which due to the presence of hydroxyl groups and van der Waals forces, can interconnect in a

parallel arrangement, establishing elementary fibrils (1.5-3.5 nm in diameter). Additionally, the aggregation of elementary fibrils gives rise to nanofibrils (10-30 nm in diameter), and a subsequent combination of them can form microfibrillar bands (diameters in the order of 100 nm). The combination of these polysaccharides are usually the main structural components of the cell walls of plants and can be further arranged in a fibril-matrix-like structure mixed with other components such as hemicelluloses and lignin (Klemm et al. 2005).

Decoupling those fibrillar structures in solution can lead to the obtention of materials in the nanometric dimensions, known as nanocellulose suspensions, which can be utilized for high-novel applications (Hubbe et al. 2017). The chemical composition of these materials, as well as the molecular organization in which they can be found, will have great impact in the properties that the materials derived from them will possess. As a result, analyzing the linkages within each component to further understand the interaction between them, is of crucial relevance. To understand these effects, there are three levels in which to study and understand the causing phenomena: atomic, molecular, and supramolecular level.

1.2.1. An insight about the components of wood and soybean

As wood is a biosynthesized product, its chemical composition varies depending on the selected tree, genus, specie, geographical location, available soil nutrients, age, environmental condition of farming, droughts, among others (Pettersen and Rowell 1984; Iglesias et al. 2020). As a general distinction, wood can be classified in two main groups, hardwoods (HW) and softwoods (SW) being differentiated mainly by their variations in morphology, types of cells, and cells arrangements (Haygreen and Bowyer 1989). Nevertheless, regardless of the type of tree; the three main general components of wood are cellulose, hemicellulose, and lignin. Within these, the polysaccharides -cellulose and hemicellulose- account for 65 to 70 % of the dry weight (Rowell et

al. 2012), which makes them the primary contributors of the physicochemical properties of the wood as a material. In addition to those, the remaining 2-5 % correspond to the presence of non-structural constituents known as extractives (Hillis 1971; Thomas 2009). Chemical composition of softwood and hardwood species is detailed in Table 1.1.

Table 1.1. Chemical composition of softwood, hardwood, and soybean hulls.

Raw material	Cellulose	Hemicellulose	Lignin	Extractive	Pectin
Softwood[1]	37-43	20-30	25-33	2-5	-
Hardwood[1]	39-45	17-35	20-25	2-4	-
Soybean hulls[2]	29-51	10-20	1-4	-	6-15
Hemp[3,4]	55	16	4	5.25-20	4

[1]Sjöström and Westermark 1999, [2]Mielenz et al. 2009, [3] Rehman et al. 2013, [4]Viswanathan et al. 2020

Considering the different alternatives to obtain crops byproducts, soybean is the second largest harvested crop in the US (FAOSTAT 2019), leading to a bulky amount of material which could be potentially used under the biorefinery concept. This crop is worldwide produced due its versatility as oil seed, proteins, and fiber source, and due the possibility of using it as a biofuel source (IAMA 2009). After the soybean seed is crushed to extract the oil, the remaining material, known as soybean hulls or coat, is rich in fiber – and therefore cellulose - content (USDA 2019) and is usually utilized as fiber source for cattle (Hult et al. 2010). Focusing on the soybean hull composition, they account in average for 35.4 % cellulose, 17.2 % hemicelluloses, and 2.3 % lignin (Yoo et al. 2011). Additionally, some proteins, oil, and ash content are present in the soybean coat (Medic et al. 2014). Nevertheless, the efficiency of the dehulling process, will have a direct impact on the final chemical composition of the soybean hulls (Rojas et al. 2014).

Another emergent crop with high fiber content is hemp, which is traditionally used for its fibers in packaging and for the extraction of the seeds oil (Rehman et al. 2013; Väisänen et al.

2019). And since it reclassification by the Farm Bill effective in 2022 (U.S. Department of Agriculture et al. 2016) it is expected to be a major product in the U.S. Composition wise, the green fibers contain 55% cellulose, 16% hemicelluloses, 18% pectin, 4% lignin and extractives between 5.25 to 20% (Rehman et al. 2013; Viswanathan et al. 2020). The high variety of structural carbohydrates make this crop of interest for modern biorefinery applications.

When bearing in mind wood or agricultural byproducts to produce nanocellulosic suspensions, it is essential to consider that cellulose fibers do not occur independently in these raw materials. Instead, they are bonded together with hemicelluloses, lignin, extractives, and pectin, depending on the source (see Table 1.1 for detail chemical composition). Nevertheless, all these materials as individual components present their own chemical functionality, thermomechanical, and morphological characteristics; those determine in turn the interactions and possible uses that they can have in different applications (Ratner et al. 2013).

1.3.Chemistry of macroscopic lignocellulosic fibers

Due to the continuous improvement of technology designed to isolate materials in the nanoscale, cellulose is of particular interest, as this biopolymer tends to bundle into nano- to microscale fibers, depending on the diameter. Analyzing in detail the characteristics of this biopolymer, cellulose is a linear homopolymer generated by repeating β (1 → 4) D-glucopyranose units. These units are covalently linked through acetal functions between the equatorial OH group of C1 and C4 (β-1,4-glucan) (Moon et al. 2011). Along the cellulose structure, covalent bonds C-O and C-C are extended through the chain. Each anhydroglucose unit (AGU) has three hydroxyl groups (OH) in carbons C6, C3, and C2, being the one in C6 the more propense to react. Two AGU linked together by the same β orientation form the repeating unit for cellulose, commonly

known as cellobiose (Klemm et al. 2005). These bonds among the AGU are accommodated in a thermodynamically preferred conformation with every other AGU, rotated at 180º in the plane (Credou and Berthelot 2014).

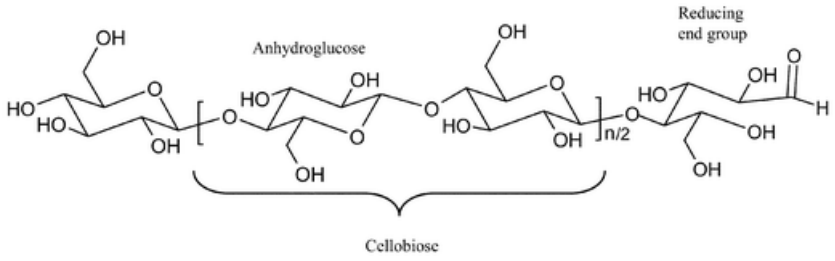

Figure 1.1. Cellulose chain structure. Reprinted from Kontturi et al. (2006) with permission from Royal Society of Chemistry.

Additionally, the presence of OH groups in carbons 2, 3, and 6 confers the possibility of forming inter- and intra- hydrogen bonds within and between OH groups from the same and different cellulose chains, giving this bio-based material the opportunity of establishing a robust supramolecular structure (Nishiyama et al. 2002). The presence of these OH groups also promote hydration interactions of the nanocellulose fibers in water, improving their dispersion in this media. As a result of the strong supramolecular arrangement of the cellulose chains, this biopolymer can be found as different polymorphic structures. The capability of cellulose chains to share protons to form H bonds opens the possibility of multiple options for crystalline packing. For example, cellulose I, commonly known as native cellulose, can be classified in cellulose Iα and Iβ depending if the crystalline structures are packed as tricyclic or monocyclic arrangements, respectively (Moon et al. 2011). The second most important type of polymorph is known as cellulose II. This is the most thermodynamically stable type of cellulose, and it appears as the result of the mercerization of cellulose with an aqueous sodium hydroxide (NaOH) or regeneration of cellulose fibers after dissolution in specific media (Aulin 2009). The main difference between cellulose I and II is the orientation of their atoms; in the former, atoms are organized in a parallel

orientation while in the later, the cellulose chains run in an antiparallel direction (Klemm et al. 2005). Additionally, when treating cellulose, I and II with ammonia, cellulose IIIα and IIIβ can be obtained. Finally, the last and less stable polymorphs are cellulose IVα and IVβ, obtained by heating cellulose IIIα and IIIβ, respectively, with glycerol (O'Sullivan 1997).

When arrange into elementary fibrils, the cellulose chain has two differentiable packing conformations, an amorphous and a crystalline domain; the previous can be dissolved by acidic hydrolysis, which when in the nanoscale diameters leaves the crystalline domain as the nanomaterial known as cellulose nanocrystals (CNCs) (Salas et al. 2014). On the other hand, if the celluloses fibers are subjected to mainly mechanical treatment, then both the amorphous and crystalline domain remain on the structure, giving rise to the obtention of cellulose nanofibrils (CNFs) (Xu et al. 2013). Additionally, when producing CNFs there are different alternatives, such as bleached or unbleached cellulose nanofibrils (BCNF and LCNF, respectively), depending on the purity of the starting raw material, in terms of cellulose content.

Hemicelluloses are also a type of polysaccharide present in lignocellulosic materials which form part in the above-mentioned fibril-matrix-like structure. Hemicelluloses are branched and less ordered polysaccharides. They are composed of several types of sugars arranged in different conformations. The most important are D-xylose, L-arabinose, D-glucose, D-galactose, D-mannose, D-glucuronic acid, 4-0-methyl-D-glucuronic acid, and D-galacturonic acid. Additionally, to a lesser extent there are also L-rhamnose, L-fucose, and various O-methylated neutral sugars (Pettersen and Rowell 1984; Sun et al. 2009). The type of hemicellulose will vary depending on the source of origin (Naimi et al. 2016) together with the different types of linkages between the sugars units, allowing branching and shorter molecular weight structures than cellulose (Eronen et al. 2011). For example, softwood are characterized for having more mannose

and galactose units than hardwood, while the later, it has a larger proportion of xylose and acetyl groups (Sixta et al. 2006a). Additionally, the structure of hemicelluloses will also be affected by the extraction method utilized. For example, cellulose fibers produced from kraft methods using hardwood sources contain a higher amount of carboxylic groups due to the initial hemicellulose content (Solala 2011). Nevertheless, similarly to cellulose, covalent C-C and C-O bonds are found among the hemicellulose structures. Due to the presence of OH groups along its structure, hemicelluloses interact extensively with cellulose through hydrogen bonds (Yi and Puri 2012). Additionally, the interactions with lignin are trough covalent bonds and when interacting with acetyl units ester linkages are formed (Sun et al. 2009).

Specifically, the presence of hemicelluloses on CNF have been found to impede the agglomeration of the nanofibrils. This effect is partly electrostatic in nature, as many hemicelluloses possess negative charges, generating repulsion between them (Arola et al. 2013). Conversely, the side chains present in some hemicelluloses contribute to steric repulsion between nanofibrils, thereby also reducing their tendency to aggregate (Hubbe and Rojas 2008; Tenhunen et al. 2014). As a result of these interactions, the presence of hemicelluloses promotes pulp fibrillation (Duchesne et al. 2001; Hult et al. 2001; Iwamoto et al. 2008; Tarrés et al. 2017) and colloidal stability of CNF suspensions (Tenhunen et al. 2014).

In addition to cellulose and hemicelluloses, the second most abundant component in lignocellulosic materials is the polyphenol biopolymer: lignin. It is a complex phenolic heteropolymer arising from the polymerization of three primary precursors; coniferyl alcohol, sinapyl alcohol, and p-coumaryl alcohol (Wang et al. 2016). Although the composition and content of lignin vary among the different lignocellulosic species, a general classification can be considered as (1) softwood species, 2:1 ratio of coniferyl alcohol: p-coumaryl alcohol; (2)

hardwood species, 1:1 ratio of coniferyl alcohol: sinapyl alcohol, and (3) grass species, with a principal amount of p-coumaryl alcohol (Jiang 1997). Furthermore, lignin structure will also be affected by the isolation method utilized, generating structural changes and cleavage of the native lignin (Wang et al. 2016). Due to the high variability of lignin, the number of functional groups will also vary. However, specific functional groups on this natural polymer are methoxy, carbonyl, phenolic, and aliphatic hydroxyl groups (Jiang 1997).

Regarding the interactions in between the above-described components present in lignocellulosic materials, the presence of OH groups allow them to interact through non-covalent links (hydrogen bonds). These interactions have been demonstrated to be essential for the structure of wood, as when the hydrogen bonding was disturbed by cycles of wetting and drying, separation of the cellulose fibrils from the lignin and hemicelluloses matrix was measured (Toba et al. 2012). Meanwhile, it has been studied that lignin and hemicelluloses can be chemically linked through covalent bonds, forming lignin-carbohydrates complexes (LCC) (Deshpande et al. 2018).

In LCNF fibers, the dominant forces occurring on the cellulose surface containing lignin and hemicelluloses are electrostatic dipole-dipole interactions. Among them, covalent and hydrogen bonding, can be considered the most important, with an important contribution by steric effects (Israelachvili 2011). The presence of lignin, hemicelluloses, and pectin in soybean fibers, may reduce the accessibility of the three OH initially available on each AGU of the cellulose chain. However, due to the heterogeneity of the sample, other functional groups may have more predominance, such as carboxylic and phenolic hydroxyl groups from the different components.

Additionally, when considering the presence of lignin, this aromatic polymer can have two, seemingly contradictory effects on pulp fibrillation, based on what kind of pulps are utilized as the starting material. On the one hand, it can hinder fibrillation, as has been demonstrated in the case

of mechanical pulps (Lahtinen et al. 2014). On the other hand, residual lignin can even significantly lower the energy consumption of fibrillation in the case of chemical pulps (Spence et al. 2011), serving as an example on how lignin structure affects its function. Moreover, the presence of residual lignin in chemical pulps has been reported to result in the formation of finer CNFs at comparable energy consumption levels (Solala et al. 2012; Rojo et al. 2015).

Assuming a complex, network-like structure for native lignin, it seems probable that the initial crosslinked structure prevents efficient fibrillation of the highest-lignin pulp grades by 'locking' the individual microfibrils together (Lahtinen et al. 2014; Hanhikoski et al. 2016). The hydrophobic character of lignin may also play an important role in preventing fiber swelling and fibrillation, as will be discussed in the next section. In contrast, the residual lignin present in chemical pulps is significantly degraded and present in much lower quantities, therefore less able to prevent fiber swelling and fibrillation. We have previously proposed (Ferrer et al. 2012; Solala et al. 2012) that the ease of fibrillation observed in lignin-containing chemical pulps is due to lignin acting as an antioxidant, preventing broken covalent bonds from being formed again.

Moreover, when studying agricultural by-products as possible sources for bio-based materials, it is crucial to consider all the components those agricultural sources may have. For example, in the case of soybean hulls, pectins could be an additional component in the CNF fibers. Soybean contains 40 % proteins, 21 % oils, 34 % carbohydrates, and 4 % of ash (Kawamura 1967). Pectins, are present mainly on the primary cell wall of plants, belonging to the polysaccharides family, forming branch and linear structures (Gawkowska et al. 2018). Pectins are composed of up to 69 % D-galacturonic acid, covalently linked (Monsoor 2005). Among the different types of pectins, the most abundant is homogalacturonan (HG). This is a linear homopolymer, composed of (1→4)-α-linkage. The main functionalities present in HG are carboxyl, acetyl, and OH groups

(Mohnen 2008). As mentioned in the previous section, hemp is another example of agricultural byproduct that besides cellulose, hemicelluloses, lignin, and pectins, contains a high percentage of extractives. In fact, extractives, are present in multiple native fibers and they vary depending on the plant source. An important characteristic of these compounds is their low molecular weight (Kontturi 2005). Extractive compounds can be classified as fatty acids, fatty alcohols, waxes, and phenolic constituents (Credou and Berthelot 2014). Most of these compounds are removed after the pulping process (Kontturi 2005). However, in species such as southern pines with relatively high extractive content, byproducts such as raw tall oil and turpentine can remain on the sample (Smook 2016).

Due to the reduction in size compared to cellulose fibers, nanocellulose suspensions are the combination of cellulose nanoparticles with enhanced surface area and, as a result, higher hydrogen bonding capability surrounded by water molecules, which confers greater stability to the suspension. Such suspensions are commonly known as colloids. The importance of understanding the interfacial interaction between colloids relays in the fact that if the colloidal particles are sufficiently close, they will exert forces that will determine the capacity to form flocs or aggregates, the rate of the formation of the aggregates, and the final characteristics of the formed structures (Meakin 1988).

1.3.1. Isolation of nanocellulosic materials and its effect in CNF chemistry

During the early '80s, Turbak et al. (1982) and Herrick et al. (1983) were the first to introduce the nanocelluloses commonly known at that time as microfibrillated cellulose (MFC). Utilizing cellulose pulp suspensions at a very low solid content (typically ~2 %wt.) as starting material, and homogenizing this suspension under pressure, they discovered that after intensive mechanical disintegration they were able to obtain a colloidal fibrous suspension with particles in

the microscale. Despite the efforts to produce MFC, the process was energy-consuming, which was why this material lost interest. Several years after, different types of mechanical treatments, including homogenization (Nakagaito and Yano 2004; Spence et al. 2011b; Moser et al. 2015), grinding (Taniguchi and Okamura 1998; Iwamoto et al. 2007; Spence et al. 2011a), ultrasonication (Zhao et al. 2007; Cheng et al. 2009; Chen et al. 2011), and cryocrushing (Dufresne et al. 1997; Chakraborty et al. 2005), together with pre-treatments such as carboxymethylation (Wågberg et al. 1987, 2008), TEMPO (2,2,6,6-tetramethylpiperidine-1-yl)oxyl radical) mediated oxidation (Saito et al. 2006, 2007), ammonium persulphate oxidation (Filipova et al. 2018), and enzymatic pre-treatments (Henriksson et al. 2007; Pääkko et al. 2007) were developed to address this problem while producing these colloidal suspensions. The new technology and pre-treatments allowed scientists to obtain what we know today as cellulose nanofibrils (CNFs), meaning that one of the fibers' dimensions were in the range of the nanometers while consuming less energy for its production compared to the initial processing techniques.

Conversely, the pretreatments selection will also add functional groups to the surface of the CNF by side reactions between the hydroxyl groups and the reagents used (Young 1994; Sixta et al. 2006b; Iglesias et al. 2020a). These new functional groups will also affect the interfacial interactions possible between the CNF and other systems, for example, both TEMPO mediated oxidized cellulose and carboxymethyl cellulose will have more negative charge than unmodified cellulose fibrils, as carboxyl groups will be present on the surfaces. However, carboxymethyl cellulose have an intermediate ether group which increases the side chain length, and with this, steric effects will also sum in the interactions generated with fibrils containing this functional group when compared with only carboxylated cellulose. Similarly, carboxylated modified CNF with different linkers can be obtained through pretreatments with anhydrides such as maleic,

succinic, or phthalic (Sehaqui et al. 2017) prior to its mechanical fibrillation; or by only chemical treatments with diluted acids (Chen et al. 2016; Zhu et al. 2021).

1.4.Nanocellulose fibers as colloidal particle

Cellulose nanomaterial suspensions are a gel-like colloidal suspension. Colloidal science's history can be traced back to the mid-eighteenth century when Francesco Selmi described the mixture of solid particles – such as silver chloride, sulfur, Prussian blue, starch, and alumina – in water as "pseudo-solutions". It was later in 1861 when Thomas Graham defined these pseudo-solutions as colloids (which means glue in Greek) (Evans and Wennerström 1999). However, there is a lot of controversy when defining what a colloid is. As a general definition, colloids are dispersions where small solid particles (solute) are embedded in a continuous liquid media (solvent) (López-Esparza et al. 2015). But the question now would be: What is small enough to be considered in the group of colloids? During Graham times, he deduced that colloidal particles should have dimensions between 1 nm and 1 μm in diameter (Evans and Wennerström 1999). Nevertheless, over the years, various solutions with larger sizes such as clays, sprays, emulsions, and fiber suspensions such as nanocellulose have been studied, showing similar characteristics to the traditionally named colloids (Myers 2002; Berg 2010). The properties of colloidal suspensions are determined by the properties of the solid particles, the media, and the interface between them (Berg 2010). Thus, understanding the fundamental behavior and interactions of CNF in water systems could help to come to a better conclusion and give an inside on how better use the suspensions for the development of different applications.

1.4.1. Interfacial interactions in nanofibrillated cellulosic systems

As mentioned earlier, CNF suspensions are obtained mainly by mechanical treatments of cellulose pulps and the extraction process of the cellulose pulp from which the nanomaterial would be obtained will also modified the available groups in the surface. When producing cellulose fibers by traditional pulping methods, such as Kraft of sulfite, fibers acquire a negative charge on the surface due to the formation of carboxylic, carbonyl, and sulfate groups, among others (Iglesias et al. 2020a). Consequently, CNF suspensions made thereof will have a substantially anionic surface charge (Olszewska 2013). Other providers of surface charge in the cellulose nanomaterial are the residual hemicelluloses and lignin that also have carboxyl groups that are exposed in this interfacial volume (Popescu et al. 2008). As a result of this charge, there will be several interactions present in a CNF suspension.

Defining the macroscopic region separating two pieces of substance of one another is relevant when discussing interfacial phenomena. This thin region that ranges from a few Angstroms to a few nanometers is commonly known as the interface. It can be applied to any surface boundary, such as liquid-gas, liquid-liquid, solid-liquid, gas-solid, and solid-solid (Berg 2010). Specifically, in a nanocellulosic suspension, the solid-liquid interface properties will be tightly related to the chemical composition of the raw material and the interactions between them (physico-chemical properties), conferring different performances (Evans and Wennerström 1999). The main characteristic of this thin layer is that it is inhomogeneous compared with the bulk material (Berg 2010). Different long and short-range interactions can occur at the interfaces when solid particles are dispersed in a liquid media. Some of them are solvation and hydration forces due to the surface swelling or the arrangement of the solvent molecules at the interface, hydrophobic forces due to the interaction between hydrophobic components in water, steric

repulsions forces generated by osmotic and entropic effects, and electrostatic and double layer forces due to the ionization of surface groups, charged surfaces, and ion adsorption (Bellmann et al. 2019). These interactions are usually categorized as interactions following the DLVO theory and non-DLVO interactions.

i. DLVO interaction forces

At a fundamental level, the most important interaction between the charged particles are (i) van der Waals forces and (ii) electrostatic repulsions (Eronen 2011). Van der Waals forces are dispersions forces generated by the fluctuation of the electronic clouds of the atoms. When two similar particles get close enough, attractive interactions occur between them, which will depend on the characteristics of the material and the medium (Israelachvili 2011). Moreover, due to the presence of charge on the surface of the fibers in aqueous solution, electrostatic repulsions interactions are also present (Eronen 2011). Ions present on the solution carrying oppose charge to that of the colloids form an electrical double layer. These two different interactions in a colloidal suspension give rise to the DLVO potential between them (named after Boris Derjaguin and Lev Landau, Evert Verwey and Theodoor Overbeek) (Figure 1.1). As two particles get closer, there is an energy barrier that the particles must overcome to get in contact. If the energy of the interaction is not enough to overcome the energy barrier, the particles will not agglomerate, and they will form stable colloidal suspensions. On the contrary, if the energy is high enough to overcome the energy barrier, the particles will fall in the primary minimum dominated by van der Waals interactions and collapse, forming aggregates (Israelachvili 2011).

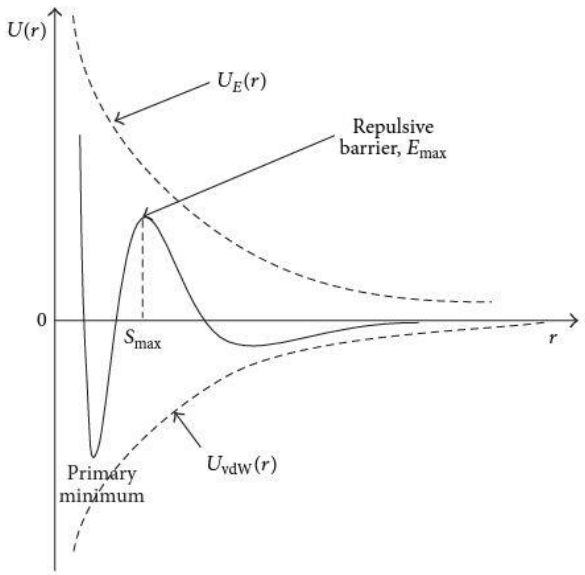

Figure 1.2. The presence of van der Waals attraction interactions together with electrostatic repulsive interactions leads to the DLVO potential interaction (Adapted from Lopez-Esparza et al. 2015).

This electrostatically driven behavior is of particular interest as ions and other charged solutes can be present in the water media. Association constants with polarized molecules and metallic ions, as well as localized acid environments formed in the interfaces will also impact the behavior of the suspension even as the bulk of the colloid behave more continuously. These localized environments, where the barrier energy is surpassed, is one of the principles for the self-assembly of gel networks with nanofibrillated cellulose (Benselfelt et al. 2019). Furthermore, the DLVO potential on the surface will impact the water retention, swelling and stability of CNF suspensions. The interactions between water and ions with the CNF will generate a mixing and ion pressure on the suspension, respectively (Karlsson et al. 2019). The ions present in the suspension can screen the charges on the surface of CNF -especially when higher concentrations than CNF are used-, facilitating the interaction with other components of the suspension, such as

water and small molecules. This impact will then depend on their kinetic constant, usually resulting in more water retained on the network (Yang et al. 2010; Karlsson et al. 2019) or in the formation of hydrogen bonding between different adjacent elements, such as the molecules or other nanofibrils when water layers are depleted (Ding et al. 2019).

ii. Non-DLVO interaction forces

In a nanocellulosic system, not only DLVO forces regarding to van der Waals and repulsion forces are present. There is a group of interactions linked more to the thermodynamic equilibrium of the suspension system, which are commonly known as the non-DLVO forces. When these interactions arise, they will impacting how the particles present in the CNF suspensions behave between them (Berg 2010).

Hydrophobic interactions are significant long-range attractive effects on nanocellulosic suspensions. They appear when hydrophobic molecules/particles approach since they are not able to bond with water molecules. The contact between water and these hydrophobic portions is entropically unfavorable (Berg 2010). As a result, the water molecules are ejected, and the hydrophobic molecules attract each other, reducing the energy of the system (Olszewska 2013). Lignin contained in LCNF also generate hydrophobic points in their phenolic structures. Due to the double bonds in the rings, the electronic clouds are contained in the interior of the structure, leaving the protons on the exterior tightly bound to the carbon, and making difficult the formation of hydrogen bonding with water (Israelachvili 2011). Thus, lignin tends to attract hydrophobic molecules to lower the expose surface.

Another type of non-DLVO forces are steric forces originated mostly when large polymer structures are present in the suspension. When polymers tails from different surfaces get in contact, two effects arise into the system; (i) when mingling of the fibers, there is an increase in the osmotic

pressure of the system due to the difference in concentration solute/solvent, and (ii) there is a loss on the freedom of the polymers chains to move, this reduction on movement decreases the entropy and as a result increases the free energy of the system, which is thermodynamically less stable. As a result, a repulsion force is generated on the system to reduce the free energy and return to the most stable position (Eronen 2011; López-Esparza et al. 2015).

Hydration forces also contribute to the non-DLVO forces. They are considered short-range structural repulsive forces. They appear due to the movement of the particles getting closer to one another. As a result, the structure and orientation of the water molecules are affected (Argyris et al. 2011), generating a repulsion between the particles. Nevertheless, it has been reported that in cellulosic systems, these forces are not observable since the steric repulsion between the fibers overcome this effect (Olszewska 2013).

An additional type of interaction is the so-called depletion interaction. In the case of nanocellulosic systems, they can appear when the surfaces of the fibers are fully saturated with water. When two particles with depletion layers come closer enough, the polymer is excluded generating osmotic pressure and, as a result leading to flocculation of the particles (Berg 2010). Finally, hydrodynamic forces are also present on cellulosic systems due to the flow of the water molecules surrounding the fibers, affecting the dynamics of the solution (López-Esparza et al. 2015).

1.5.Relevant suspension properties

Other essential properties to describe in nanocellulosic suspensions are charge density, zeta potential, and surface free energy. Surface charge density is related to surface charge coming from functional groups on the surface of the fibers from lignin, hemicelluloses, or in the case of soybean

CNF from residual pectins. The most commons groups that contribute to the surface charge density are carboxyl and carboxymethyl (Henriksson et al. 2007; Isogai et al. 2011). Zeta potential, is related to the surface potential and surface charge of the sample, is a valuable measurement to indicate the colloidal stability of the sample (Foster et al. 2018). The zeta potential is a result of the screening of the surface charge with a tightly bound layer of ions or water, that in turn will interact with and structure water layers, contributing to the hydration and depletion forces present in the suspension and determining then the colloidal stability.

Finally, the surface free energy of a material is an important parameter that can provide information about its compatibility with other species. This can be estimated as the sum of the dispersive intermolecular forces, the polar interactions, and the hydrophobic attractions (Israelachvili 2011), as well as the wettability of the surface (Wang et al. 2009). Knowing the surface free energy on a solid surface can help to predict (i) its behavior when interacting with liquids, including water; and (ii) the energy required to propitiate the intermolecular and interatomic interactions with other surfaces, phenomena also known as adhesion (Awaja et al. 2009). It has been reported in the literature that LCNF films possess a lower surface free energy than their bleached counterpart (Rojo et al. 2015). This can be related to the presence of lignin which has a more hydrophobic behavior, reducing, as a result, the interactions with water.

1.5.1. Viscoelastic properties

When characterizing colloidal suspensions made from bleached and unbleached cellulose nanofibrils, it is essential to consider all the information detailed above about the chemistry of the different natural components. Additionally, if the system is not in equilibrium, which is usually the case, and external forces are applied, hydrodynamic interactions will need to be considered. Hydrodynamic forces start playing a role when the solvent where the solid particles are embedded

flows. Then, the dynamics of the particles changed. For distant particles, the expression to calculate the force of the particle proposed by George Stokes is relatively simple (Israelachvili 2011). However, for more concentrated samples, the interactions between particles cannot be neglected. This being said, if the objective is to study the rheological behavior of the cellulose nanofibrils suspensions, with entangled structures and with varying chemical composition, then the rheological analysis becomes more complicated due to the shape, flexibility, size polydispersity, transient physical entanglements, and physicochemical interactions.

It has been extensively reported in the literature that nanocellulosic suspensions at different concentrations present shear-thinning behavior (Pääkko et al. 2007; Herrera et al. 2018). Additionally, rheological studies of lignin-containing cellulose nanofibrils with varying chemical composition show the same trend (Iglesias et al. 2020b). Due to the anisotropy of the particles in nanocellulosic suspensions, this behavior in which the viscosity of the sample decreases as the velocity of the deformation increases is expected (Berg 2010). During this process, the velocity gradients break down the flocks between the fibrils, allowing their alignment and movement (Berg 2010). However, when lignin is present on the surface of the particles in suspension, covalent linkages between lignin and hemicelluloses (Smook 2016), and hydrogen-bond interactions with the cellulose chain could be the reason why the viscosity of the LCNF samples are always higher than their bleached counterpart at low shear rates. Furthermore, the same rheological behavior was found for bleached and unbleached samples from soybean fibers (Iglesias et al. 2021a). Moreover, the unbleached CNF sample from soybean has a yield stress, which can be due to the gel formation of the sample or flocculation. Thus, the presence of pectins from soybean could be responsible for this behavior due to the gelling properties of pectins (Gawkowska et al. 2018).In summary, as detailed in the previous sections, there are several different interactions present in nanocellulosic

particles and systems, which will result in the properties of the suspensions. The surface groups will contribute to the surface free energy, but other factors such as position, surface structure, atomic neighbors, and even shape would also be important to determine it. Thus, understanding all the properties of the nanocellulosic system will contribute to gain a better insight into the interactions with other materials when utilizing nanocellulosic suspensions for different applications.

1.6.Examples of applications and the influence of the interfacial interactions

As explained throughout this text, nanocellulose suspensions over a concentration range possess a gel-like structure and are the combination of cellulose nanoparticles with enhanced hydrogen bonding capability surrounded by and entrapping water molecules, which confers stability to the colloidal suspension. Due to this property, CNFs have demonstrated to have an excellent potential for being incorporated in formulations for thickeners and emulsifiers for food, cosmetics, and paints (Turbak et al. 1982; Herrick et al. 1983; Lavoine et al. 2012). Furthermore, CNFs present high aspect ratio, low density and thermal expansion, high strength modulus and stiffness (Hsieh et al. 2008; Eichhorn et al. 2010; Siró and Plackett 2010), as well as remarkable film-formability when dried (Spence et al. 2011a); properties that make them attractive in terms of producing high-strength composites and barrier materials from renewable resources. Hence, the following sections aim to relate the interactions present on these suspensions and their use in some applications.

1.6.1. Interfacial interactions between CNF systems and wood adhesives

Over the years, UF has been positioned as one of the most utilized wood binders in the wood panel industry (Riegler et al. 2012). Based on the literature trends, during the last decade, we observed an increased interest in research replacing wood-based adhesives to a certain extent for more renewable alternatives, such as nanocellulose (Veigel et al. 2011; Mahrdt et al. 2016). The idea of replacing petroleum-based adhesives and improving the mechanical and dimensional stability of the wood panels with a natural filler has been the driver for such growing interest.

UF is a thermosetting amino resin characterized for being water-soluble, with good adhesion properties, highly curing rates, and relatively low cost (Christjanson et al. 2006). They are synthesized from two components: urea and formaldehyde. The structure of this resin is highly changeable due to the variety of reactions that can occur during the obtention process. UF is formed by a mixture of linear and branch macromolecules (Jada 1988), containing different functional groups. Among the most predominant functional groups, carboxyl and amine groups (Christjanson et al. 2006). Additionally, as UF is produced in an aqueous formaldehyde solution, these resins are soluble in water. Among the interactions at an atomic level, they are mainly covalent bonds and van der Wall interactions.

When utilizing bleached and unbleached CNF as a replacement of UF in particle boards, interfacial interactions occur between them. Compared with the fully bleached CNF samples, it is expected an additional surface charge on the fibers due to the presence of lignin, hemicelluloses, and even pectins (in the case of soybean CNF), improving the interactions of these materials with the UF (Iglesias et al. 2021b). These components will interact through non-covalent links (hydrogen bonds). Additionally, steric repulsion can occur, increasing the osmotic pressure of the system.

The incorporation of LCNF to the UF resins can decrease its surface free energy due to the hydrophobic behavior of this natural polymer. Due to the chemistry on the surface of both components, lignin could adhere to the surface of the adhesive, repelling the adhesion of water molecules, thus, reducing the wettability of the surface (Israelachvili 2011; Iglesias et al. 2021b). In order to measure these characteristics, contact angle, in particular the sessile drop method, can be used. By obtaining a contact angle lower than 90º, the surface presents hydrophilic properties. If oppositely, the contact angle is >90º, then the surface behaves more hydrophobic (Berg 2010).

As mentioned before, UF has been widely used in the wood adhesive industry due to the advantages it presents for industrial applications (Veigel et al. 2012). Nevertheless, the release of aldehydes and formaldehyde from products such as particle board, medium density fiberboard (MDF), and oriented strand board (OSB) panels over time and also during the pressing of the products is what increased the necessity of its modification and/or replacement with more environmentally friendly alternatives (Dunky 1998; Baumann et al. 2000). Based on these issues, isocyanate wood binders were introduced to the German market in the early 1970's (Papadopoulos et al. 2002). More specific, the use of MDI (4,4'-methylenediphenyl isocyanate) with a variety of functionalities, reactivity, and different structures (Frazier 2003) made this polymer a suitable alternative for the forest products market.

pMDI is an aromatic polymer containing two isocyanate groups per monomer. The reactivity of this polymer is highly variable due to the variability of the isocyanate groups. These functional groups reactivity will vary depending on their substitution (Frazier 2003). The aromatic structure on this adhesive confers rigidity as well as more hydrophobic characteristics. Isocyanates groups are highly reactive in contact with hydroxyl groups, forming polyurethanes and releasing

CO_2 as consequence (Frazier 2003). Due to the available OH groups in the structure, LCNF could be a better option to interact with pMDI than bleached CNF (Hornus et al. 2020).

1.6.2. Solubilization and regeneration of nanocellulosic systems

Another example of the impact of the interactions of the media with the material can have on the properties is the solubilization of cellulose in sodium-urea solutions. Cellulose is insoluble in water due to the high crystallinity of the formed molecules and fibers, which the high density of hydrogen bonding generated have a more stronger interaction between them, than the interactions that could form with the water (Pinkert et al. 2010). However, if these bonds are broken, solubilization of cellulose could be possible. To achieve this, one can make use of ions such as the ion sodium, which has a high electro-attractive force (ion-dipole), high enough that the surface hydroxyl groups release the bound proton and interact with it, breaking some of the H-bonds formed (Beck et al. 2015). However, solvation (the complete surrounding of water to the molecule to become a solvate) is still not possible as other type of interactions are still present, such as hydrophobic interactions on the surface. To eliminate this, urea is able to attach to this plane on the crystals while also interacting with the water, allowing the dissolution (Zhou and Zhang 2000; Cai and Zhang 2005; Xiong et al. 2014; Huber et al. 2016). The high concentration of the sodium and urea also come with an alkaline pH, so when the solution is dropped into an acid bath, the solubility of the cellulose drops, regenerating its crystalline structure and forming 3-D compacted bead hydrogels (Trivedi et al. 2016), however the resulting new structure will be cellulose II, as hydrogen bonding arrangement will be most beneficial here (Li et al. 2015). Here, the interactions not only affect the solubility, but the surface and crystalline structure is modified.

In this last example, the molecular interactions and its changes were the only thing needed to generate a 3-D structure during regeneration (Trygg 2015; Trivedi et al. 2016; Gomez-

Maldonado et al. 2021; Gomez-Maldonado et al. 2021). Likewise, composite materials can be generated from cellulose without the formation of covalent bonds. As mentioned before, the hydroxyl groups of cellulose are exposed in the equatorial axis (Alekozai 2013), which makes the surface rich in hydroxyl groups. These groups can be used to form hydrogen bonding with other β-lineal polysaccharides such as chitosan or alginate (Orelma et al. 2011), which would add functionality to the surface, and therefore surface energy, as the available groups of these new polymers would be exposed in the new generated surface (Gomez-Maldonado et al. 2021). Here the surface energy is decreased by the intermediate state where salts form an intermediate species where they displace the present hydrogen before being displaced by the new polymer, enhancing the density of hydrogen bond interactions, and irreversibly adsorbing onto the surface.

1.7.Conclusions

As a summary, when utilizing different raw materials to produce and apply nanocellulose suspensions into products, two main characteristics need to be considered to understand the interfacial interactions; (1) all the different chemical components present of the selected raw material, and (2) the utilized treatments to obtain the colloidal suspension (chemical, mechanical, and/or enzymatical), which will confer different properties to the fibers (Ratner et al. 2013). Understanding of the atomic and molecular interactions will help to take full advantage of the wood and soybean derivates, mainly the cellulose nanomaterials and enable applications based on these renewable and sustainable materials. Enhancing the use of the forest, and increasing its potential value for the US, will provide a more environmentally friendly alternative to displace many fossil-based polymer applications.

1.8.Literature cited

Alabama Farmers Federation (2021) Alabama Hemp Farms Set To Jump Significantly In 2020. In: https://alfafarmers.org/alabama-hemp-farms-set-to-jump-significantly-in-2020/

Alekozai E (2013) Enhanced Multiscale Sampling of the Cel7A-Cellulose Interaction. Ruperto-Carola University of Heidelberg

Argyris D, D. Ashby P, Striolo A (2011) Structure and Orientation of Interfacial Water Determine Atomic Force Microscopy Results: Insights from Molecular Dynamics Simulations. ACS Nano 5:2215–2223. doi: 10.1021/nn103454m

Arola S, Malho JM, Laaksonen P, et al (2013) The role of hemicellulose in nanofibrillated cellulose networks. Soft Matter 9:1319–1326. doi: 10.1039/c2sm26932e

Aulin C (2009) Novel oil resistant cellulosic materials. Royal Institute of Technology

Awaja F, Gilbert M, Kelly G, et al (2009) Adhesion of polymers. Prog Polym Sci 34:948–968. doi: 10.1016/j.progpolymsci.2009.04.007

Azizi Samir MAS, Alloin F, Dufresne A (2005) Review of Recent Research into Cellulosic Whiskers, Their Properties and Their Application in Nanocomposite Field. Biomacromolecules 6:612–626. doi: 10.1021/bm0493685

Baumann M, Lorenz L, Batterman S, Zhang G-Z (2000) Aldehyde Emissions From Particleboard and Medium Density Fiberboard Products. For Prod J 50:75–82

Beck S, Méthot M, Bouchard J (2015) General procedure for determining cellulose nanocrystal sulfate half-ester content by conductometric titration. Cellulose 22:101–116. doi: 10.1007/s10570-014-0513-y

Bellmann C, Caspari A, Moitzi C, Babick F (2019) Dynamic and Electrophoretic Ligth Scattering , First. Anton Paar GmbH, Austria

Benselfelt T, Nordenström M, Hamedi MM, Wågberg L (2019) Ion-induced assemblies of highly anisotropic nanoparticles are governed by ion-ion correlation and specific ion effects. Nanoscale 11:3514–3520. doi: 10.1039/c8nr10175b

Berg JC (2010) An introduction to interfaces & colloids: the bridge to nanoscience. World Scientific, Hackensack, NJ

Cai J, Zhang L (2005) Rapid dissolution of cellulose in LiOH/urea and NaOH/urea aqueous solutions. Macromol Biosci 5:539–548. doi: 10.1002/mabi.200400222

Chen L, Zhu JY, Baez C, et al (2016) Highly thermal-stable and functional cellulose nanocrystals and nanofibrils produced using fully recyclable organic acids. Green Chem 18:3835–3843. doi: 10.1039/c6gc00687f

Christjanson P, Pehk T, Siimer K (2006) Structure formation in urea-formaldehyde resin synthesis. Proc Est Acad Sci Chem 55:212–225

Cox M, Nelson DL (2021) Lehninger Principles of Biochemistry, Eight Edit. W. H. Freeman & Company

Credou J, Berthelot T (2014) Cellulose: from biocompatible to bioactive material. J Mater Chem B 2:4767–4788. doi: 10.1039/C4TB00431K

Department of Economic and Social Affairs (2019) World Population Prospects 2019

Deshpande R, Giummarella N, Henriksson G, et al (2018) The reactivity of lignin carbohydrate complex (LCC) during manufacture of dissolving sulfite pulp from softwood. Ind Crops Prod. doi: 10.1016/j.indcrop.2018.02.038

Ding Q, Zeng J, Wang B, et al (2019) Effect of nanocellulose fiber hornification on water fraction characteristics and hydroxyl accessibility during dehydration. Carbohydr Polym 207:44–51. doi: 10.1016/j.carbpol.2018.11.075

Duchesne I, Hult E, Molin U, et al (2001) The influence of hemicellulose on fibril aggregation of kraft pulp fibres as revealed by FE-SEM and CP/MAS13C-NMR. Cellulose 8:103–111. doi: 10.1023/A:1016645809958

Dunky M (1998) Urea-formaldehyde (UF) adhesive resins for wood. Int J Adhes Adhes 18:95–107. doi: 10.1016/S0143-7496(97)00054-7

Eronen P (2011) Adsorption studies on cellulose surfaces by combinations of interfacial techniques. Aalto University

Eronen P, Österberg M, Heikkinen S, et al (2011) Interactions of structurally different hemicelluloses with nanofibrillar cellulose. Carbohydr Polym 86:1281–1290. doi: 10.1016/j.carbpol.2011.06.031

Evans DF, Wennerström H (1999) The Colloidal Domain: Where Physics, Chemistry, Biology, and Technology Meet, 2nd Edition. Wyley-VCH, Canada

FAOSTAT 2019 http://www.fao.org/faostat/en/#data/QC

Ferrer A, Quintana E, Filpponen I, et al (2012) Effect of residual lignin and heteropolysaccharides in nanofibrillar cellulose and nanopaper from wood fibers. Cellulose 19:2179–2193. doi: 10.1007/s10570-012-9788-z

Filipova I, Fridrihsone V, Cabulis U, Berzins A (2018) Synthesis of nanofibrillated cellulose by combined ammonium persulphate treatment with ultrasound and mechanical processing. Nanomaterials 8:. doi: 10.3390/nano8090640

Filpponen I, Peresin MS, Nypelö T (eds) (2020) Lignocellulosics, First Edit. Elsevier

Foster EJ, Moon RJ, Agarwal UP, et al (2018) Current characterization methods for cellulose nanomaterials. Chem. Soc. Rev. 2609–2679

Frazier C (2003) Isocyanate Wood Binders. In: Handbook of Adhesive Technology,

Revised and Expanded

Gawkowska D, Cybulska J, Zdunek A (2018) polymers Structure-Related Gelling of Pectins and Linking with Other Natural Compounds: A Review. doi: 10.3390/polym10070762

Geyer R, Jambeck JR, Law KL (2017) Production, use, and fate of all plastics ever made. Sci Adv 3:25–29. doi: 10.1126/sciadv.1700782

Gironi F, Piemonte V (2011) Bioplastics and petroleum-based plastics: Strengths and weaknesses. Energy Sources, Part A Recover Util Environ Eff 33:1949–1959. doi: 10.1080/15567030903436830

Gomez-Maldonado D, Filpponen I, Hernandez-Díaz JA, et al (2021) Simple functionalization of cellulose beads with pre-propargylated chitosan for clickable scaffold substrates. Cellulose 28:6073–6087. doi: 10.1007/s10570-021-03905-8

Gomez-Maldonado D, Filpponen I, Johansson L, et al (2021) Environmentally dependent adsorption of 2,4-dichlorophenol on cellulose-chitosan self-assembled composites. Biopolymers 112:1–9. doi: 10.1002/bip.23434

Gumpert J, Material Connexion (2021) Bio-based vs. Biomaterial vs. Bioplastics // Material ConneXion

Hanhikoski S, Solala I, Lathinen P, et al (2016) Lignocellulosic nanofibrils from neutral sulphite pulps. 251st ACS National Meeting & Exposition, San Diego, USA

Harding KG, Dennis JS, von Blottnitz H, Harrison STL (2007) Environmental analysis of plastic production processes: Comparing petroleum-based polypropylene and polyethylene with biologically-based poly-β-hydroxybutyric acid using life cycle analysis. J Biotechnol 130:57–66. doi: 10.1016/j.jbiotec.2007.02.012

Haygreen JG, Bowyer JL (1989) Forest products and wood science: and introduction,

Second edition. Iowa State University Press, Iowa

Henriksson M, Henriksson G, Berglund LA, Lindström T (2007) An environmentally friendly method for enzyme-assisted preparation of microfibrillated cellulose (MFC) nanofibers. Eur Polym J 43:3434–3441. doi: 10.1016/j.eurpolymj.2007.05.038

Herrera M, Thitiwutthisakul K, Yang X, et al (2018) Preparation and evaluation of high-lignin content cellulose nanofibrils from eucalyptus pulp. Cellulose 25:3121–3133. doi: 10.1007/s10570-018-1764-9

Hestin M, Mitsios A, Said SA, et al (2017) Deloitte Sustainability - Blueprint for Plastics Packaging Waste: Quality Sorting & Recycling - Final report. 41

Hillis WE (1971) Distribution, properties and formation of some wood extractives. Wood Sci Technol 4:272–289

Hornus M, Via BK, Gallagher T, Peresin MS (2020) Partial substitution of pMDI with lignin containing cellulose nanofibrils: low density oriented strand board. Wood Mater Sci Eng 1–6. doi: 10.1080/17480272.2020.1769722

Hubbe MA, Ferrer A, Tyagi P, et al (2017) Nanocellulose in thin films, coatings, and plies for packaging applications: A review. BioResources 12:2143–2233

Hubbe MA, Rojas OJ (2008) Colloidal stability and aggregation of Lignocellulosic materials in aqueous suspension: A review. BioResources 3:1419–1491

Huber T, Starling K, Cen WS, et al (2016) Effect of Urea Concentration on the Viscosity and Thermal Stability of Aqueous NaOH / Urea Cellulose Solutions. 2016:

Hult EL, Iotti M, Lenes M (2010) Efficient approach to high barrier packaging using microfibrillar cellulose and shellac. Cellulose 17:575–586. doi: 10.1007/s10570-010-9408-8

Hult ELL, Larsson PT, Iversen T, et al (2001) Cellulose fibril aggregation - An inherent

property of kraft pulps. Polymer (Guildf) 42:3309–3314. doi: 10.1016/S0032-3861(00)00774-6

IAMA (2009) International Food and Agribusiness Management Review. Texas

IEA Bioenergy (2009) Biorefineries: adding value to the sustainable utilisation of biomass. In: Task 42 Bookl.

Iglesias MC, Gomez-Maldonado D, Via BK, et al (2020a) Pulping processes and their effects on cellulose fibers and nanofibrillated cellulose properties: A review. For Prod J 70:10–21. doi: 10.13073/FPJ-D-19-00038

Iglesias MC, Hamade F, Aksoy B, et al (2021a) Correlations between Rheological Behavior and Intrinsic Properties of Nanofibrillated Cellulose from Wood and Soybean Hulls with Varying Lignin Content. BioResources 16:4831–4845. doi: 10.15376/biores.16.3.4831-4845

Iglesias MC, McMichael PS, Asafu-Adjaye O, et al (2021b) Interfacial interactions between urea formaldehyde and cellulose nanofibrils (CNFs) of varying chemical composition and their impact on particle board (PB) manufacture. Cellulose 28:7969–7979. doi: 10.1007/s10570-021-04007-1

Iglesias MC, Shivyari N, Norris A, et al (2020b) The effect of residual lignin on the rheological properties of cellulose nanofibril suspensions. J Wood Chem Technol. doi: 10.1080/02773813.2020.1828472

Isogai A, Saito T, Fukuzumi H (2011) TEMPO-oxidized cellulose nanofibers. Nanoscale 3:71–85. doi: 10.1039/c0nr00583e

Israelachvili JN (2011) Intermolecular and surface forces. Academic press

Iwamoto S, Abe K, Yano H (2008) The effect of hemicelluloses on wood pulp nanofibrillation and nanofiber network characteristics. Biomacromolecules 9:1022–1026. doi: 10.1021/bm701157n

Jada SS (1988) The structure of urea—formaldehyde resins. J Appl Polym Sci 35:. doi: 10.1002/app.1988.070350614

Jiang Z-H (1997) Advances and applications of quantitative 31P NMR for the structural elucidation of lignin. McGill University

Karlsson RMP, Larsson PT, Hansson P, Wågberg L (2019) Thermodynamics of the Water-Retaining Properties of Cellulose-Based Networks. Biomacromolecules 20:1603–1612. doi: 10.1021/acs.biomac.8b01791

Kawamura S (1967) Quantitative paper chromatography of sugars of the cotyledon, hull, and hypocotyl of soybeans of selected varieties. 香川大学農学部学術報告

Klemm D, Heublein B, Fink HP, Bohn A (2005) Cellulose: Fascinating biopolymer and sustainable raw material. Angew Chemie - Int Ed 44:3358–3393. doi: 10.1002/anie.200460587

Kontturi EJ (2005) Surface chemistry of cellulose : from natural fibres to model surfaces. Technische Universiteit Eindhoven

Kontturi E, Tammelin T, Österberg M (2006) Cellulose—model films and the fundamental approach. Chem Soc Rev 35:1287–1304. doi: 10.1039/B601872F.

Lahtinen P, Liukkonen S, Pere J, et al (2014) A Comparative study of fibrillated fibers from different mechanical and chemical pulps. BioResources 9:2115–2127. doi: 10.15376/biores.9.2.2115-2127

Li R, Wang S, Lu A, Zhang L (2015) Dissolution of cellulose from different sources in an NaOH/urea aqueous system at low temperature. Cellulose 22:339–349. doi: 10.1007/s10570-014-0542-6

López-Esparza R, Balderas Altamirano MA, Pérez E, Gama Goicochea A (2015) Importance of molecular interactions in colloidal dispersions. Adv. Condens. Matter Phys.

Mahrdt E, Pinkl S, Schmidberger C, et al (2016) Effect of addition of microfibrillated cellulose to urea-formaldehyde on selected adhesive characteristics and distribution in particle board. Cellulose 23:571–580. doi: 10.1007/s10570-015-0818-5

Meakin P (1988) Models for Colloidal aggregations. Ann Rev Phys Chern 39:237–67

Medic J, Atkinson C, Hurburgh CR (2014) Current knowledge in soybean composition. JAOCS, J. Am. Oil Chem. Soc.

Meereboer KW, Misra M, Mohanty AK (2020) Review of recent advances in the biodegradability of polyhydroxyalkanoate (PHA) bioplastics and their composites. Green Chem 22:5519–5558. doi: 10.1039/d0gc01647k

Mielenz JR, Bardsley JS, Wyman CE (2009) Fermentation of soybean hulls to ethanol while preserving protein value. Bioresour Technol 100:. doi: 10.1016/j.biortech.2009.02.044

Mohnen D (2008) Pectin structure and biosynthesis. Curr. Opin. Plant Biol. 11:266–277

Monsoor MA (2005) Effect of drying methods on the functional properties of soy hull pectin. Carbohydr Polym 61:362–367. doi: 10.1016/j.carbpol.2005.06.009

Moon RJ, Martini A, Nairn J, et al (2011) Cellulose nanomaterials review: structure, properties and nanocomposites. Chem Soc Rev Chem Soc Rev 40:3941–3994. doi: 10.1039/c0cs00108b

Myers D (2002) Surfaces, Interfaces, and Colloids: Principles and Applications, 2nd Edition. Wyley-VCH, New York

Naimi LJ, Sokhansanj S, Bi X, Lim CJ (2016) Development of a Size Reduction Equation for Woody Biomass: The Influence of Branch Wood Properties on Rittinger's Constant. Am Soc Agric Biol Eng 59:1475–1484. doi: 10.13031/trans.59.11347

Nishiyama Y, Langan P, Chanzy H (2002) Crystal Structure and Hydrogen-Bonding

System in Cellulose I from Synchrotron X-ray and Neutron Fiber Diffraction. Dtsch Chem Ges 7:9074–9082. doi: 10.1021/ja0257319

O'Sullivan AC (1997) Cellulose: the structure slowly unravels. Cellulose 4:173–207. doi: Chemistry and Materials Science

Oksman K, Mathew AP, Bismarck A, et al (eds) (2014) Handbook of Green Materials, First edit. World Scientific, Singapore

Olszewska AM (2013) Interfacial forces in nanocellulose based composite materials. Aalto University

Orelma H, Filpponen I, Johansson LS, et al (2011) Modification of cellulose films by adsorption of cmc and chitosan for controlled attachment of biomolecules. Biomacromolecules 12:4311–4318. doi: 10.1021/bm201236a

Pääkko M, Ankerfors M, Kosonen H, et al (2007) Enzymatic hydrolysis combined with mechanical shearing and high-pressure homogenization for nanoscale cellulose fibrils and strong gels. Biomacromolecules 8:1934–1941. doi: 10.1021/bm061215p

Papadopoulos AN, Hill CAS, Traboulay E, Hague JRB (2002) Isocyanate resins for particleboard: PMDI vs EMDI. Holz als Roh - und Werkst 60:81–83. doi: 10.1007/s00107-001-0275-8

Patel P, Tullo A (2020) The future of plastic. c&en

Pettersen RC, Rowell RM (1984) The Chemical Compostition of Wood. In: Rowell R (ed) The chemistry of solid wood. American Chemical Society, Washington, pp 57–126

Philp J (2015) Balancing the bioeconomy: Supporting biofuels and bio-based materials in public policy. Energy Environ Sci 8:3063–3068. doi: 10.1039/c5ee01864a

Pinkert A, Marsh KN, Pang S (2010) Reflections on the solubility of cellulose. Ind Eng

Chem Res 49:11121–11130. doi: 10.1021/ie1006596

Plackett D V (ed) (2011) Biopolymers - New Materials for Sustainable Films and Coatings, First Edit. John Wiley & Sons, Ltd.

Popescu CM, Tibirna CM, Raschip IE, et al (2008) Bulk and Surface Characterization of Unbleached and Bleached Softwood Kraft Pulp Fibres. Cellul Chem Technol 42:525–547

Ratner BD, Hoffman AS, Schoen FJ, Lemons JE (2013) Biomaterials Science: An Introduction to Materials, Third Edit. Academic Press

Rehman MSU, Rashid N, Saif A, et al (2013) Potential of bioenergy production from industrial hemp (Cannabis sativa): Pakistan perspective. Renew Sustain Energy Rev 18:154–164. doi: 10.1016/j.rser.2012.10.019

Riegler M, Gindl-Altmutter W, Hauptmann M, Müller U (2012) Detection of UF resin on wood particles and in particleboards: potential of selected methods for practice-oriented offline detection. Eur J Wood Wood Prod 70:. doi: 10.1007/s00107-012-0628-5

Rojas MJ, Siqueira PF, Miranda LC, et al (2014) Sequential proteolysis and cellulolytic hydrolysis of soybean hulls for oligopeptides and ethanol production. Ind Crops Prod 61:. doi: 10.1016/j.indcrop.2014.07.002

Rojo E, Peresin MS, Sampson WW, et al (2015) Comprehensive elucidation of the effect of residual lignin on the physical, barrier, mechanical and surface properties of nanocellulose films. Green Chem 17:1853–1866. doi: 10.1039/C4GC02398F

Roy D, Berry E, Dempster DM (2021) “If it is not made easy for me, I will just not bother”. Barriers and Facilitators to Recycling Plastics. PsyArXiv. doi: 10.31234/OSF.IO/BKPQW

Sehaqui H, Kulasinski K, Pfenninger N, et al (2017) Highly Carboxylated Cellulose Nanofibers via Succinic Anhydride Esterification of Wheat Fibers and Facile Mechanical

Disintegration. Biomacromolecules 18:242–248. doi: 10.1021/acs.biomac.6b01548

Sixta H, Potthast A, Krotschek AW (2006a) Raw material for pulp. In: Sixta H (ed) Handbook of Pulp. WILEY-VCH Verlag GmbH &Co. KGaA, Weinheim, Lenzing Austria, pp 21–61

Sixta H, Potthast A, Krotschek AW (2006b) Chemical Pulping Processes. In: Handbook of Pulp. WILEY-VCHVerlag GmbH&Co., Lenzing Austria, pp 109–229

Sjöström E, Westermark U (1999) Chemical Composition of Wood and Pulps: Basic Constituents and Their Distribution. Analytical Methods in Wood Chemistry, Pulping, and Papermaking. Springer, Berlin, Heidelberg

Smook G (2016) Handbook for Pulp and Paper Technologists, 4th edn. TAPPI Press, Georgia

Solala I (2011) Mechanochemical reactions in lignocelluloseic materials. Dissertation, Aalto Universty

Solala I, Volperts A, Andersone A, et al (2012) Mechanoradical formation and its effects on birch kraft pulp during the preparation of nanofibrillated cellulose with Masuko refining. Holzforschung 66:477–483. doi: 10.1515/HF.2011.183

Spence KL, Venditti RA, Rojas OJ, et al (2011) A comparative study of energy consumption and physical properties of microfibrillated cellulose produced by different processing methods. Cellulose 18:1097–1111. doi: 10.1007/s10570-011-9533-z

Sun R, F. Sun X, Tomkinson J (2009) Hemicelluloses and Their Derivatives

Tardy BL, Mattos BD, Otoni CG, et al (2021) Deconstruction and Reassembly of Renewable Polymers and Biocolloids into Next Generation Structured Materials. Chem Rev. doi: 10.1021/acs.chemrev.0c01333

Tarrés Q, Ehman NV, Vallejos ME, et al (2017) Lignocellulosic nanofibers from triticale straw: The influence of hemicelluloses and lignin in their production and properties. Carbohydr Polym 163:20–27. doi: 10.1016/j.carbpol.2017.01.017

Tenhunen TM, Peresin MS, Penttilä PA, et al (2014) Significance of xylan on the stability and water interactions of cellulosic nanofibrils. React Funct Polym 85:157–166. doi: 10.1016/j.reactfunctpolym.2014.08.011

Thomas RJ (2009) Wood: Structure and Chemical Composition

Toba K, Yamamoto H, Yoshida M (2012) Mechanical interaction between cellulose microfibrils and matrix substances in wood cell walls induced by repeated wet-and-dry treatment. Cellulose 19:1405–1412. doi: 10.1007/s10570-012-9700-x

Trivedi P, Trygg J, Saloranta T, Fardim P (2016) Synthesis of novel zwitterionic cellulose beads by oxidation and coupling chemistry in water. Cellulose 23:1751–1761. doi: 10.1007/s10570-016-0939-5

Trygg J (2015) Functional Cellulose Microspheres For Pharmaceutical Applications

U.S. Department of Agriculture, Office of the Secretary, Drug Enforcement Administration, Food and Drug Administration (2016) Statement of Principles on Industrial Hemp

USDA 2019 Survey. In: https://quickstats.nass.usda.gov/results/5C031FE5-0931-3E14-A2AE-5C9B57901334

Väisänen T, Kilpeläinen P, Kitunen V, et al (2019) Effect of steam treatment on the chemical composition of hemp (Cannabis sativa L.) and identification of the extracted carbohydrates and other compounds. Ind Crops Prod 131:224–233. doi: 10.1016/j.indcrop.2019.01.055

Veigel S, Müller U, Keckes J, et al (2011) Cellulose nanofibrils as filler for adhesives:

Effect on specific fracture energy of solid wood-adhesive bonds. Cellulose 18:1227–1237. doi: 10.1007/s10570-011-9576-1

Veigel S, Rathke J, Weigl M, Gindl-Altmutter W (2012) Particle board and oriented strand board prepared with nanocellulose- reinforced adhesive. J Nanomater 2012:1–8. doi: 10.1155/2012/158503

Viswanathan MB, Park K, Cheng MH, et al (2020) Variability in structural carbohydrates, lipid composition, and cellulosic sugar production from industrial hemp varieties. Ind Crops Prod 157:112906. doi: 10.1016/j.indcrop.2020.112906

Wang C, Kelley SS, Venditti RA (2016) Lignin-based thermoplastic materials. ChemSusChem 9:770–783. doi: 10.1002/cssc.201501531

Wang S, Zhang Y, Abidi N, Cabrales L (2009) Wettability and Surface Free Energy of Graphene Films. Langmuir 25:. doi: 10.1021/la901402f

Xiong B, Zhao P, Hu K, et al (2014) Dissolution of cellulose in aqueous NaOH/urea solution: role of urea. Cellulose 21:1183–1192. doi: 10.1007/s10570-014-0221-7

Xu X, Liu F, Jiang L, et al (2013) Cellulose nanocrystals vs. Cellulose nanofibrils: A comparative study on their microstructures and effects as polymer reinforcing agents. ACS Appl Mater Interfaces 5:2999–3009. doi: 10.1021/am302624t

Yamane C, Aoyagi T, Ago M, et al (2006) Two different surface properties of regenerated cellulose due to structural anisotropy. Polym J 38:819–826. doi: 10.1295/polymj.PJ2005187

Yang S, Fu S, Li X, et al (2010) Preparation of salt-sensitive and antibacterial hydrogel based on quaternized cellulose. BioResources 5:1114–1125. doi: 10.15376/biores.5.2.1114-1125

Yang Y, Suh S (2015) Changes in environmental impacts of major crops in the US. Environ Res Lett 10:094016. doi: 10.1088/1748-9326/10/9/094016

Yi H, Puri VM (2012) Architecture-Based Multiscale Computational Modeling of Plant Cell Wall Mechanics to Examine the Hydrogen-Bonding Hypothesis of the Cell Wall Network Structure Model. Plant Physiol 160:1281–1292. doi: 10.1104/pp.112.201228

Yoo J, Alavi S, Vadlani P, Amanor-Boadu V (2011) Thermo-mechanical extrusion pretreatment for conversion of soybean hulls to fermentable sugars. Bioresour Technol 102:. doi: 10.1016/j.biortech.2011.04.092

Young RA (1994) Comparison of the properties of chemical cellulose pulps. Cellulose 1:107–130. doi: 10.1007/BF00819662

Zhou J, Zhang L (2000) Solubility of cellulose in NaOH Urea.pdf. 32:866–870

Zhu JY, Agarwal UP, Ciesielski PN, et al (2021) Towards sustainable production and utilization of plant-biomass-based nanomaterials: a review and analysis of recent developments. Biotechnol Biofuels 14:1–32. doi: 10.1186/s13068-021-01963-5

2. Research Objectives

2.1. General objectives

Traditionally, the primary objective of pulping processes has been to isolate the different chemical components present in lignocellulosic bioresources to gain better access to them, primarily trying to keep the cellulose fibers intact while also eliminating lignin and hemicelluloses. Nevertheless, the emergence of bio-based nanotechnology, and increased concern about the environmental impact of the pulping processes on the raw materials, has created a need for a more in-depth analysis and understanding of their effects on the cellulose fibers (Iglesias et al. 2020a).

Additionally, there has been a tendency for research focus on the utilization of purely bleached cellulose pulps to produce cellulose nanofibers (CNFs). Thus, involving extra bleaching steps that require the utilization of chemicals, and therefore, an impact on the properties of the fibers. Recently, researchers have started looking into the alternative of utilizing lignin-containing cellulose nanofibrils (LCNFs), and taking advantage of the characteristics that residual lignin and hemicelluloses can confer to the nanocellulose performance (Solala et al. 2019).

It is well known that nanocellulose suspensions are materials in which particles in the nanoscale are embedded in a liquid media. The characteristics of these colloidal suspensions will be determined by the chemical composition of the solid particles, the media, and the interfaces between them (López-Esparza et al. 2015). Chapter 1 of the dissertation is a literature review focused on the interfacial interactions between different chemical components in lignocellulosic materials. The review is centered to not only consider the chemical bonds and electrostatic interactions in each component but also the interactions and affinities between them (PAPER I). Additionally, the nature of the raw material (i.e., where the fibers came from), as well as the

processes used to produce the nanofibers, will dictate the properties of the colloidal suspensions, and will influence their performance when handling and processing, mainly their viscoelastic properties (PAPER II). Thus, Chapter 3 has been centered on studying bleached and unbleached CNFs from soybean hulls and wood. The effect of raw materials and chemical composition on their characteristics, such as charge density, morphology, and crystallinity, was discussed and related to the viscoelastic properties of the suspensions.

Among the essential intrinsic properties of lignin, their rheological behavior can dictate the viability of utilizing this material for different applications. Rheology, study the deformation and flow of materials when an external force is applied and permits inferring the aqueous suspensions microstructure to correlate it with the intrinsic properties of the material. Thus, Chapter 4 is center on the rheological study of four different softwood LCNFs samples with lignin contents from <0.1 to 16.8% (PAPER III).

To better understand how the intrinsic properties of the nanocellulose can be related to the final performance of the material, in Chapter 5 the behavior of bleached and unbleached CNFs at the interface with resins for wood panel composites (PAPER IV) was studied. We observed an improvement of the properties of the panels by using unbleached CNF, which was corresponded with the interaction at the interface and with the reduction of the surface free energy due to the more hydrophobic nature of the samples containing lignin.

Finally, in Chapter 6 as a future work, it was proposed to elucidate the effect of lignin on the mechanical treatment of cellulose pulps, studying the scavenging ability of lignin on wood samples with a large variation in lignin content. This idea arose from the fact that when producing nanocellulose out of cellulose pulp by mechanical treatments, activation energy is generated on the cellulose fibers, allowing the chain to break (Hon 1983) and it has been suggested in the

literature that LCNF presents a better defibrillation (i.e., small fibers diameters) due to the presence of lignin (Rojo et al. 2015). This theory is supported by the antioxidant property of lignin, which can stabilize the cellulosic mechanoradicals formed during the mechanical process (Solala et al. 2012). As an additional topic within this work, and since some radicals can recombine in a short period of time, we propose to study the most unstable radicals (i.e., those generated as soon as the samples were produced), and the radicals remaining on the specimens after ten days.

2.2. Objectives for each chapter

Chapter 1:

i. To research about the published literature regarding interfacial interactions between the chemical components presented in lignocellulosic materials.

Chapter 2:

i. To define the research objectives and the hypothesis of the work

Chapter 3:

i. To produce CNF suspensions from wood and soybean hulls fibers
ii. To fully characterize the produced CNFs
iii. To correlate the intrinsic properties of wood and soybean CNF, with their viscoelastic performance

Chapter 4:

i. To produced cellulose pulps from softwood with different chemical composition in controlled conditions
ii. To produce LCNFs and fully characterize them

iii. To deeply understand the viscoelastic properties of wood LCNF suspensions, with a large variation in lignin content, and to correlate their viscoelasticity with the additional intrinsic properties

Chapter 5:

i. To produce CNF suspensions from wood with different chemical composition

ii. To fully characterize the produced CNFs

iii. To study the interfacial interactions between wood resins and CNFs with different chemical compositions

iv. To correlate the interfacial interactions between the adhesive and the CNFs with the final performance of particleboards.

Chapter 6:

i. To analyze the scavenging ability of lignin and how its presence improve the defibrillation of the fibers when producing LCNF suspensions

ii. To quantify the free radicals generation during the production of LCNF fibers

iii. To correlate the scavenging ability of lignin for each sample with its intrinsic properties

2.3. Hypothesis

i. Raw material is the main characteristic affecting CNF properties

ii. Functional groups present in lignin will improve the interfacial interactions between CNF and wood-based adhesives.

iii. Chemical composition on wood CNFs will directly affect the viscoelastic properties of CNFs suspensions

iv. Due to lignin scavenging ability, unbleached cellulose fibers are more manageable to

defibrillate than their bleached counterpart.

2.4. Literature cited

Abbati de Assis C, Houtman C, Phillips R, et al (2017a) Conversion Economics of Forest Biomaterials: Risk and Financial Analysis of CNC Manufacturing. Biofuels, Bioprod Biorefining 11:682–700. doi: 10.1002/bbb.1782

Abbati de Assis C, Iglesias MC, Bilodeau M, et al (2017b) Cellulose micro- and nanofi brils (CMNF) manufacturing - financial and risk assessment. Biofuels, Bioprod Biorefining 12:251–264. doi: 10.1002/bbb.1835

Hon DNS (1983) Mechanochemical reactions of lignocellulosic materials. In: J. Appl. Polym. Sci.: Appl. Polym. Symp. United States

Iglesias MC, Gomez-Maldonado D, Via BK, et al (2020a) Pulping processes and their effects on cellulose fibers and nanofibrillated cellulose properties: A review. For Prod J 70:10–21. doi: 10.13073/FPJ-D-19-00038

Iglesias MC, Hamade F, Aksoy B, et al (2021a) Correlations between Rheological Behavior and Intrinsic Properties of Nanofibrillated Cellulose from Wood and Soybean Hulls with Varying Lignin Content. BioResources 16:4831–4845. doi: 10.15376/biores.16.3.4831-4845

Iglesias MC, McMichael PS, Asafu-Adjaye O, et al (2021b) Interfacial interactions between urea formaldehyde and cellulose nanofibrils (CNFs) of varying chemical composition and their impact on particle board (PB) manufacture. Cellulose 28:7969–7979. doi: 10.1007/s10570-021-04007-1

Iglesias MC, Shivyari N, Norris A, et al (2020b) The effect of residual lignin on the rheological properties of cellulose nanofibril suspensions. J Wood Chem Technol. doi: 10.1080/02773813.2020.1828472

López-Esparza R, Balderas Altamirano MA, Pérez E, Gama Goicochea A (2015)

Importance of molecular interactions in colloidal dispersions. Adv. Condens. Matter Phys.

Rojo E, Peresin MS, Sampson WW, et al (2015) Comprehensive elucidation of the effect of residual lignin on the physical, barrier, mechanical and surface properties of nanocellulose films. Green Chem 17:1853–1866. doi: 10.1039/C4GC02398F

Solala I, Iglesias MC, Peresin MS (2019) On the potential of lignin-containing cellulose nanofibrils (LCNFs): a review on properties and applications. Cellulose 27:1853-1877. doi: 10.1007/s10570-019-02899-8)

Solala I, Volperts A, Andersone A, et al (2012) Mechanoradical formation and its effects on birch kraft pulp during the preparation of nanofibrillated cellulose with Masuko refining. Holzforschung 66:477–483. doi: 10.1515/HF.2011.183

Villada Y, Iglesias MC, Casis N, et al (2018) Cellulose nanofibrils as a replacement for xanthan gum (XGD) in water based muds (WBMs) to be used in shale formations. Cellulose 25:7091–7112. doi: https://doi.org/10.1007/s10570-018-2081-z(0123456789().,-volV()0123456789().,-volV)

Villada Y, Iglesias MC, Olivares ML, et al (2020) Di-carboxylic acid cellulose nanofibril (DCA-CNF) as an additive in water-based drilling fluids (WBMs) applied to shale formations. Cellulose. doi: 10.1007/s10570-020-03502-1

3. Correlations between rheological behavior and intrinsic properties of nanofibrillated cellulose from wood and soybean hulls with varying lignin content

This chapter has been published in "Iglesias, M. C., Hamade, F., Aksoy, B., Jiang, Z., Davis, V. A., & Peresin, M. S. (2021). Correlations between rheological behavior and intrinsic properties of nanofibrillated cellulose from wood and soybean hulls with varying lignin content. *BioResources*, 16(3), 4831"

3.1. Abstract

Effects of raw material and chemical composition were considered relative to the intrinsic properties and the rheological behavior of nanofibrillated cellulose aqueous suspensions (CNFs). Atomic force microscopy, Fourier-transform infrared spectroscopy, surface chemistry analysis, thermal gravimetrical analysis, and zeta-potential were used to study the morphology, chemical composition, charge density, as well as thermal and colloidal stability of the different CNFs. Regarding the rheological properties of the samples, steady-state and oscillation studies of the CNF aqueous suspensions obtained from wood and soybean hulls were performed. An interesting correlation was found between the rheological behavior of CNF suspensions and their intrinsic properties. Soybean CNF presented lower viscosities than wood samples, which could be related to their morphology and charge density. Additionally, unbleached soybean CNF (sb-LCNF) showed yield stress compared with the other samples, which could be attributed to the presence of pectin. Furthermore, the different chemical compositions between the samples affected their thermal properties, as well as on their crystallinity.

3.1.1. Index words

Lignin-containing cellulose nanofibrils; LCNFs; Rheology; Residual lignin; Ligno-nanofibers; Cellulosic nanofibers; Soybean hulls; Soybean cellulose nanofibrils

3.1.2. Project partners

The Forest Products Development Center worked in collaboration with the Department of Chemical Engineering, Samuel Ginn College of Engineering and the Alabama Center for Paper and Bioresource Engineering, from Auburn University.

This work was supported by the USDA National Institute of Food and Agriculture, Hatch program (ALA013-17003) and McIntire-Stennis program (1022526). The School of Forestry and Wildlife Sciences at Auburn University's financial support to complete this work is much appreciated.

3.2. Introduction

Over the last decade, the utilization of nanocellulose for novel applications, such as stabilizers for Pickering emulsions, 3D printing, carriers for drug delivery, and packaging have positioned this renewable source as a promising alternative substitution for petroleum-based materials (Hubbe *et al.* 2017a). Nanocellulose is well known for being obtained through the isolation of cellulose fibers and transformed to the nanoscale by chemical and/or mechanical treatments. Furthermore, nanocellulose has shown remarkable properties such as the aspect ratio, low density, and its ability to be chemically modified (Klemm *et al.* 2011).

Although commercial nanocellulose is mainly isolated from wood sources, over the years different resources have been found as alternatives for nanocellulose production. This opens the possibility of conferring value to side streams of agroindustry that were often considered

underutilized waste streams. Banana (Tarrés *et al.* 2017) and pineapple leaves (Deepa *et al.* 2015), sugarcane bagasse (Feng *et al.* 2018), lotus leaf stalks (Chen *et al.* 2015), jute (Ahuja *et al.* 2018), cotton (Sangeetha *et al.* 2019), corn stover (Xu *et al.* 2018), waste from the agave plant (Palacios Hinestroza *et al.* 2019) and pomelo peel (Tang *et al.* 2020b), are some of the alternative raw materials presented on the literature.

Soybean is one of the most relevant agricultural sources in the United States (US). Within its composition, soybean contains proteins, oils, carbohydrates, and ash in the amount of 40, 21, 34, and 4%, respectively (Kawamura 1967). In 2019, the US was reported as the second leading worldwide soybean producer with 27% of the total production (FAOSTAT 2019). During the same year, 64.7% of this production was crushed to extract the oil contained in the seed (USDA 2019), giving little commercial value to the remaining fibrous material named soybean hulls. This by-product is also known as seed coat and is mainly utilized as a fiber source for cattle (Hult *et al.* 2010).

Due to their availability and their chemical composition versatility, several researchers have focused on utilizing soybean fibers as a source for nanocellulose production. Efforts to extract fibrous materials from soybean hulls has also been driven by efforts to increase the value of this waste material (Debiagi *et al.* 2020).

Debiagi *et al.* (2020) obtained nanofibrillated cellulose, which is also known as cellulose nanofibrils (CNFs) by reactive extrusion followed by bleaching of the soybean hulls and studied how this process affected the properties of the nanofibers with respect to the original soybean fibers. Additionally, Li *et al.* (2019) studied the effect of alkaline and acidic pretreatments on the fiber properties, corroborating how their properties can be altered depending on the extraction/purification methods. Similarly, Ferrer *et al.* (2016) characterized microfibers and

microparticles obtained from soybean utilizing mechanical and chemical processes and compared their properties with CNF obtained from fully bleached cellulose pulp. Due to their abundance and versatility, soybean hull-based CNFs have recently been utilized in the development of novel applications such as in feed binders and in gas detectors for food spoilage and ripening (Aksoy *et al.* 2020).

This work focused on comparing the effect of the chemical composition of soybean hulls and wood fibers on the rheological behavior of bleached and unbleached nanocellulose suspensions. Rheology provides a useful assessment of differences between materials, since properties vary with concentration, material structure, and interactions that are affected by surface chemistry. In addition, the materials were characterized by atomic force microscopy (AFM) to determine structure and dimensions, X-ray diffraction (XRD) for crystal structure, Fourier-transform infrared spectroscopy (FTIR) for chemical composition, surface charge for charge density, and thermogravimetric analysis (TGA) for thermal stability. These techniques provide insight into the materials' morphology and resulting microstructure.

3.3. Experimental

3.3.1. Materials

Never-dried hardwood kraft pulps: i) bleached (lignin content of < 0.1 %), and ii) unbleached (lignin content of 2.25%) were kindly provided by a US mill. Soybean hulls were provided by Republic Mills, Inc., of Okolona, Ohio. Fibers from the soybean hulls were extracted as described in Alemdar and Sain (2008). Additionally, one portion of the material was bleached following a conventional Elemental Chlorine Free (ECF) bleaching sequence (D_0EpD_1), where the first and third steps used sodium chlorite ($NaClO_2$) and the second step was a hydrogen peroxide

(H_2O_2) supplemented alkaline extraction process utilizing sodium hydroxide (NaOH). Details of the bleaching process are as follows; first, $NaClO_2$ was incorporated into the fibers at 5 wt% and kept at 70 °C for 1 hour at a pH of 2.8. Second, H_2O_2 supplemented alkaline extraction was performed on the fibers at 4 wt.%, adding NaOH until pH was 10.5 and left for 2 hours at 80 °C. Finally, $NaClO_2$ was added to the fibers at 2 wt.% and maintained at 70 °C for 1 h at a pH of 2.8. Unless clarified in the text, all the concentrations in the text are expressed on a dry mass basis.

For charge density measurements, 0.01 N polydiallyldimethylammonium chloride (Poly-DADMAC, sample #920) and 0.01 N polyvinylsulfuric acid potassium salt (PVSK, sample #919) were purchased from BTG Americas Inc. A low viscosity silicon oil (Brookfield 1000, 980 cp) purchased from Brookfield Engineering Laboratories, Inc., was used to seal the sample edge for ensuring no solvent evaporation during rheological measurements.

3.3.2. Methods

3.3.2.1. CNF production

Prior to the defibrillation process, suspensions containing 2.0 wt.% of the fibers mentioned above were prepared using deionized water. The suspensions were then subjected to mechanical defibrillation using a Masuko supermasscolloider MKZA10-15J IV (Masuko Sangyo Co., Ltd., Japan), passing them ten times between one stationary and one rotating stone. The same procedure was performed for both kraft and soybean fibers. After the mechanical treatment, a ~2.0 wt% cellulose nanofibril with a gel-like consistency was obtained. For this work, the abbreviations BCNF and LCNF correspond to bleached and unbleached cellulose nanofibrils, respectively. Additionally, the prefixes w- and sb- have been utilized to indicate the raw materials wood and soybean, respectively. For example, sb-BCNF represents bleached cellulose nanofibrils made from soybean. The materials studied in this work are sb-BCNF, sb-LCNF, w-BCNF, and w-LCNF.

3.3.2.2. Characterization of CNF suspensions

i. Dry content, pH, and surface charge

Dry content of the samples was measured following TAPPI Standard T550 om-08. Measurements were performed by triplicate, and the results were averaged. Equation 3.1 was utilized for the calculations of moisture content as:

$$MC\% = \frac{mass_{wet} - mass_{dry}}{mass_{dry}} \times 100\% \quad (3.1)$$

Then, the dry content was calculated as the difference between 100% and the MC% value. The pH of the CNF suspensions was assessed by using a VWR® SympHony Benchtop Multiparameter Meter B30PCI. Samples were measured with 15 runs, with the average calculated and reported. The charge density of the nanofibers was measured using a Chemtrac Lab Charge Analyzer (Chemtrac Systems Inc., Model LCA01, USA), following a protocol adapted from Carrasco *et al.* (1998). Negatively charged CNF suspensions were prepared at 0.04 wt.% consistency in ultrapure water. Samples were placed in an ice bath, where they were sonicated for 10 min using a Sonics Vibra Cell Sonicator (Sonics & Materials, Inc., Newton, CA, Model VC750). Subsequently, 25 mL of 0.01 N polyDADMAC was mixed with 15 mL of CNF suspension, and the mixture was centrifuged at 3000 rpm for 15 min in an Eppendorf Centrifuge 5415R (Eppendorf AG, Hamburg). After centrifugation, 10 mL of the supernatant was analyzed in the charge analyzer using the anionic polymer 0.01 N PSVK as the titrant. Charge density was measured with 6 runs and calculated using equation 3.2 (Carrasco *et al.* 1998),

$$Charge\ density = \frac{(C * V_c - A * V_A)}{W} \quad (3.2)$$

where C is the concentration of the cationic polymer polyDADMAC, V_C is the volume of polyDADMAC, A is the concentration of the anionic polymer (PVSK), V_A is the volume of PVSK, and W is the weight of CNF that is consumed to reach a streaming current value (SCV) equal to zero.

ii. Chemical composition

The chemical composition of the nanofiber suspensions was analyzed by Fourier-transform infrared spectroscopy with attenuated total reflectance accessory (ATR-FTIR). This was performed using a Perkin Elmer Spotlight 400 FTIR imaging system equipped with deuterated triglycine sulfate DTGS detector and built-in ATR module with a germanium crystal. All spectra were recorded over the spectral range from 4000 to 400 cm^{-1} at room temperature and after 64 scans.

iii. Thermal behavior

The thermal stability of the samples was assessed by thermogravimetric analysis (TGA) with a TGA-50 from Shimadzu (Kyoto, Japan) using nitrogen as a sweep fluid at a flow rate of 20 mL/min. The samples were placed in aluminum pans and heated from 10 to 600 °C at a heating rate of 10 °C/min. About 15 mg of each sample was analyzed with measurements performed in duplicate. The data was processed with the Shimadzu TA60 software (version 2.11).

iv. Morphology

The morphology of the cellulose nanofibers was investigated by atomic force microscopy (AFM) utilizing an Anton Paar TOSCA^{TM} 400 AFM (Graz, Austria). The images were obtained with a silicon cantilever in tapping mode, and the scan size area was set at 3x3 µm. Data visualization and analysis was performed with Gwyddion open software (Source Forge, Version

2.49). For AFM imaging, before the CNF deposition, silicon surfaces were cleaned using UV ozone for 30 min and submerged for 15 min into 0.1 wt% polyethylenimine (PEI), which was used as an anchoring solution. CNF suspensions were prepared at 0.01 wt.% and placed in a cold bath to avoid sample heating while sonicating using a Vibra Cell sonicator (Newtown, CA) for 10 min with 20 kW and 25 % amplitude to promote delamination and prevent their agglomeration. Then, 80 µL of suspension was spin coated onto the PEI-silicon at 3200 rpm for 1 min. Surfaces were placed in the oven at 80 °C for 20 min and stored in a desiccator until use.

v. Crystallinity

X-ray powder diffraction (XRD) was performed using a 1-Dimension Bruker AXS D8 Discover equipped with a LYNXE detector and Cu Kα irradiation. Measurements were performed at a continuous scan speed of 0.1 second/step, from 5 to 90 degrees. Data was acquired using the DiffracPlus Eva version 13.0.0.3 by Bruker. The crystallinity index (CI) was calculated utilizing Segal's method, defined by equation 3.2 (Segal *et al.* 1959):

$$CI = \frac{I_{002} - I_{Am}}{I_{002}} \tag{3.3}$$

vi. Rheological behavior

Rheological properties of the prepared bleached and unbleached CNF from soybean and hardwood sources were measured at 25 °C using an Anton Paar Physica MCR301 (Graz, Austria) strain-controlled rotational rheometer. Prior to the measurements, 2.0 wt% dispersions were tip-sonicated, and then allowed 3 h of relaxation before loading onto the rheometer. Rheological measurements were primarily performed on 25 mm diameter parallel plates. Some tests were repeated using other geometries to ensure that there were no artifacts in the data. All tests were

performed with a silicon oil coating along the edge of the fixture and a solvent trap of deionized water to prevent water loss during testing. After loading the sample on the rheometer, the sample was allowed to equilibrate for 10 min before investigation of rheological properties. A preliminary shear protocol using a shear rate of 0.001 s^{-1} for 20 min was used to further reduce artifacts from shear induced microstructural changes during sample loading. The dispersion microstructures were investigated with oscillatory shear measurements, where amplitude sweeps were used to determine the linear viscoelastic region (LVR). Then, frequency sweeps were performed at 0.2 % strain (within the LVR) to measure the storage (*G*') and loss (*G*") moduli as a function of angular frequency (ω). Steady shear viscosity tests were then performed to investigate the effect of shear on the structures. Constant shear step rate tests were performed to determine the time for samples to reach a steady viscosity, which was then used for the flow curves. Flow curves were performed to determine the dependence of steady shear viscosity η on shear rate $\dot{\gamma}$.

3.4. Results and discussion

3.4.1. Characterization of CNFs Suspensions

3.4.1.1. Lignin content, dry content, pH, and surface charge

The main components of soybean hulls are cellulose (39.7%), hemicellulose (25.5%), pectin (12.7%), lignin (9.1%), proteins (13.1%), and ash (0.6%) (Cassales *et al.* 2011). Nevertheless, after chemical treatment of the hulls to obtain fibers, these components are partially eliminated, while only cellulose, hemicelluloses, pectin, and lignin remain (Alemdar and Sain 2008). For wood as a raw material, the main components for hardwood samples are cellulose (41.0%), hemicellulose (29.8%), lignin (22.0%), and extractives (3.2%) (Sjostrom *et al.* 1993). Like soybean hulls, after the pulping process of wood to obtain cellulose fibers, the chemical

composition changes due to the partial elimination of some components (Smook 2016). It is worth mentioning that the differences in the chemical composition of the starting materials will be translated to differences in the nanocelluloses fibers made thereof. Table 3.1 shows the lignin content, dry content, pH, and charge density data for the set of samples utilized in this work.

As shown in Table 3.1, sb-LCNF showed the highest value of charge density. To corroborate the differences of the mean between the samples, a statistical analysis with ANOVA was performed. By performing a Tukey test, the charge density for sample sb-LCNF was confirmed to be significantly different from the rest of the specimens. However, the other three were not significantly different. The high charge density on the sb-LCNF could be attributed to the presence of pectin in the sample. Furthermore, the charge density of the wood CNFs was smaller than sb-LCNF and slightly greater than sb-BCNF. These discrepancies may be attributed not only to the presence of pectin in the sb-LCNF sample but also to the effect of the chemical treatments on the surface of the wood fibers. It is known that during kraft pulping, free phenolic hydroxyl groups are formed, together with lignin-carbohydrate complexes (Iglesias *et al.* 2020a), which modify the properties of the fibers.

Table 3.1. Lignin Content, Dry Content, pH, and Charge Density

Property	**Unit**	**w-BCNF**	**w-LCNF**	**sb-BCNF**	**sb-LCNF**
Lignin content	%	<1*	2.3*	<1**	~2.5**
Dry Content	wt.%	1.9 ± 0.0	2.0 ± 0.0	2.0 ± 0.0	2.1 ± 0.0
pH	-	6.1 ± 0.0	6.1 ± 0.0	6.0 ± 0.0	6.0 ± 0.0
Charge density	µeq/gr	206.1 ± 10.0	206.7 ± 6.0	191.1 ± 43.5	310.0 ± 24.1

*Lignin content was estimated from the Kappa number provided in the datasheet.

**Lignin content was estimated from Alemdar and Sain 2008.

3.4.1.2 Thermal behavior

The thermal behavior of the samples is presented in Figure 3.1. The corresponding T_{onset} and T_{max} values of all the samples are summarized in Table 3.2, where T_{onset} refers to the initial visually apparent inflection mass decrease and T_{max} refers to the temperature corresponding to the maximum in the derivative peak. Analysis of the graphs shows that T_{onset} is around 346 °C for wood samples, while for soybean samples this temperature increases to approximately 361 °C. The derivative peaks convey that the values of T_{max} were equivalent; the actual values of 406.5 °C and 408.5 °C are within the instrument error. Cellulose and hemicelluloses present degradation temperature ranges between 315-400 °C and 220-315 °C, respectively (Yang *et al.* 2007). This explains the peak breadth for all four samples. Regarding the wood nanofibers, the w-LCNF mass loss derivative curve shows an additional small peak between 200 and 250 °C. This is attributed to lignin degradation; it has been reported that due to its complex composition, lignin decays in a range of temperatures from 200 to over 500 °C (Brebu and Vasile 2010). Alemdar and Sain (2008), reported that untreated soybean hull fibers start to decompose at 209 °C, while the nanofibers produced from those fibers have a notably higher decomposition temperature of 290 °C.

Table 3.2. T_{onset} and T_{max} Temperatures for Wood and Soybean CNFs

Suspension	**w-BCNF**	**w-LCNF**	**sb-BCNF**	**sb-LCNF**
$\boldsymbol{T_{onset}}$ **(°C)**	346.0	346.8	361.0	361.0
$\boldsymbol{T_{max}}$ **(°C)**	406.5	406.5	408.5	408.5

In the set of nanocellulose samples, greater thermal stability was observed for soybean CNFs compared with wood CNFs. These results are in accordance with the data reported by Ferrer *et al.* (2016), where the decomposition temperature for soybean CNF was 305 °C while for bleached CNF from wood, it occurred at 282 °C. The amount of hemicelluloses in hardwood CNFs

with similar characteristics to those presented in this work, has been reported to be between 19.2% and 18.4% (Iglesias *et al.* 2020b). In contrast, utilizing the extraction method proposed by Alemdar and Sain (2008), the CNFs from soybean hulls contained only 3.5% of hemicelluloses after the alkali and acidic treatment. As a result, the lower thermal stability for wood CNFs can be attributed to the higher amount of hemicelluloses in these samples that have a low degradation temperature compared to the other components.

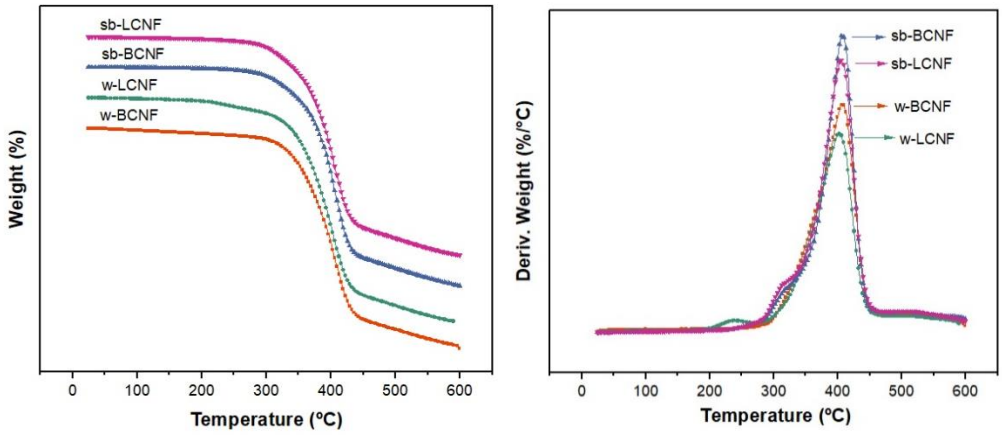

Figure 3.1. TGA curves in nitrogen atmosphere including weight (%) and the derivative weight (%/ºC) of the set of nanocellulose samples as indicated in the plots.

3.4.2.3. Chemical composition

As can be observed in Figure 3.2 in the region between 4000 and 3250 cm^{-1}, the FTIR spectra are dominated by the peaks at 3335 cm^{-1} reflecting the aromatic and aliphatic stretching vibrations for O-H groups, which is consistent with spectra previously reported (Alemdar and Sain 2008; Tang *et al.* 2020a). Additionally, in the range between 2922 and 2855 cm^{-1}, the bands correspond to stretching vibrations of CH_3, CH_2, and CH (Debiagi *et al.* 2020).

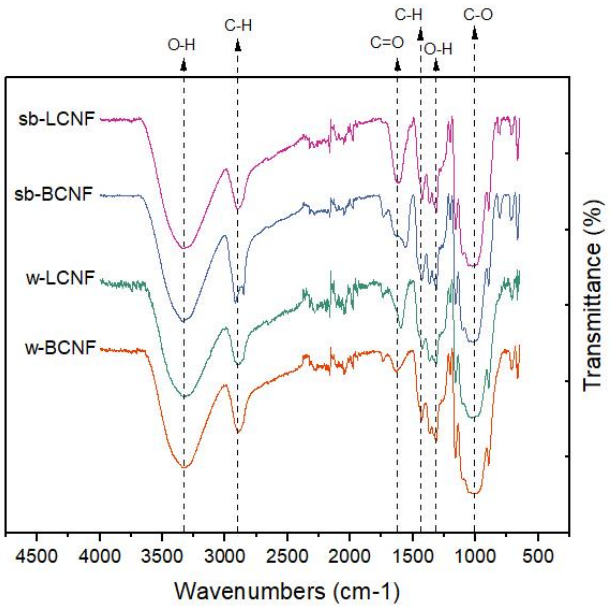

Figure 3.2. FTIR spectra of samples (from top to bottom) sb-LCNF, sb-BCNF, w-BCNF, and w-LCNF.

At 1604 cm^{-1} there is a peak for the sb-LCNF sample, which is assigned to C=O stretching vibrations corresponding to carboxylic groups. As described by Alemdar and Sain (2008), this peak can be related to the absorption of water. Its intensity decreases for sb-BCNF due to the partial removal of hemicelluloses during the bleaching process. The differences in relative peak intensities among the different samples can be attributed to the different initial chemical compositions of the raw material and the strength of the chemical treatment utilized to obtain the nanofibers. The absorption peaks at 1430 and 1319 cm^{-1} result from CH_2 and O-H deformations, respectively (Larkin 2011). Additionally, the shoulder at 1240 cm^{-1} corresponds to bending vibrations from O-H, C-H, and CH_2. Finally, the high-intensity peak at 1026 cm^{-1} observed in all samples is attributed to C-O stretching vibrations from polysaccharides and lignin, confirming the presence of the latter on the samples.

3.4.2.4. Crystallinity

X-ray powder diffraction (XRD) was used to measure the crystallinity of nanocellulose samples. Crystallinity is affected by both the crystallinity of the precursor material and the chemical treatment utilized to produce the samples (Ferrer *et al.* 2016). All the samples exhibited a major peak at a 2θ value between 21.5° and 22.5°, and a smaller peak around 15.5°. Data were normalized and presented in Figure 3.3. Results showed that w-BCNF and w-LCNF had a CI of 40.42 ± 0.01% and 46.14 ± 0.03%, respectively. Additionally, the CI for soybean samples was 54.07 ± 0.01% and 48.09 ± 0.01% for sb-BCNF and sb-LCNF, respectively. Based on the obtained data, soybean CNFs had a higher crystallinity than wood CNFs. The present results are in agreement with those reported by Ferrer *et al.* (2016). Comparing the CNFs from both sources, the differences in crystallinity for soybean and wood nanofibrils could be also attributed to the preparation process, which may produce heavier damage to the supramolecular structure of the wood fibers, thus decreasing their crystallinity. This can be correlated in the following section with the morphology of the samples.

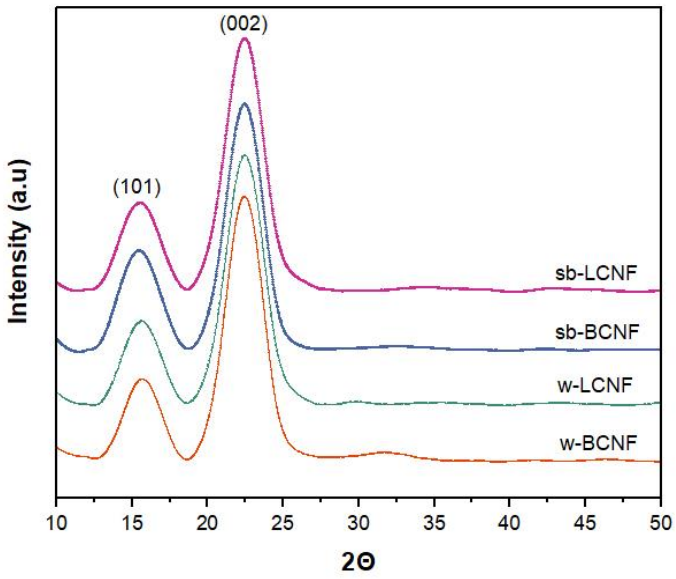

Figure 3.3. XRD spectra of samples (from bottom to top) w-BCNF, w-LCNF, sb-BCNF, and sb-LCNF. (Data acquired by Dr. Ann Norris, Virginia Tech)

Additionally, the present crystallinity results were in accordance with the findings obtained in the thermal analysis discussed in the previous sections, where larger degradation temperatures can be related to larger crystallinity of the samples due to the increase in cellulose content (Espinosa *et al.* 2017; Debiagi *et al.* 2020; Yuan *et al.* 2021).

Regarding the soybean CNFs, the higher CI of sample sb-BCNF compared with sb-LCNF is related to the reduction of lignin, hemicelluloses, and pectin content, which are the components that contribute to the amorphous or non-crystalline material (Espinosa *et al.* 2017). With regards to the wood samples, the w-BCNF shows a lower crystallinity than w-LCNF, even when the latter contains lignin and hemicelluloses. A disadvantage of the chemical process necessary to bleach the wood sample is the possibility of degrading and damaging the samples, which reduces their crystallinity (Debiagi *et al.* 2020).

3.4.2.5. Morphology

The morphology of the samples was analyzed by AFM, and the topographic images are presented in Figure 3.4. CNF from wood had a greater amount of fibril bundles when compared with CNF from soybean hulls. The AFM images suggest heterogeneous samples, containing both thick and long microfibril and microparticle bundles as well as a network of very fine irregular fibrils. CNFs from soybean hulls seem to be thicker and shorter than the CNFs from wood. Nevertheless, a broader understanding of the morphology of the samples will be discussed in depth in the rheological behavior of the suspensions. As mentioned in the previous section, the morphology of the samples could be also related to their crystallinity. CNFs from soybean hulls present thicker structures than CNFs from wood. It is possible that during the production process, soybean fibers suffered less damage than wood fibers, which could be the reason for the higher crystallinity of sb-CNFs.

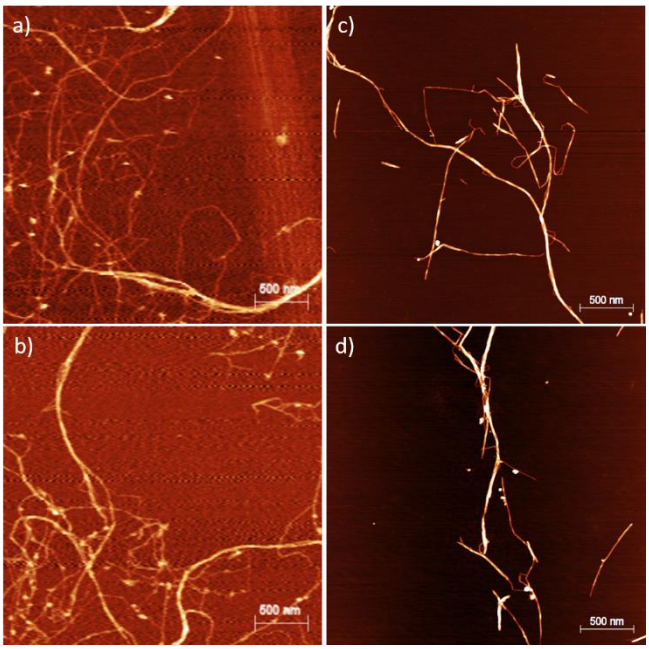

Figure 3.4. AFM topographic microscopies, of a) w-BCNF, b) w-LCNF, c) sb-BCNF, and d) sb-LCNF. With image size of 3µm x 3µm and scale bar of 500 nm.

3.4.2.6. Rheological behavior

The rheological behavior of dispersions of all wood and soybean CNFs dispersions was determined. Rheology is a bulk measurement method that is sensitive to solid content, charge density, pH, and morphology (Macosko 1994). The CNFs from wood showed a viscosity ten times larger than that corresponding to soybean CNFs. The sb-LCNF had the lowest shear viscosity value. The reduction in viscosity could be attributed to the interparticle repulsion, which favors the colloidal stability of the sample, decreasing the tendency of the particles to form agglomerates (Hubbe *et al.* 2017b). Additionally, the presence of hemicelluloses and pectin include additional negative charges to the suspensions which may contribute to the repulsion between fibers (Hubbe *et al.* 2008). Nevertheless, charge density is not the only factor affecting viscosity. Although sb-BCNF shows a slightly lower charge density than the CNFs from wood, the sb-LCNF has a lower viscosity than those samples. This variance could be attributed to the differences in morphology; while wood samples are entangled and long structures, soybean CNFs are short fibers that can be expected to have higher mobility and therefore, lower viscosity.

As expected, all the samples exhibited non-Newtonian shear-thinning behavior (Figure 3.5), such that the viscosity of the samples decreased as a function of shear rate. (Pääkko *et al.* 2007; Iotti *et al.* 2011; Iglesias *et al.* 2020b). This is attributed to alignment of the fibrils with increasing shear rate. The steady shear rheology data was fit to models to enable more detailed comparison between samples. The data is presented in Table 3.3 and the power index <1 confirmed the shear-thinning behavior for non-Newtonian fluids (Macosko 1994). Additionally, the power law index is slightly larger for soybean samples than for the wood samples, which could indicate a dependence on the raw material of the CNFs.

Table 3.3. Power-law and Herschel-Bulkley Parameters Fitted to the Data $\eta = k\dot{\gamma}^{n-1}$ for sb-BCNF, w-BCNF, and w-LCNF, and $\tau = \tau_0 + k\dot{\gamma}^n$ for Sample sb-LCNF.

Sample	k	n	τ_0 (Pa)
sb-BCNF	53.7	0.13	-
sb-LCNF	4.3	0.60	14.0
w-BCNF	97.8	0.06	-
w-LCNF	256.9	0.08	-

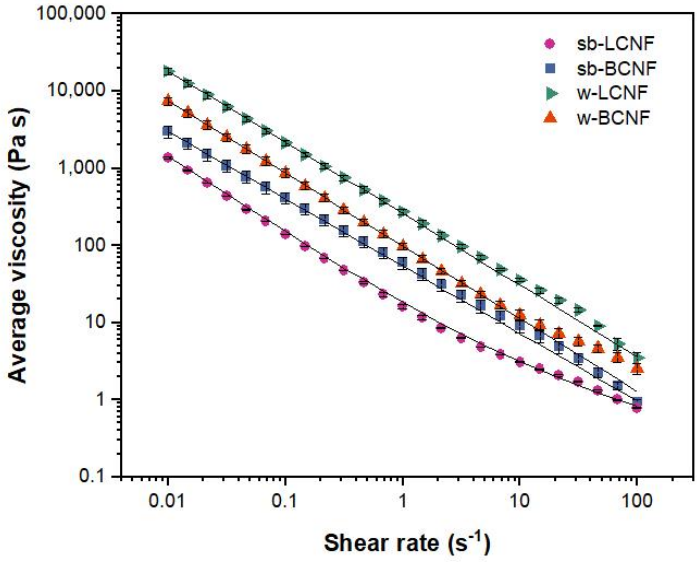

Figure 3.5. Steady state flow curves for sb-LCNF (●), sb-BCNF (■), w-LCNF (▶), and w-BCNF (▲). The curves represent model fits to the data, where the power-law model was fit to sb-BCNF, w-LCNF, and w-BCNF and the Herschel-Bulkley model was fit to sb-LCNF. (Data acquired by Fatima Hamade, Auburn University).

For the w-BCNF, w-LCNF, and sb-BCNF, the power-law model (equation 3.4) described the behavior.

$$\eta = k\dot{\gamma}^{n-1} \tag{3.4}$$

where η is the viscosity, k is the consistency index, $\dot{\gamma}$ is the shear rate, and n is the power law index. However, sample sb-LCNF exhibited a well-defined yield stress. There was one order of magnitude decrease in viscosity at a shear stress of 14 Pa. As a result, the Herschel-Bulkley model (equation 3.5) provided a better fit for the sb-LCNF data,

$$\tau = \tau_0 + k\dot{\gamma}^n \tag{3.5}$$

$$\eta = \tau * \dot{\gamma}$$

Where τ is the shear stress at a given shear rate and τ_0 is the yield stress. This result is surprising, since it was the only sample to show a yield stress, but in other studies specimens with the highest charge density show decreased yield stress due to repulsion between the fibers (Horvath and Lindström 2007). However, in this study both the differences in the morphology (figure 3.4) and chemistry affected the flow behavior. As mentioned previously, soybean hulls contain pectin, interacting in the primary cell wall with cellulose and hemicelluloses (Medic *et al.* 2014). Although the chemical treatment reduces the amount of hemicelluloses, lignin, and pectin on the extracted soybean fibers (Alemdar and Sain 2008), remnants of pectin on the sample could act as a gelling agent (Monsoor and Proctor 2001) between the different lignocellulosic components. This could restrict the movement of the fibers and generate the yield stress observed on the unbleached soybean CNF.

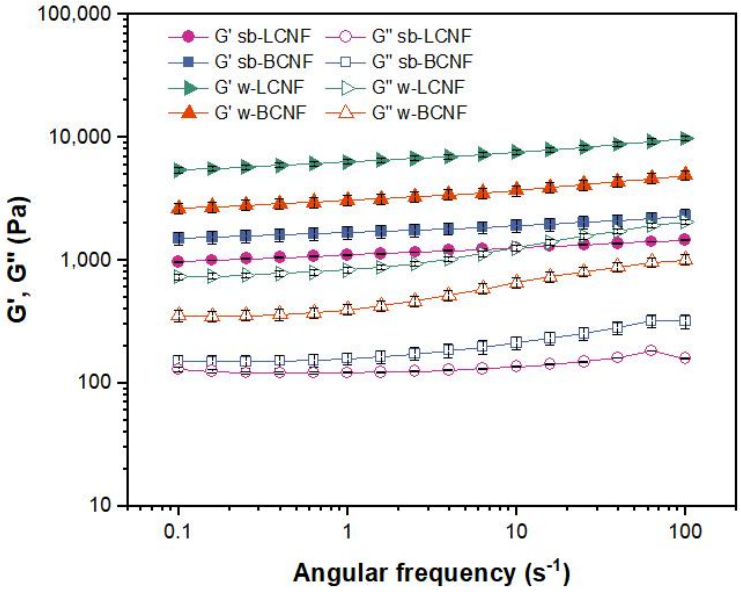

Figure 3.6. Oscillatory frequency sweeps for the set of nanocelluloses at 0.2% of strain. G' (bold) and G'' (empty) for sb-LCNF (●,○), sb-BCNF (■,□), w-LCNF (▶,▷), and w-BCNF (▲,△). (Data acquired by Fatima Hamade, Auburn University).

Small amplitude oscillatory shear (SAOS) was used to gain more insight into the samples' viscoelastic nature. Figure 3.6 shows that all samples were primarily elastic, the storage moduli were greater than the loss moduli (G'>$\underline{G}$") with tan(δ) = G"/G' ~ 0.1. For both G' and G" the wood samples had higher values than the soybean CNFs. In a similar fashion as the steady shear results, this can be attributed to the more entangled structures observed in the AFM images. Compared to the soybean CNFs, wood CNFs show higher G' and G", which could be related to the thick and long fibers bundles observed in the AFM images. Interestingly, the lower slope of the soybean samples suggests that they were the closest to achieving percolated network formation.

3.5. Conclusions

Cellulose nanofibrils (CNFs) were prepared from two different sources, wood and soybean hulls. In order to better understand how the chemical composition of each raw material affects the characteristics of nanocellulose suspensions, CNF was prepared from bleached and unbleached fibers from each of the materials.

The samples were fully characterized in terms of chemical composition, morphology, thermal, and rheological behavior. A higher thermal stability of the soybean hulls samples was observed compared with the CNFs produced from wood. This was correlated with a higher crystallinity of the soybean hulls nanocellulose samples.

Additionally, the morphology of the samples showed entangled structures for wood samples, which was in agreement with the higher viscosity and more elastic behavior observed in the rheological assessment. Furthermore, the charge density of these samples fell between those obtained for sb-LCNF and sb-BCNF. Although no trend was observed between wood and soybean fibers in terms of charge density, it is concluded that the differences are not only due to their chemical composition but also due to the chemical treatments used to produced them.

Finally, the samples were fully characterized in terms of their rheological behavior. All the specimens presented a shear-thinning behavior and were primarily elastic. This was more noticeable for wood CNFs, which was mainly attributed to the morphology of these fibers. Furthermore, the modeling of the rheological properties and the yield stress found on the sb-LCNF when performing oscillatory measurements also introduced a novelty on the rheological behavior of the samples.

3.6. Literature cited

Ahuja, D., Kaushik, A., and Singh, M. (2018). "Simultaneous extraction of lignin and cellulose nanofibrils from waste jute bags using one pot pre-treatment," *Int. J. Biol. Macromol*. DOI: 10.1016/j.ijbiomac.2017.09.107

Aksoy, B., Jiang, Z., Aksoy, M., and Beck, B. (2020). "Using liberated and modified fibers, micro, nano fibers and cellulose from lignocellulosic plant fibers, and algae as feed binders in compound feeds," US Provisional patent application No.: 63/054,907.

Alemdar, A., and Sain, M. (2008). "Biocomposites from wheat straw nanofibers: Morphology, thermal and mechanical properties," *Compos. Sci. Technol.* 68, 557-565. DOI: 10.1016/j.compscitech.2007.05.044

Brebu, M., and Vasile, C. (2010). "Thermal degradation of lignin—A review," *Cellul. Chem. Technol.* 44, 353-363.

Carrasco, F., Mutjé, P., and Pelach, M. A. (1998). "Control of retention in paper-making titration and zeta potential techniques," *Wood Sci. Technol.* 32, 145-155. DOI: 10.1007/BF00702595

Cassales, A., de Souza-Cruz, P. B., Rech, R., and Záchia Ayub, M. A. (2011). "Optimization of soybean hull acid hydrolysis and its characterization as a potential substrate for bioprocessing," *Biomass and Bioenergy* 35(11), 4675-4683. DOI: 10.1016/j.biombioe.2011.09.021

Chen, Y., Wu, Q., Huang, B., Huang, M.-J., and Ai, X.-L. (2015). "Isolation and characteristics of cellulose and nanocellulose from lotus leaf stalk agro-wastes," *BioResources* 10(1), 684-696. DOI: 10.15376/biores.10.1.684-696

Debiagi, F., Faria-Tischer, P. C. S., and Mali, S. (2020). "Nanofibrillated cellulose obtained

from soybean hull using simple and eco-friendly processes based on reactive extrusion," *Cellulose* 72(4), 1975-1988. DOI: 10.1007/s10570-019-02893-0

Deepa, B., Abraham, E., Cordeiro, N., Mozetic, M., Mathew, A. P., Oksman, K., Faria, M., Thomas, S., and Pothan, L. A. (2015). "Utilization of various lignocellulosic biomass for the production of nanocellulose: A comparative study," *Cellulose* 22, 1075-1090. DOI: 10.1007/s10570-015-0554-x

Espinosa, E., Domínguez-Robles, J., Sánchez, R., et al. (2017). "The effect of pre-treatment on the production of lignocellulosic nanofibers and their application as a reinforcing agent in paper," *Cellulose* 24, 2605-2618. DOI: 10.1007/s10570-017-1281-2

FAOSTAT (2019). http://www.fao.org/faostat/en/#data/QC

Feng, Y. H., Cheng, T. Y., Yang, W. G., Ma, P.-T., He, H.-Z., Yin, X.-C., and Yu, X.-X. (2018). "Characteristics and environmentally friendly extraction of cellulose nanofibrils from sugarcane bagasse," *Ind. Crops Prod*. 111, 285-291. DOI: 10.1016/j.indcrop.2017.10.041

Ferrer, A., Salas, C., and Rojas, O. J. (2016). "Physical, thermal, chemical and rheological characterization of cellulosic microfibrils and microparticles produced from soybean hulls," *Ind. Crops Prod*. 84, 337-343. DOI: 10.1016/j.indcrop.2016.02.014

Horvath, A. E., and Lindström, T. (2007). "The influence of colloidal interactions on fiber network strength," *J. Colloid Interface Sci.* 22, 824-830. DOI: 10.1016/j.jcis.2006.08.066

Hubbe, M. A., Ferrer, A., Tyagi, P., Yin, Y., Salas, C., Pal, L., and Rojas, O. J. (2017a). "Nanocellulose in thin films, coatings, and plies for packaging applications: A review," *BioResources* 12, 2143-2233.

Hubbe, M. A., Tayeb, P., Joyce, M., Tyagi, P., Kehoe, M., Dimic-Misic, K., and Pal, L. (2017b). “Rheology of nanocellulose-rich aqueous suspensions: A review,” *BioResources* 12(4), 9556-9661. DOI: 10.15376/biores.12.1.2143-2233

Hubbe, M. A., Rojas, O. J, Lucia, L, and Sain, M. (2008). "Cellulosic nanocomposites: A review," *BioResources* 3, 929-980. DOI: 10.15376/biores.3.3.929-980

Hult, E. L., Iotti, M., and Lenes, M. (2010). "Efficient approach to high barrier packaging using microfibrillar cellulose and shellac," *Cellulose* 17, 575-586. DOI: 10.1007/s10570-010-9408-8

Iglesias, M. C., Gomez-Maldonado, D., Via, B. K., Jiang, Z.-H., and Peresin, M. S. (2020a). "Pulping processes and their effects on cellulose fibers and nanofibrillated cellulose properties: A review," *For. Prod. J.* 70, 10-21. DOI: 10.13073/FPJ-D-19-00038

Iglesias, M. C., Shivyari, N., Norris, A., Martin-Sampedro, R., Eugenio, M. E., Lahtinen, P., Auad, M. L., Elder, T., Jiang, Z.-H., Frazier, C. E., and Peresin, M. S. (2020b). "The effect of residual lignin on the rheological properties of cellulose nanofibril suspensions," *J. Wood Chem. Technol*. 40(6), 370-381. DOI: 10.1080/02773813.2020.1828472

Iotti, M., Gregersen, Ø. W., Moe, S., and Lenes, M. (2011). "Rheological studies of microfibrillar cellulose water dispersions," *J. Polym. Environ*. 19, 137-145. DOI: 10.1007/s10924-010-0248-2

Kawamura, S. (1967). "Quantitative paper chromatography of sugars of the cotyledon, hull, and hypocotyl of soybeans of selected varieties," Kagawa University, Departmental Bulletin Paper, 18(2), 117-131.

Klemm, D., Kramer, F., Moritz, S., Lindström, T., Ankerfors, M., Gray, D., and Dorris, A. (2011). "Nanocelluloses: A new family of nature-based materials," A*ngew. Chemie - Int. Ed.* 50,

5438-5466. DOI: 10.1002/anie.201001273

Larkin, P. J. (2011). "Unknown IR and Raman spectra," in: *IR and Raman Spectroscopy - Principles and Spectral Interpretation*, Elsevier, United States, pp. 177-212.

Li, P., Wang, Y., Hou, Q., Liu, H., Liang, C., and Li, X. (2019). "Effect of pretreatment on the structure and properties of nanofibrillated cellulose from soybean residues," *BioResources* 14(1), 554-560. DOI: 10.15376/biores.14.1.554-560

Macosko, C. W. (1994). "Rheology: Principle, measurements, and applications," WILEY-VCH Verlag GmbH &Co., Canada

Medic, J., Atkinson, C., and Hurburgh, C. R. (2014). "Current knowledge in soybean composition," *J. Am. Oil Chem. Soc*. 91, 363-384. DOI 10.1007/s11746-013-2407-9.

Monsoor, M. A., and Proctor, A. (2001). "Preparation and functional properties of soy hull pectin," *J. Am. Oil Chem. Soc.* 78, article no. 709. DOI: 10.1007/s11746-001-0330-z

Pääkko, M., Ankerfors, M., Kosonen, H., Nykänen, A., Ahola, S., Österberg, M., Ruokolainen, J., Laine, J., Larsson, P T., Ikkala, O., and Lindström, T. (2007). "Enzymatic hydrolysis combined with mechanical shearing and high-pressure homogenization for nanoscale cellulose fibrils and strong gels," *Biomacromolecules* 8, 1934-1941. DOI: 10.1021/bm061215p

Palacios Hinestroza, H., Hernández Diaz, J. A., Esquivel Alfaro, M., Toriz, G., Rojas, O. J., and Sulbarán-Rangel, B. C. (2019). "Isolation and characterization of nanofibrillar cellulose from *Agave tequilana* Weber bagasse," *Adv. Mater. Sci. Eng*. 2019, article no. 1342547. DOI: 10.1155/2019/1342547

Sangeetha, V. H., Varghese, T. O., and Nayak, S. K. (2019). "Isolation and characterisation of nanofibrillated cellulose from waste cotton: Effects on thermo-mechanical properties of polylactic acid/MA-g-SEBS blends," *Iran Polym. J.* (English Ed.) DOI: 10.1007/s13726-019-

00733-3

Segal, L., Creely, J. J., Martin, A. E., and Conrad, C. M. (1959). "An empirical method for estimating the degree of crystallinity of native cellulose using the X-ray diffractometer," *Text. Res. J*. 29, 786-794. DOI: 10.1177/004051755902901003

Sjöström, E. (1993). *Wood Chemistry, Fundamentals and Applications*, Second Ed., Elsevier, Academic Press Inc., California, San Diego.

Smook, G. (2016). "Kraft pulping," in: *Handbook for Pulp & Paper Technologist*, 4th Ed., M. Kocurek (ed.), TAPPI Press, Atlanta, pp. 76-85.

Tang, F., Li, S., Yu, H.-Y., Wang, C., Li, Y.-Z., Li, Z.-H., Yao, J.-M., Tang, J.-H., and Zhu, J.-Y. (2020a). "Tailoring commercial cellulose membranes into janus conductive electronic skin via diffusion-controlled polymerization," *ACS Sustain. Chem. Eng.* 8, 17458-17465. DOI: 10.1021/acssuschemeng.0c05913

Tang, F., Yu, H., Hussain Abdalkarim, S. Y., Sun, J.-H., Fan, X-M., Li, H.-Z., Zhou, Y., and Tam, K. C. (2020b). "Green acid-free hydrolysis of wasted pomelo peel to produce carboxylated cellulose nanofibers with super absorption/flocculation ability for environmental remediation materials," *Chem. Eng. J.* 395, 125070. DOI: 10.1016/j.cej.2020.125070

Tarrés, Q., Espinosa, E., Domínguez-Robles, J., Rodríguez, A., Mutjé, P., and Delgado-Aguilar, M. (2017). "The suitability of banana leaf residue as raw material for the production of high lignin content micro/nano fibers: From residue to value-added products," *Ind. Crops Prod.* 99, 27-33. DOI: 10.1016/j.indcrop.2017.01.021

USDA (2019). https://quickstats.nass.usda.gov/results/F248CF7B-0665-3904-A2BE-F9CF1A1A80DD

Xu, J., Krietemeyer, E. F., Boddu, V. M., Liu, S. X., and Liu, W.-C. (2018). "Production

and characterization of cellulose nanofibril (CNF) from agricultural waste corn stover," *Carbohydr. Polym.* 192, 202-207. DOI: 10.1016/j.carbpol.2018.03.017

Yang, H., Yan, R., Chen, H., Lee, D. H., and Zheng, C.-G. (2007), "Characteristics of hemicellulose, cellulose and lignin pyrolysis," *Fuel* 86, 1781-1788. DOI: 10.1016/j.fuel.2006.12.013

Yuan, T., Zeng, J., Wang, B., Cheng, Z., and Chen, K.-F. (2021). "Lignin containing cellulose nanofibers (LCNFs): Lignin content-morphology-rheology relationships," *Carbohydr. Polym*. 254, article no. 117441. DOI: 10.1016/j.carbpol.2020.117441

4. Elucidating the effect of varying chemical composition of the starting material on the rheological properties of lignin-containing cellulose nanofibrils (LCNFs)

4.1. Abstract

Nanocellulose suspensions are commonly referred to as colloidal suspensions, where particles in the nano to the micro size range are dispersed in a liquid media (Berg 2010). The characteristics of these colloidal suspensions will be determined by the chemical composition of the solid particles, the media, and the interfaces between them (Berg 2010). When considering cellulosic nanomaterials, cellulose nanocrystals (CNCs) and cellulose nanofibrils (CNFs) have different morphologies and chemistries, which directly impact their dispersions viscoelastic properties. Specifically, the lignin containing cellulose nanofibrils (LCNFs) colloidal systems have been understudied due to their complexity. Rheology is the science of understanding the deformation and flow of materials when an external force is applied. Such understanding is crucial since all the different unit operations at which materials are subjected during processing/application will introduce deformations on them. Studying the rheological behavior of a suspension can offer information such as the stability of the sample over time, its viscoelastic behavior, the alignment/entanglement of the fibrils when applying shear, among many others.

In this work, we focused on understanding the effect of chemical composition on the rheological properties of Kraft softwood cellulose pulps with different amounts of residual lignin and hemicelluloses using steady-state and dynamic state analysis. Different geometries were utilized and compared to one another. Additionally, we studied the intrinsic properties of the colloidal suspensions in terms of morphology, chemical composition, charge density, thermal, and colloidal stability by atomic force microscopy (AFM), Fourier-Transform infrared spectroscopy

(FT-IR), surface chemistry analysis, thermal gravimetric analysis (TGA), and dynamic light scattering (DLS) techniques.

4.1.1. Index words

Lignin-containing cellulose nanofibrils, LCNF, cellulose nanofibrils, rheology, lignocellulosic fibers, CNF, viscoelastic behavior.

4.2. Introduction

Over the years, the field of materials science and nanotechnology have grown extensively, including the advance of analytical techniques, allowing researchers to explore and study alternatives that were not even possible a while ago. It is estimated that the nanotechnology market will have a compound annual growth rate of 19.4% from 2018 to 2023 (BBC Publising 2019). The possibility of having materials in various dimensions make them suitable for specific applications and introduces the necessity of being more precise and meticulous when studying their properties to better understand their behaviors and long-term impact in processes, health, and the environment. Rheology is a science that provides powerful characterization information, that allows understanding how a material will behave when introducing a stress/deformation on the sample (Macosko 1994). This is crucial since all the different procedures at which materials are subjected during processing/application will introduce deformations on them, e.g., during coating and spraying, samples can be exposed to shear rates of 10 and 1000 s^{-1}, respectively (Mezger 2014). Studying the rheological behavior of suspensions, can offer information such as their stability over time, their viscoelastic behavior, the alignment/entanglement of nanofibrils when applying shear, among many others (Guan Gong 2014).

When considering cellulosic nanomaterials, cellulose nanocrystals (CNCs) and cellulose nanofibrils (CNFs) have been the two most characterized types of dispersions. CNCs are usually obtained by purely chemical treatments, mainly utilizing sulfuric acid as a reagent that dissolves the amorphous regions of the cellulose elementary fibrils. As a result, the final nanoparticles presents a rod-like structure with 0.05-0.5 μm in length and 3-5 nm in width (Klemm et al. 2011, Moon et al. 2011). The presence of sulphate groups on the crystals surface allows for a stable colloidal suspension in water. On the other hand, CNFs can be produced by various methods, always having as a common denominator the mechanical defibrillation of the fibers (Dufresne 2019). When making this type of nanomaterial, both the crystalline and amorphous regions of the cellulosic elementary fibrils are preserved. As a result, CNF suspensions are characterized for having particle lengths in the range of a hundred microns while the diameters can reach a few nanometers (Moon et al. 2011). Regarding the rheological behavior, the different morphologies and chemical compositions of both types of nanomaterials will directly impact their viscoelastic properties (Moberg et al. 2017).

While researchers have been focusing on the rheological properties of CNCs and CNFs during recent years, there are still many doors to explore to predict their behavior (Hubbe 2021). The possibility of producing nanocellulosic materials without the necessity of utilizing extra chemicals, other than the ones necessary for the pulping process, is the motivation on focusing on CNF suspensions. Furthermore, although much work has been published on the study of fully bleached cellulose nanofibrils (BCNF), the alternative of utilizing lignin-containing cellulose nanofibrils (LCNFs), where chemical components such as lignin and hemicelluloses remain on the fibers, present an exciting opportunity to be considered for high-end applications such as coatings, composites, among others (Solala et al. 2019). Lignin is well known for its more hydrophobic

nature when compare with the other wood components (Solala et al. 2019), and its presence can introduce differences on the surface properties as well as on the defibrillation degree of the fibers (Rojo et al. 2015). In our recent study, we demonstrated how the presence of lignin, affect the rheological properties of the suspensions, increasing the viscosity of the samples which could be attribute due to the entanglement of the fibers and as a result of lignin-lignin interactions present on the suspensions, thus preventing the material to flow (Iglesias et al. 2020b). Additionally, Lê et al. (2018) demonstrated how lignin influences the elasticity of the fibrillar network due to its presence on the fibers surface and within the fibrils on the solution. Furthermore, following the same trend, Yuan et al. (2021b) investigated the rheological properties of LCNFs from bleached-chemi-thermo-mechanical pulps, determining that the lignin content on the samples was the main property affecting morphology and viscoelastic properties. Thus, as a general observation, it is also worth mentioning that not only the chemical composition of the sample but also the raw material and the treatments at which the sample are subjected, will have a direct impact on the rheological behavior of the samples which is related with size, aspect ratio, flexibility, and chemical components (Iglesias et al. 2021a).

To better understand the effect of chemical composition on the rheological properties of LCNFs, four different softwood cellulose pulps were produced from a kraft pulping process pulps varying the times and applying a bleaching stage when considered. Once the LCNFs were produced, we studied their viscoelastic properties by steady shear and dynamic analysis. Additionally, the stability of the suspensions over time was assessed. Furthermore, we investigated the intrinsic properties of the colloidal suspensions in terms of morphology, chemical composition, charge density, thermal, and colloidal stability by atomic force microscopy (AFM), Fourier-Transform infrared spectroscopy (FT-IR), surface chemistry analysis, thermal gravimetric analysis

(TGA), and dynamic light scattering (DLS) techniques. All the data was processed using Origin Student Version 2021. Otherwise, will be specified along the manuscript.

4.3. Experimental

4.3.1. Materials

For this work, softwood chips were kindly provided by a US mill. For the pulping process, sodium hydroxide pellets (Macron, Chemicals) and sodium sulfide hydrate (Honeywell) were utilized. Bleaching was carried out utilizing sodium chloride (BTC Beantown Chemical), hydrochloric acid 36.5-38% assay (EMD Millipore), and sodium hydroxide pellets (Macron, Chemicals).

For charge density measurements, poly(diallyldimethylammonium chloride) (pDADMAC) solution and potassium polyvinyl sulfate (PVSK), were acquired from BTG Americas Inc, (Norcross, GA, USA) both at 0.001 N concentration. For the surface preparation, polyethyleneimine (PEI) was purchased from Sigma Aldrich (Saint Louis, MO, USA) and the silicon oil B1000 for the rheological measurements was acquired from Brookfield Ametek (Middleboro, MA, USA).

4.3.2. Methods

4.3.2.1. Cellulose pulps with varying chemical composition processing

For the purpose of this work, four variations on the Kraft cooking process were carried out. Softwood chips were cooked at different periods of time in order to reach different lignin contents on the samples. A scheme of the process can be observed in Figure 4.1.

The wood ships were air dried and stored in polyethylene bags at 25 ºC until use. Moisture content before use was 7% wt. Kraft cooking was performed in a 2 L batch reactor furnished with a recirculation system and heating of the cooking liquor. Cooking conditions were: 500 g of dry chips, liquor to wood ratio was 4:1, 20 % active alkali (AA), 30 % sulfidity, 170 ºC cooking temperature, and 3 hours to maximum temperature. Time was varied to obtain different H-factor values which means different lignin contents can be reached. The H-factor was calculated according to the following equation:

$$H = \int_0^t e^{\left(43.2 - \frac{16115}{T}\right)} dt \qquad (4.1)$$

in which T is the temperature (K) and t the time (hours) (Table 4.1).

Table 4.1. Calculated H factors based on the cooking time and temperature

Cellulose pulps	Cooking time (h)	H factor	Bleaching stage
P1	0.5	459	No
P2	1	919	No
P3	3	2756	No
P4	3	2756	Yes

Figure 4.1. Pulping process sequence, a) white liquor, b) wood chips inside the reactor vessel, c) closed reactor during the pulping process, d) discharging the black liquor, and e) wood chips after the kraft process.

After the cooking process was completed, the chips were discharged into the blow tank, washed using abundant water, disintegrated, and screened to remove uncooked material. The cellulose pulp suspension was placed inside the screener constantly adding tap water to avoid the clogging of the equipment. During this process, cooked chips were separated into accepted and rejected fibers. In order to recover as much fibers as possible, the rejected material was placed inside a blender and mixed for 10 min with abundant water following by screening the sample again as showed in Figure 4.2. After the pulping and screening process, P4 was bleached using the conditions described in the following section.

Figure 4.2. Screening process sequence, a) wood chips desintagrated into the blow tank, b) pulp screener, c) adding small amount of fibers with abundant water to the screener, and d) the accepted fibers are collected in a fabric bag and further washed with abundant water.

4.3.2.2. Bleaching process

This process was performed in three stages (Table 4.2) as depicted in Figure 4.3. For all the different stages, suspensions were initially prepared at 3 %wt. After each process, the cellulose pulp was washed using a fabric bag and abundant water. Briefly, for the first stage, sodium chlorite ($NaClO_2$) was incorporated while adjusting the suspension pH to 4 using 1 M hydrochloric acid (HCl). Cellulose pulp was placed in a plastic bag and submerged in a hot water bath at 50 ºC for 1 hour. The sample was mixed every 15 min to improve heat transfer. For the second stage, pH

was adjusted to 11.5 using 1 M sodium hydroxide (NaOH) and the sample was placed in a hot water bath at 80 ºC for 1 hour, and mixed every 15 min. Finally, during the last step, $NaClO_2$ was incorporated, and the pH adjusted to 2.8 using 1 M HCl. The suspension was placed in a hot water bath at 70 ºC for 3 hours and mixed every 15 min. When the time was completed, the cellulose pulp was washed using a fabric bag and abundant water.

Finally, four different cellulose pulps with different chemical composition were further utilized to produced LCNF suspensions. The full characterization of the cellulose pulps can be founded in the Appendix of this dissertation.

Table 4.2. Bleaching conditions summary

Reagent	**Suspension consistency**	**Temperature**	**Time**	**Initial pH**
	(%wt.)	(ºC)	(Hrs)	
D0*	3	50	1	2.8
E**	3	80	1	11.5
D1	3	70	3	4.0

*D = ClO2, **E = alkaline extraction using NaOH

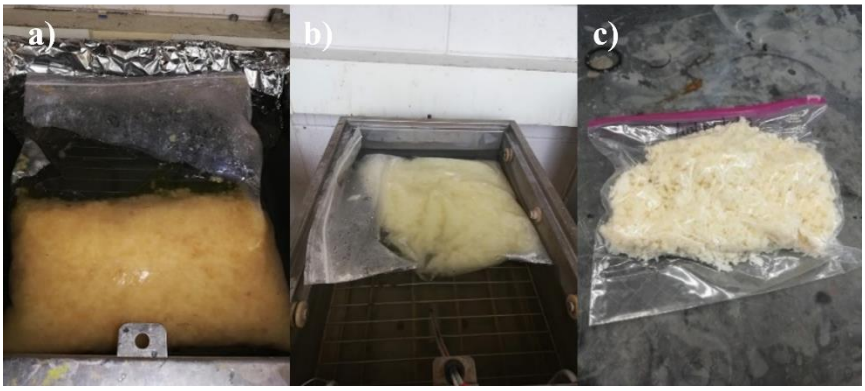

Figure 4.3. Bleaching process cellulose fibers, a) during first beaching step, b) after second bleaching step, c) once the process was completed.

4.3.2.3. LCNFs production

Lignin containing cellulose nanofibrils (LCNFs) were produced at the Forest Products Development Center of Auburn University. Suspensions at 2 wt.% were prepared using DI water. The suspensions were fibrillated using the Masuko Supermasscolloider (MKZA-10-15J, Japan). A total of 14 passes through the equipment were used and controlling at each step the gap between the disks. Additionally, different disks combination was used to improve the defibrillation of the sample. After the mechanical process, a gel-like consistency was obtained.

4.3.2.4. Characterization of LCNFs samples

i. Zeta potential

The zeta potential of the samples was measured by dynamic light scattering (DLS) utilizing a Litesizer 500 with dosing system (Anton Paar, Austria). Samples were prepared at 0.1 %wt. at a pH=7.1 and mixed using a magnetic stirrer during 10 min. Measurements were performed 10 times and averaged.

ii. Charge density

The charge density of the fibers, was measured by a polyelectrolyte titration method, adapted from Espinosa et al. (2016). Briefly, LCNF suspensions were diluted to reach 0.04 wt.% consistency, at a pH=7. Samples were sonicated for 10 min with a cold bath. Then, 25 ml of the positive polyelectrolyte (pDADMAC) were added and mixed with 15 ml of the resulting LCNF suspensions. Afterwards, the samples were centrifuged for 15 min at 3000 rpm. Once centrifugation was completed, 10 ml of the supernatant were separated and measured in a Laboratory Charge Analyzer Chemtrac LCA-1, (Norcross, GA, USA). An anionic titrant (PSVK)

was used until a 0 streaming current value (SCV) was obtained. Charge density was calculated using Equation 4.2.

$$Charge\ density = \frac{\left([pDADMAC] * V_{p-DADMAC}\right) - ([PVSK] * V_{PVSK})}{W_{dry\ LCNF\ sample}} \quad (4.2)$$

where $[pDADMAC]$ is the solutions concentration of the cationic polymer, $V_{pDADMAC}$ is the used volume of p-DADMAC added to the mix, $[PVSK]$ is the concentration of the stock anionic titrant, V_{PVSK} is the used volume for the titration, and $W_{dry\ LCNF\ sample}$ is the dry weight of the LCNF samples. Measurements were performed six times per each sample.

iii. Thermal behavior

The thermal behavior of the samples containing different amounts of lignin was analyzed by TGA in order to study the thermal decomposition of the material as a function of temperature. Measurements were performed using a TGA-50 from Shimadzu (Kyoto, Japan) Approximately 15 mg of sample were placed on aluminum pans and pre-heated at 120 °C for 20 min to eliminate the moisture content. Afterwards, they were heated to 600 °C at a rate of 10 °C/min in a nitrogen atmosphere. Measurements were performed by duplicated and averaged.

iv. Chemical composition

FT-IR with attenuated total reflectance accessory (ATR-FTIR) was utilized to determine chemical and structural composition of the samples. A PerkinElmer Spotlight 400 FT-IR Imaging System (Massachusetts, USA) with an ATR accessory with diamond/ZnSe crystal was utilized. A background spectrum in air was recorded before each different sample measurement. All spectra were collected from 400 to 4000 cm^{-1} with a 4 cm^{-1} wavenumber resolution after 128 continuous

scans. The baseline was corrected, and the data was normalized using the Spectrum 6 Spectroscopy Software (PerkinElmer, Massachusetts, US).

v. Crystallinity

X-ray powder diffraction (XRD) was performed using a Rigaku 2-Dimension G SmartLab X-Ray Diffractometer equipped with a HyPix-3000 detector, Cu Kβ irradiation filter, and a Bragg-Brentano geometry. Measurements were performed at a continuous scan speed of 0.1 second/step, from 10 to 80 degrees. Data was acquired using the DiffracPlus Eva version 13.0.0.3 by Bruker. The crystallinity index (CI) was calculated utilizing Segal's method, defined by equation 4.3 (Segal et al. 1959):

$$CI\ (\%) = \frac{I_{002} - I_{Am}}{I_{002}} \tag{4.3}$$

vi. Morphology

AFM and scanning electron microscopy (SEM) techniques were utilized to study the morphology of the samples. For AFM imaging, silicon wafers were prepared as described in Iglesias et al. (2021b). AFM images size was 5 μm x 5 μm were obtained in tapping mode utilizing an Anton Paar TOSCATM 400 (Graz, Austria) with a silicon cantilever. Images were processed with Gwyddion software 2.49 (SourceForge).

For SEM measurements, dispersions were prepared at 0.1 %wt. and deposited onto Sil-wafers. Surfaces were air dried and stored in a desiccator until used. Previous to the image acquisition, all the surfaces were coated under an argon atmosphere with a gold layer using a EMS 550 Sputter Coating Device. Then, SEM analyses were performed using a Carl Zeiss Supra 35VP SEM and all images were acquired at a magnification of 2.0 KX.

The width distribution of the fibrils was analyzed with the AFM images utilizing the ImageJ Software (Kimura et al. 1999). Two hundred measurements were performed for each sample and the results are plotted in Figure 4.8.

In order to corroborate the presence of lignin on the samples as well as to have a better insight about where lignin is located on the suspension, a Nikon A1R MP Multiphoton and Confocal Microscope (Tokyo, Japan) was utilized. Images were acquired at 1/32 frame per sec and a size of 512. To imaging lignin autofluorescence, a FTIC Laser was utilized at an excitation wavelength of 488 nm.

vii. Absorbance

The absorbance of the LCNF suspension at 0.1 %wt. consistency was measured by a Genesys 50 UV-Visible Spectrophotometer from Thermo Scientific (Waltham, MA U.S.) at a wavelength range from 220 to 800 nm. Milli Q water was utilized as reference. Samples were measured four times and averaged.

viii. Rheological behavior

Rheological properties of the CNFs were measured using a strain-controlled rotational rheometer (Physica MCR302, Anton Paar, Austria). Rheological measurements were performed using a 25 mm diameter parallel plate geometry (PP25), 50 mm diameter parallel plate geometry (PP50), 25 mm diameter sandblasted parallel plate (PP25/P3), and 27 mm diameter concentric cylinders (CC27). Suspensions at a concentration of 1.0 % wt. CNFs were loaded on the rheometer and allowed to equilibrate for 15 min before investigation of rheological properties. In the case of parallel plate geometries. once the samples were loaded into the fixtures, a standard oil seal around the fixture was utilized together with a solvent trap of deionized water to prevent water evaporation due to extensive testing. A preliminary pre-shear protocol was performed at a shear rate of 0.001 s^{-}

[1] with the objective of reset the sample before measuring oscillatory dynamics. The dispersion microstructure was investigated with amplitude sweeps to determine the linear viscoelastic region (LVR) without severe structure deformation and frequency sweeps at 0.1 % strain within LVR to measure storage (G') and loss (G") moduli across a range of angular frequencies. Finally, flow curves were measured to investigate structure deformation under shear across a range of shear rates. Measurements were performed at a constant temperature of 25 ºC. For all the samples presented in this chapter and for the data that is not shown here but discussed, all of them were measured by triplicate loadings.

4.4. Results and discussion

4.4.1. Colloidal stability and surface properties

The colloidal stability as well as the surface properties of the suspensions were measured in terms of zeta potential and charge density, respectively. In general, it has been reported that suspensions with zeta potential ± 30 mV can be considered as stable colloids (Isogai et al. 2011). Additionally, it is considered that as the charge density of the fibrils increases, the repulsion between the fibrils is larger, improving, as a result, the colloidal stability of the suspensions (Bian et al. 2017).

Figure 4.4 shows that as the lignin content increases, the charge density of the suspensions increases accordingly. This can be related to the presence of remaining lignin and also hemicelluloses, which contribute to the amount of carboxylic groups present on the fibrils surface (Popescu et al. 2008). Nevertheless, we observed a decrease on the colloidal stability as the lignin content of the samples increases. Although these values will indicate that our samples are not stable colloids, phase separation over time has not occurred.

In order to understand the differences within samples, an ANOVA statistical test was performed for both characterization techniques. For zeta potential measurements, samples are significantly different with exception of 16.8 and 6.9% lignin. Regarding charge density data, the mean of the samples is significatively different except for suspensions with 6.9 and 2.8% lignin content.

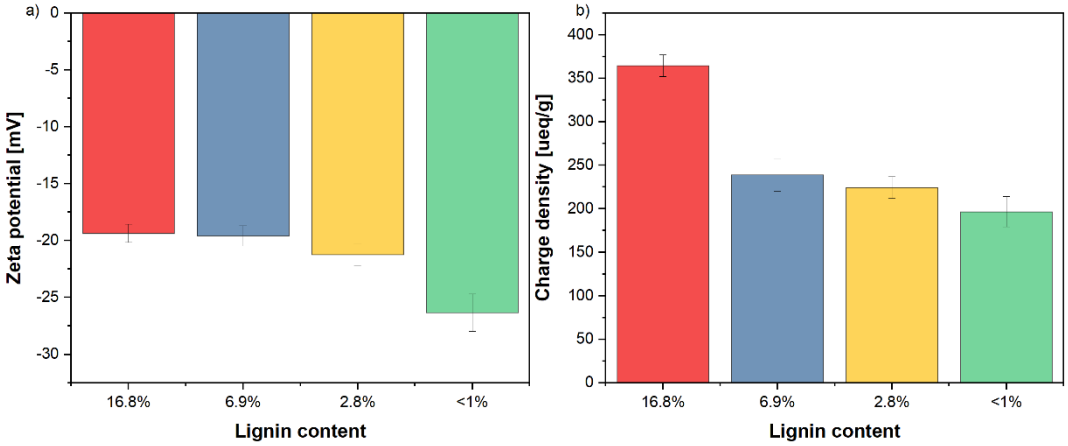

Figure 4.4. a) Zeta potential and b) Charge density of LCNFs with different lignin content.

4.4.2. Thermal decomposition

Figure 4.5 shows the thermogram of all four samples in nitrogen and Table 4.3 summarizes the different temperatures of their thermal decomposition.

Analyzing the temperatures at which the thermal decomposition begins (T_{onset}), it is possible to observe that as the lignin content on the suspensions increases, the thermal decomposition begins at higher temperatures. This differences on the T_{onset}, can be attribute due to the different chemical composition of the samples. It is well known that cellulose starts decomposing at approximately 300 ºC. Meanwhile, lignin presents a broad range of temperature from 200 to 900 ºC due to the presence of bulky groups which are more thermically stables, which could be the reason why the T_{onset} is shifted towards higher temperatures (Yang et al. 2007).

Table 4.3. T_{onset} and T_{max} of LCNF samples.

Sample (% lignin)	T_{onset} (ºC)	T_{max} (ºC)
16.8	328	360
6.9	325	356
2.8	320	352
<1.0	317	350

Differences were also observed in the solid residues remaining after the pyrolysis, mainly for the sample containing the highest amount of lignin. This can be related with the difficulties of lignin to decompose (Herrera et al. 2018) up to 600 º C.

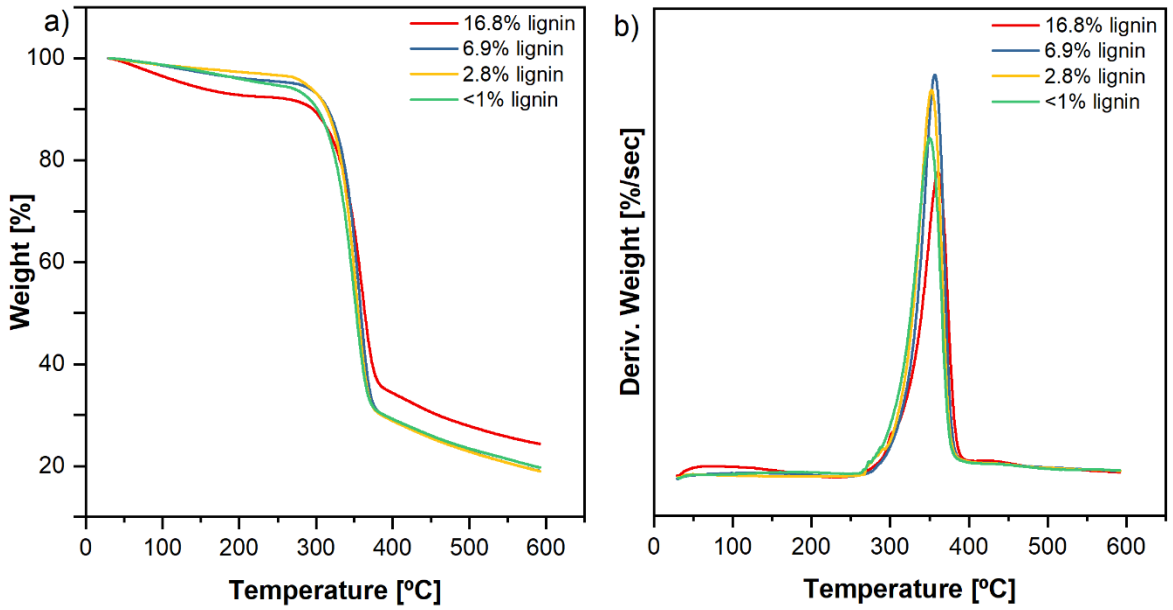

Figure 4.5. Thermogram of the samples containing different % of lignin.

4.4.3. Chemical composition

A qualitative analysis of the chemical composition of the samples was performed by FTIR and the results are presented in Figure 4.6. In the spectra, we can observe similarities between all the spectrum since no chemical treatment was applied to the fibrils. The main differences between

the samples can be attributed due to the difference in lignin content. The band at 1599 cm^{-1} could be assigned due to the C=C vibrations present on the residual lignin on the samples (Diop et al. 2017). Additionally, there is a slightly difference in the peaks at 1266 cm^{-1} corresponding to the C-OH stretching which arise from the phenolic groups (Diop and Lavoie 2017). More detail about each of the bands for similar lignocellulosic CNF suspensions can be found in Iglesias et al. (2020).

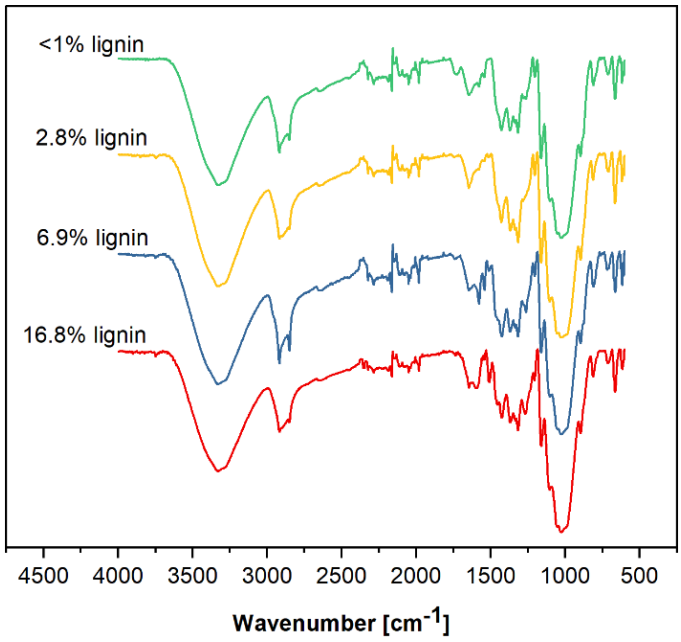

Figure 4.6. FT-IR spectra for samples with different lignin content.

4.4.4. Crystallinity

The crystallinity of the samples was analyzed by X-ray powder diffraction and the spectra is presented in Figure 4.7. As can be observed, all the samples have a major peak at a 2θ between 22.5° correspond to the crystalline plane with 200 Miller index (Chen et al. 2018). The crystallinity index (CI%) was calculated using equation 4.3, resulting in 52.6 ± 1.43, 67.3 ± 0.95, 68.9 ± 0.13, and 68.3 ± 0.18 for samples containing 16.8, 6.9, 2.8, and <1.0 % lignin content, respectively.

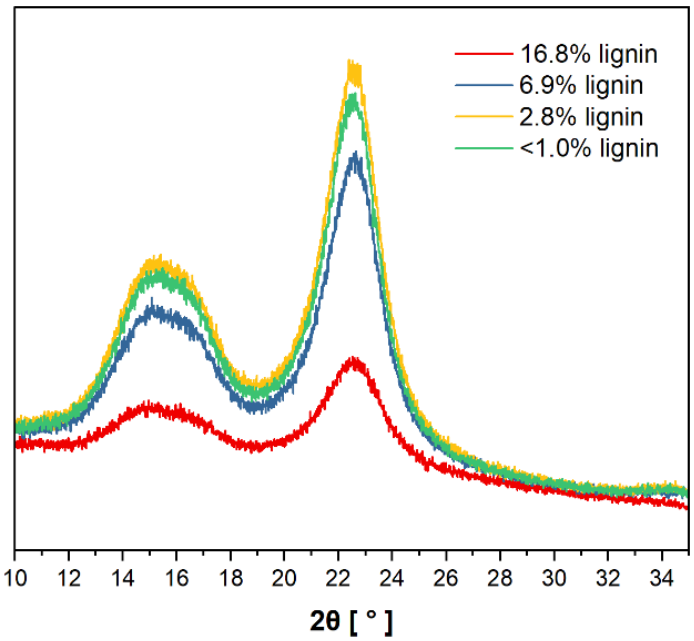

Figure 4.7. XRD spectra for LCNF samples with different lignin content.

It can be concluded that as the lignin content of the samples decrease, the crystallinity index (%) increases. This pattern could be explained due to the presence of lignin and hemicellulose which are characterized for having from less ordered to amorphous structures compared with the well organized and compact cellulose crystals (Larkin 2011). It is important mentioning that the sample containing 2.8 % lignin presents a slightly larger crystallinity than the fully bleached LCNF containing <1.0 % lignin. This could be related to the bleaching process, which can produce damage to the crystallinity of the fibers (Debiagi et al. 2020). These results correlate with the crystallinity index of the precursor pulps, presented in Appendix material of this dissertation.

4.4.5 Morphology

The morphology of the samples was analyzed by AFM and SEM images as presented in Figure 4.8. As can be observed in Figure 4.8 (A4 to D4), as the lignin content of the samples increases, the fibrils appear thinner and shorter. Our results are in agreement with previous data reported in the literature, where the presence of lignin is considered to favor the fibrillation of the

samples, due to its scavenging ability (Solala 2011; Rojo et al. 2015). Additionally, it can be consider that the presence of lignin as well as the higher charge density of the suspensions affect the fibrillation of the samples, allowing to obtain LCNF fibers with smaller diameters and less propense to entangle (Espinosa et al. 2019).

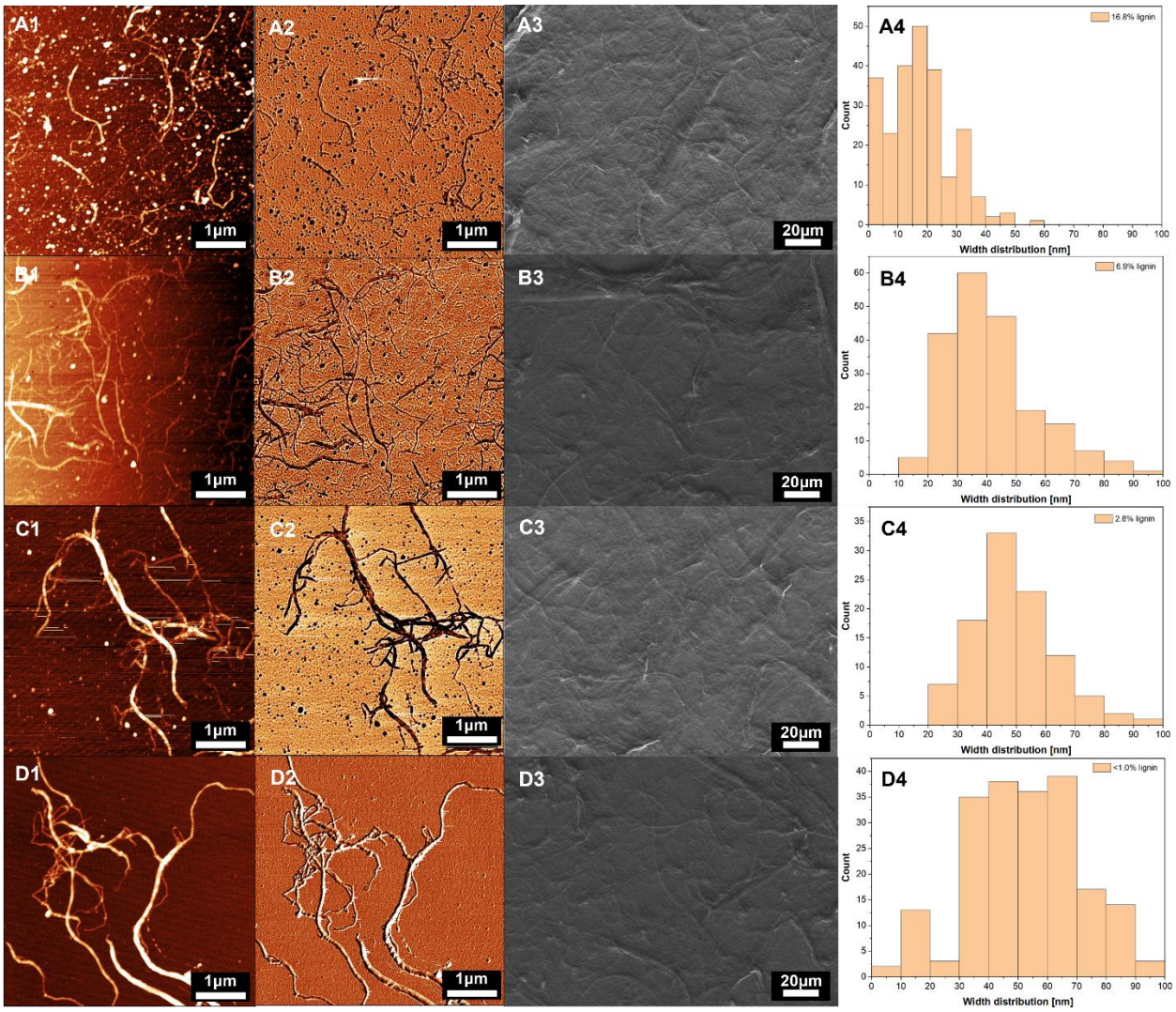

Figure 4.8. AFM height (1) and phase (2) images, SEM images (3), and width distribution (4) of LCNF samples containing A) 16.8, B) 6.9, C) 2.8, and D) <1 % lignin.

Lignin autofluorescence was measured and presented in Figure 4.9. As can be observed, the differences in lignin content on the samples can be clearly noticed. The bright area on the

images indicates the higher lignification of the samples. As the lignin content is reduced, the fluorescence intensity is also reduced. Similar results have been reported for LCNF films (Chen et al. 2018).

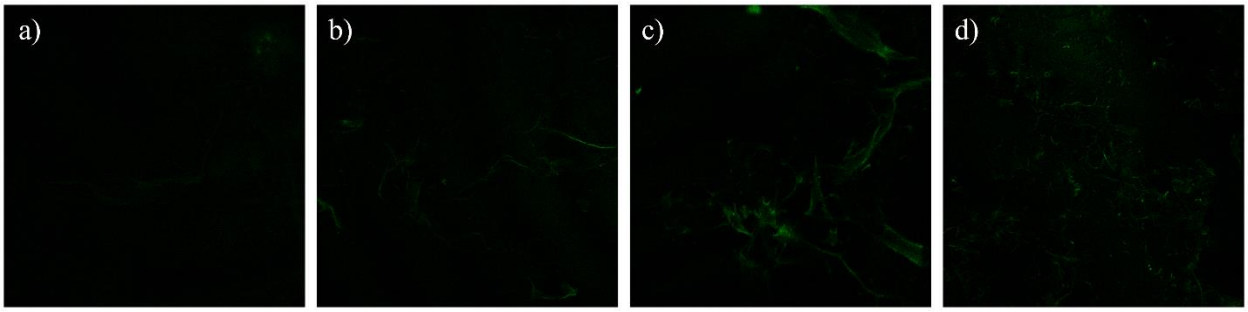

Figure 4.9. Fluorescence mapping of LCNF samples containing a) <1.0, b) 2.8, c) 6.9, and d) 16.8 % lignin.

The absorbance of 0.1 wt. %. LCNF suspensions at 0.1 %wt. was measured as a complimentary technique to corroborate the presence of lignin on the samples, and in an attempt of finding out more specifics on where the lignin is localized after the fibrillation process. As can be observed in Figure 4.10, as the lignin content of the samples increases, the absorbance values are larger, mainly in the region from 220 to 400 nm. All the samples with exception of the bleached CNF, show an absorbance peak at 280 nm which is attributed to the ability of the chromophores groups present on softwood lignin to absorb light (Jiang et al. 2020).

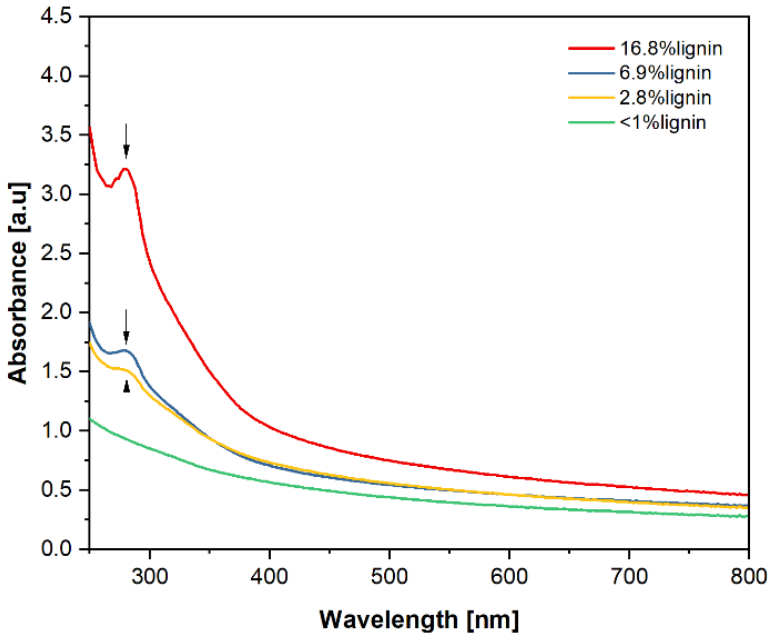

Figure 4.10. Absorbance of LCNF samples from 220 to 800 nm.

4.4.6. Rheological behavior

When analyzing the shear steady viscosity, all suspensions showed shear thinning behavior. They exhibit a particular performance when using parallel plates geometry, as the suspensions are ejected from the gap, except for sample containing 16.8 % lignin. Considering that all the LCNFs were measured at 1.0 % wt. of consistency, the suspension ejection occurred at 31.6 s^{-1} for sample containing 6.9 % lignin and at 46.4 s^{-1} for samples contain 2.8 and <1 % lignin content. The suspension with 16.8 % lignin content, did not come out from the geometry, as can be observed in Figure 4.11. It is worth mentioning that measurements were performed at different gaps, to probe the independence of the measurements with the gap height.

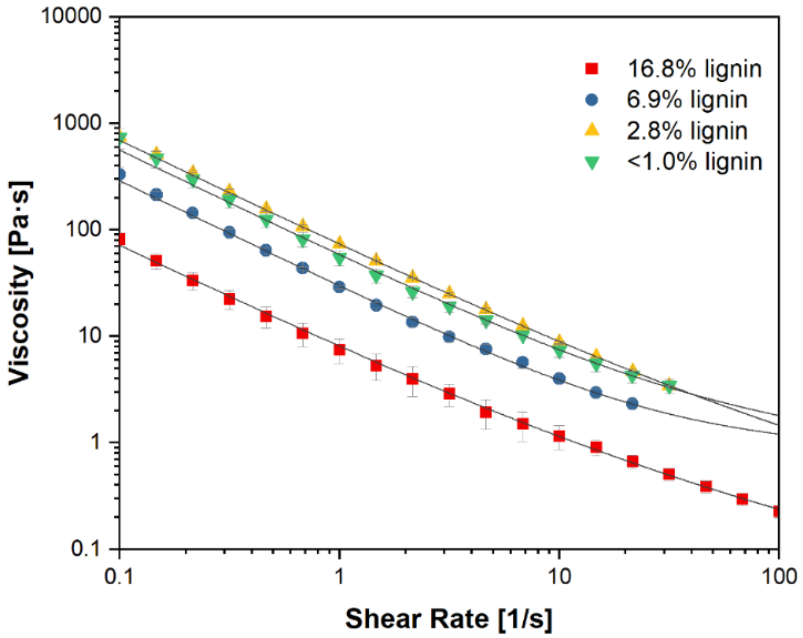

Figure 4.11. Steady-shear flow curves of samples with different lignin content. The Herschel Bulkley model was fitted to the data.

A similar behavior was reported by Nazari et al. (2016) for CNF samples with consistencies between 2 and 7 % wt. The event was attributed to the formation of flocs during the increase shear. It is proposed that such flocs present different tangential velocities. As a result, when two adjacent flocs get in contact, one can push the other outside the gap. In their publication, they attributed the formation of flocs due to the increase of solid content on the samples. Nevertheless, although our suspensions present the same consistency, a clear difference was observed on the size of the fibers (Figure 4.8).

In addition, from Figure 4.11, we can observe a decrease on the viscosity as the lignin content of the samples increases. There are several differences among the published literature regarding this behavior. In our past work, we analyzed the rheological behavior of hardwood suspensions with different lignin content and they showed increasing viscosity as the lignin content of the samples increases (Iglesias et al. 2020b). The raw material utilized to produce those LCNF

fibers were processed differently than the ones presented in this work. Mainly the cooking times were different which could affect the solubilization of the lignin and thus, the final properties of the nanofibrils made thereof. On the other hand, in agreement to data presented in Figure 4.11, it has been reported in the literature that an increase of the suspensions viscosity is observed as the lignin content of the samples is reduced (Chen et al. 2018; Fu et al. 2021; Yuan et al. 2021). Chen et al. (2018) attributed this behavior to the presence of lignin, altering the interaction between the fibers, and impeding the formation of more robust networks. Yuan et al. (2021) analyzed the rheological behavior of LCNF samples with different lignin contents and different defibrillation degrees. They conclude that the viscoelastic behavior of LCNFs is a tradeoff between the applied shear rate, the lignin content, and the defibrillation process applied on the pulps to obtain the suspensions. In our study, the sample containing 16.8% lignin showed smaller fibers when compared with its fully bleached counterpart. Thus, for this specific study, we consider that morphology could be the primary variable affecting the viscosity. Fiber size may contribute to the formation of larger flocs, and therefore, to the expulsion of the sample from the geometry. Additionally, larger fibers could surpass the effect of lignin on the suspensions, increasing their viscosity, as observed in Figure 4.11. Furthermore, samples containing 2.9 and <1.0% lignin present a similar rheological behavior, which demonstrates that there is a percentage of lignin above which lignin effects can be neglected on the performance of the samples.

Samples exhibited a well-defined yield stress and fit the Herschel-Bulkley model (Equation 4.4). The fitted parameters are presented in Table 4.4.

$$\eta = \tau_0 + k\dot{\gamma}^n \qquad (4.4)$$

$$\eta = \tau * \dot{\gamma}$$

Where η is the viscosity, τ is the shear stress at a given shear rate, τ_0 is the yield stress k is the consistency index, $\dot{\gamma}$ is the shear rate, and n is the power law index.

Table 4.4. Fitted parameters from Herschel-Bulkley modeling ($\eta = \tau_0 + k\dot{\gamma}^n$) for samples using PP25.

Lignin content (%)	τ_0 **(Pa)**	k **(Pa s^n)**	n	**R^2**
16.8	6.83 ± 0.28	1.27 ± 0.28	0.56 ± 0.05	0.981
6.9	28.86 ± 0.49	1.05 ± 0.32	0.97 ± 0.08	0.959
2.8	67.12 ± 2.00	6.33 ± 1.40	0.55 ± 0.05	0.991
<1.0	55.71 ± 2.42	2.89 ± 1.11	0.81 ± 0.08	0.971

As the lignin content of the samples decreased, an increase on the yield stress was observed. This yield stress represents the stress at which the sample needs to be subjected to disrupt the fibril network structure to be able to flow. Nevertheless, sample containing 2.8% lignin has the highest yield stress, even higher than the fully bleached sample containing <1.0% lignin. This could be related with the flexibility of the fibers, which increases the fiber-fiber interactions, thus, increasing the yield stress of the sample (Eberle et al. 2011).

Oscillatory measurements were performed to study the viscoelastic nature of the samples. Initially, three different amplitude sweeps were measured per load, to analyze the deformation of the samples over time and to define the necessary strain (%) within the linear viscoelastic region (LVR) to perform the following frequency sweeps. In a period of 1 hour, samples containing 16.8, 6.9, 2.8, and <1.0% lignin suffered were stable ± 8%. Regarding the storage modulus (G') and loss modulus (G''), measurements were performed at 0.1 % strain, within the LVR of the samples. As can be observed in Figure 4.12 a) and b), G' and G'' were larger as the lignin content of the samples decreased. This indicates the formation of a strong fibrillar network, which agrees with the previous data presented in Figure 4.11. Making use of oscillatory measurements we can also gain

useful insight on the elastic or viscous nature of the suspensions. For all the LCNFs, G' is almost one order of magnitude larger than G'', indicating that the samples present a more predominant elastic nature than viscous.

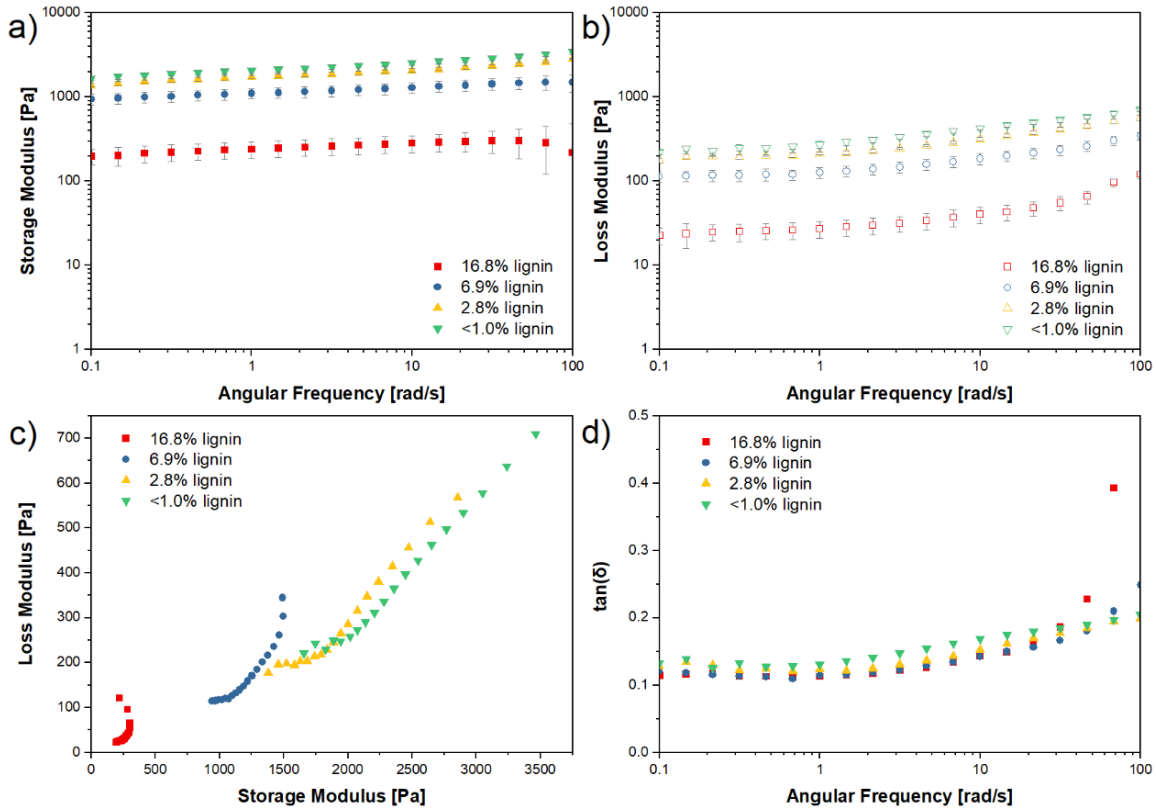

Figure 4.12. Oscillatory frequency sweeps for LCNF samples using a strain of 0.1%; a) storage modulus (G' solid symbols), and b) loss modulus (G'' empty symbols) as a function of angular frequency, c) Cole-Cole plot, and d) loss tangent as function of the angular frequency.

Figure 4.12 c) shows a Cole-Cole plot where G' is plotted against G''. As can be observed, for samples containing 2.8 and <1.0% lignin, their viscoelasticity is almost the same while for samples containing 6.9 and 16.8% lignin their behavior shows greater differences. Regarding the loss tangent as function of the angular frequency (Figure 4.12 d) we can observe that as G' >> G'' then tan(δ) <1 representing an elastic rheological behavior for all the samples.

In the case of non-Newtonian fluids, it was proposed by Cox and Merz (1958) that the apparent viscosity obtained through steady state measurements, could be considered analogous to the complex viscosity obtained by dynamic tests when the angular frequency (ω) match the steady shear rate ($\dot{\gamma}$). This could be particularly useful in situations where the sample inertia affects its permanence within the geometry at high shear rates. Then, the complete behavior of the samples cannot be fully observed in steady shear, but it could be estimated making use of the complex viscosity. In the early 2000's a research group probed the veracity of the hypothesis proposed by Cox and Merz for two polystyrene solutions. However, they also demonstrated that more concentrated solutions do not necessarily follow the same principle (Gleissle and Hochstein 2003). Furthermore, in agreement with this, some research has been published regarding nanocellulosic suspensions, where due to their complicate structure, the complex viscosity tends to be larger than the steady shear viscosity (Shafiei-Sabet et al. 2012; Nazari et al. 2016).

As presented in Figure 4.11, for most of the samples it was not possible to observe the apparent viscosity through all the shear rate range. However, when comparing with the complex viscosity, we observed no correlation of their behavior since the complex viscosity is an order of magnitude larger for all samples, compared to the apparent viscosity (Figure 4.13). As previously reported by Nazari et al. the complex viscosity does not overlap with the apparent viscosity, thus the Cox-Merz rule is not obeyed by LCNF samples with different lignin content. When performing steady shear tests, the microstructure of the suspension breaks down, generating less torque, and as a result, less resistance to flow (Nazari et al. 2016). On the other hand, during linear viscoelastic conditions, the microstructure of the material is not altered, reason why the complex viscosity has larger values.

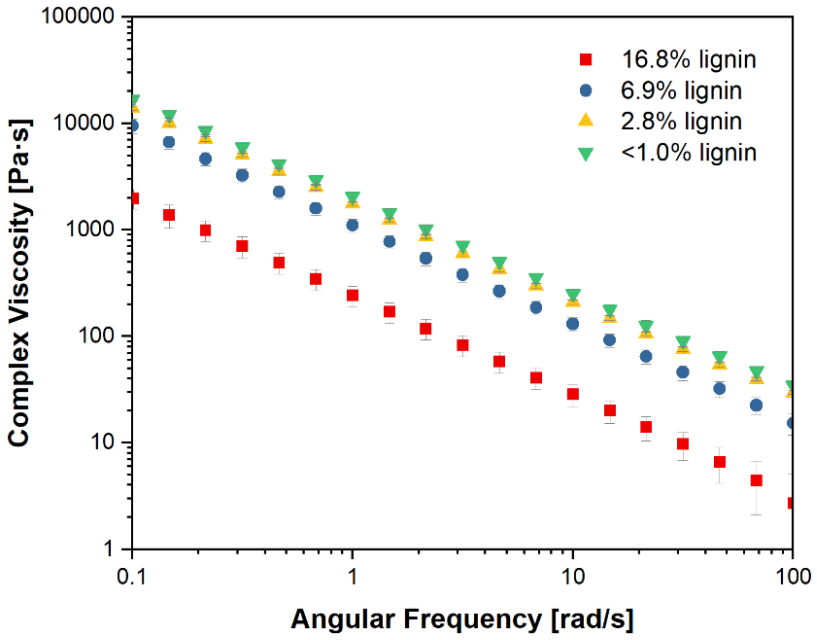

Figure 4.13. Complex viscosity of LCNFs as function of the angular frequency.

In the field of the nanocellulosic materials, many research groups have described the utilization of textured geometries for to avoid wall slip of the samples (Dimic-Misic et al. 2018; Lê et al. 2018). In order to gain a better understanding on how the rugosity/smoothness of the geometries affected the rheological result of the suspensions, a 25 mm diameter sandblasted parallel plate (PP25/P3) was utilized to measure the viscoelasticity of sample containing <1.0% lignin. As a result, we observed a decrease on the viscosity of the sample, compared with the 25 mm diameter smooth parallel plate geometry. Similar to the behavior presented in Figure 4.11, sample came out from the geometry at high shear rates. Thus, the textures geometry did not help to prevent the expulsion of the sample from the geometry, and it also did not overlap with the previous data.

Additionally, in order to corroborate the rheological results obtained by parallel plates 25 mm, the same rheological protocol was performed utilizing a 27 mm diameter concentric cylinders (CC27). Samples were measured at 1.0 % wt. under the same conditions. Although the

rheological characteristics of a sample should be independent of the geometry, our data did not show consistency while using different geometries. Only with the exception of sample containing 16.8% lignin, we observed the formation of big fiber clusters in all the samples, as shown in Figure 4.14.

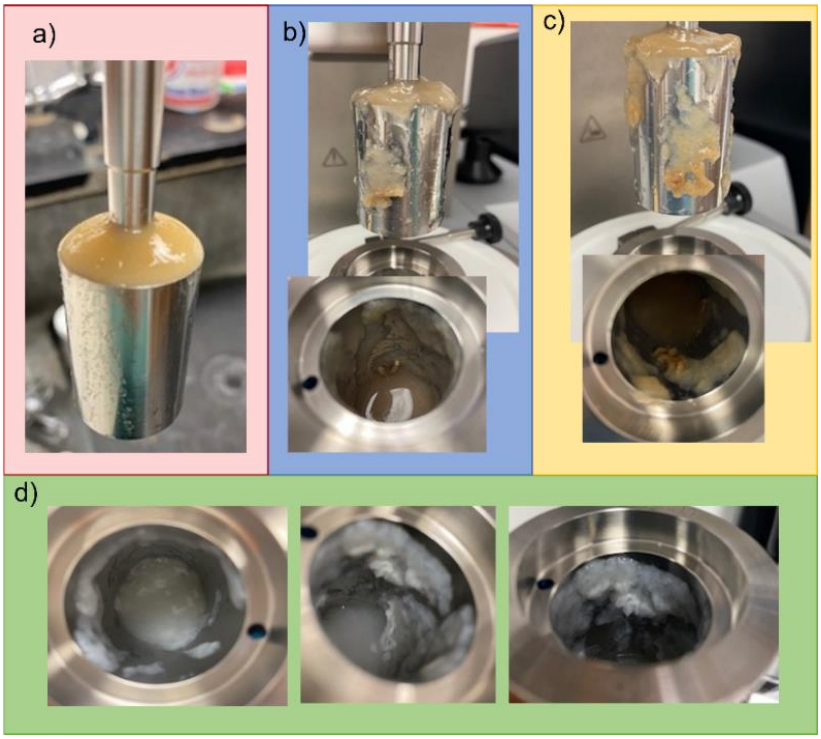

Figure 4.14. Fiber clusters formation using concentric cylinders for samples containing a) 16.8, b) 6.9, c) 2.8, and d) <1.0% lignin.

As mentioned above, the flow curves using CC27 were not consistent with the data corresponding to PP25. Similar results were reported by Nazari et al. (2016) were for the same sample, the data did not intersect when using parallel plate and concentric cylinders. They attribute these results due to the formation of water layer within the geometries and the suspensions, which may have different stability depending on the geometry used.

In addition to the results presented above, we utilized a 50 mm diameter parallel plate (PP50) to measure the same protocol on the samples. Again, the rheological behavior of the sample did not overlap with the previous data measured with geometry PP25 or CC27. Although they are in the same order of magnitude, the results were not consistent. The data acquired using PP50 was consistent with that one from the textured geometry PP25/P3. Data in presented in Figure 4.15. It has been reported that parallel plate geometry generates an inhomogeneous velocity field on the fibers, inducing excessive fiber-fibers interactions, increasing the hurdles to obtain reproducible data (Eberle et al. 2009).

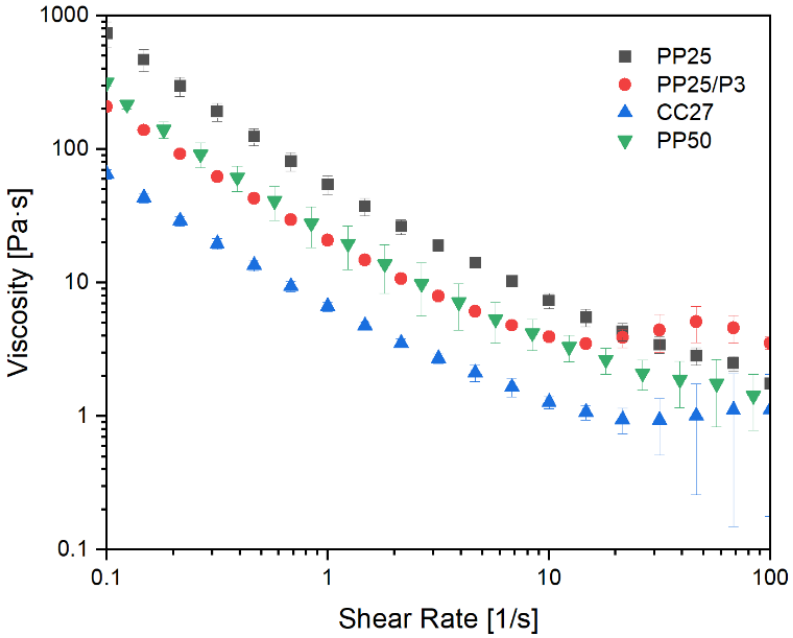

Figure 4.15. Steady-shear flow curves of LCNF containing <1.0% lignin using different geometries.

As observed in Figure 4.14, the formation of big agglomerates on the samples occurs while studying their viscoelastic behavior under rotational measurements. To gain a better insight regarding the formation of agglomerates on the fibers during the measurements, step rate analysis at different shear rates for 15 min were performed. This could give us a better indication about the

critical shear rate at which the fibers on the samples started entangling until reach the formation of the agglomerates. The analysis was performed using PP50 at 1, 5, 10, 40, and 100 s^{-1} as pre-shear. As can be observed in Figure 4.16, at low pre-shears the suspensions does not show a stable behavior over time. It is possible that longer times are needed when using small pre-shear for the sample to be able to accommodate better and to reach a stable viscosity value. Still when analyzing the results at 5 and 10 s^{-1}, the viscosity did not reach a stable value during 15 min. Additionally, for larger pre-shear values (0 and 100 s^{-1}), there is a clear disruption on the curves at the beginning of the measurement indicating that sample may goes out from the geometry at the beginning of te measurement. Then, the viscosity became constant, but it may not be representative of the viscosity of the sample at those pre-shear values.

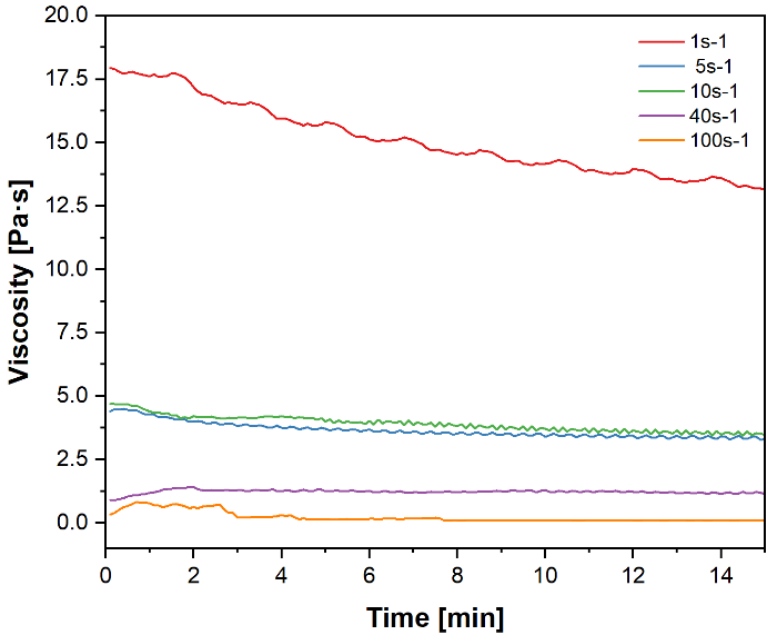

Figure 4.16. Step rate measurements at different shear rates using PP50 for sample containing <1.0% lignin.

While performing the pre-shear analysis, pictures were taken after each measurement, shown in Figure 4.17. After the measurements at 1 s^{-1}, the edges of the sample were in perfect

conditions, no disruption was observed. At 5 and 10 s^{-1} the sample presented an edge disturbance, which could indicate beginning in the formation of agglomerates at low shear rates. At shear rates of 40 and 100 s^{-1} fibers clusters were formed and expelled from the geometry.

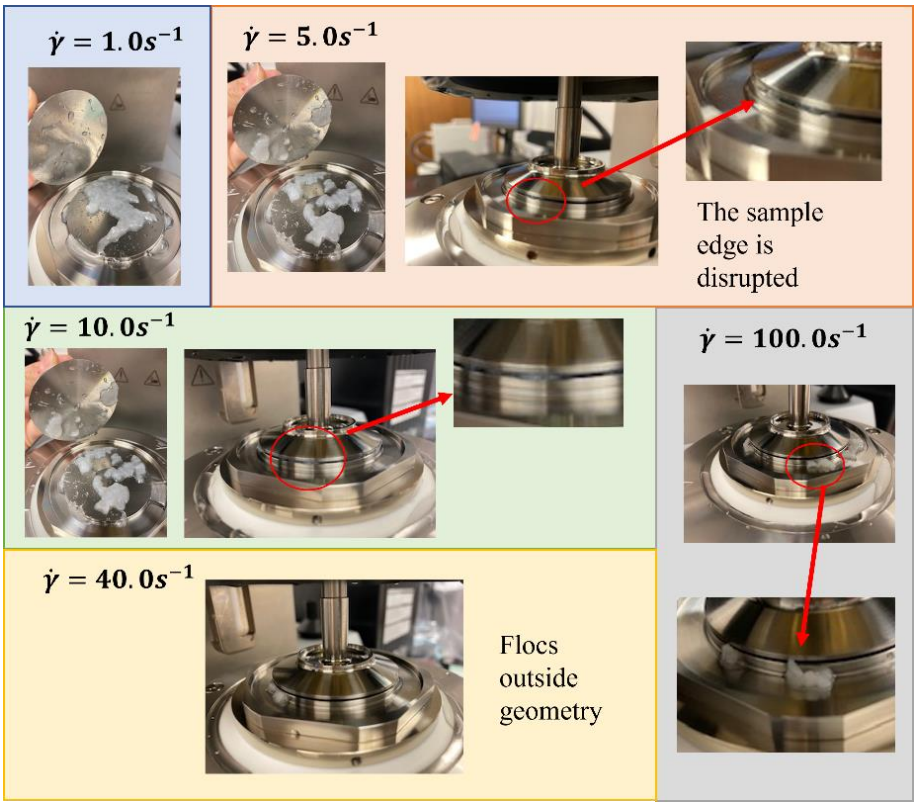

Figure 4.17. Sample containing <1.0% lignin after step rate measurements applying different pre-shear.

When performing rheological measurements, samples may be subjected to long periods of time inside the equipment. Thus, it is important to analyze their stability over the time that the experiment will last. We measured amplitude sweeps every 15 min for 3 hours for samples containing 16.8 and <1.0% lignin. The measurements were stopped once the samples reached a 5 % deformation to maintain them always within the LVR. Then, the deformation of the sample at each step was calculated. The results for twelve amplitude sweep curves were averaged and presented in Figure 4.18. After three hours, sample containing 16.8 and <1.0% lignin deformed

14.5 and 9.6, respectively. For both samples, after three hours there was evaporation of the sample even when utilizing an oil barrier and the water trap system. This was observed due to the change in the suspension edge shape.

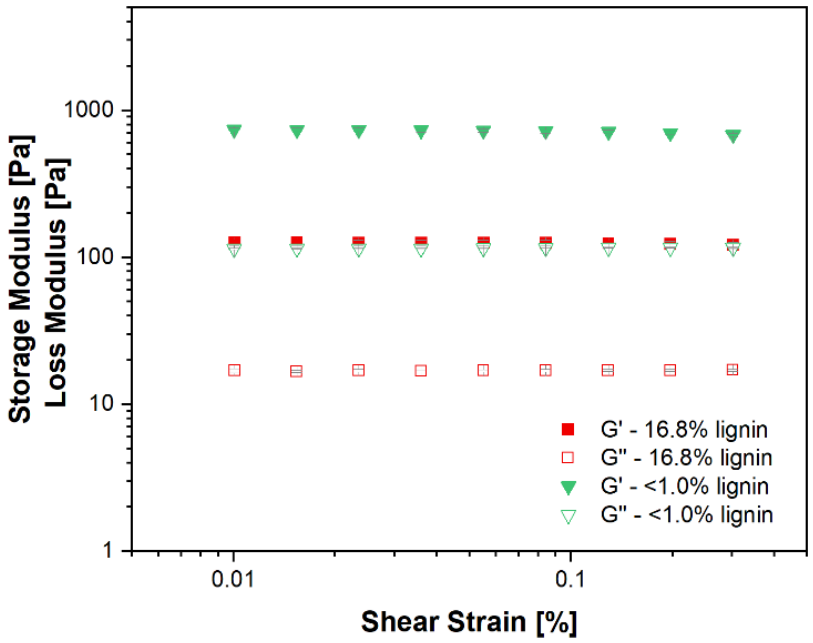

Figure 4.18. Amplitude sweep curves for samples containing 16.8 and <1.0% lignin.

4.5. Conclusions

As frequently mentioned in the literature, acquiring meaningful rheological data on the flow behavior of cellulose nanofibrils is a complicated task. Even in controlled conditions, small differences on how the samples are processed, handled, loaded, among many others, can affect their structure, leading to variations in the observed rheological response.

The morphology of the samples is one of the most important parameters to take into consideration, since this will affect the surface area, and as a result the fiber-fiber interactions, as well as the interactions between the particles and the media. This will be even more affected if we think on samples with different chemical composition. The chemical components present on the

suspensions have been related with their ability to defibrillate; higher lignin content on the samples, gives rise to smaller and better fibrillated suspensions; higher hemicelluloses content, give rise to larger repulsion between the fibers. All of this will influence the flexibility of the fibers, their interactions, and the fibrillar network they may form.

Rheology is a powerful technique, sensitive to all these intermolecular interactions. It is because of this sensitivity, that small changes can generate big variations on the rheology response of the samples. An example of this is the variation of the data when using different geometry, or when variating the gap height. Variations within sample were also observed, meaning that LCNF suspensions are complex and tricky materials.

When comparing the rheological behavior of LCNF samples, it is not possible to standardize them, as each case should be analyzed and interpreted independently. The processing conditions of the CNF fibers have to be considered, as well as the raw material and the different chemical components the suspension may have. Frequently, literature reporting rheological behavior shows flow curves data as a representation of the viscoelastic behavior of a certain suspension, but this information can be misleading, as rheological characterization should not be standardized but customized according to the specific system.

4.6. Literature cited

BBC Publising (2019) 2019 Nanotechnology and Advanced Materials Research Review. In: https://www.bccresearch.com/market-research/nanotechnology/nanotechnology-fuel-cell-research-review.html

Berg JC (2010) An introduction to interfaces & colloids: the bridge to nanoscience. World Scientific, Hackensack, NJ.

Bian H, Chen L, Dai H, Zhu JY (2017) Integrated production of lignin containing cellulose nanocrystals (LCNC) and nanofibrils (LCNF) using an easily recyclable di-carboxylic acid. Carbohydr Polym 167:167–176. doi: 10.1016/j.carbpol.2017.03.050

Chen Y, Fan D, Han Y, et al (2018) Effect of high residual lignin on the properties of cellulose nanofibrils/films. Cellulose 25:6421–6431. doi: 10.1007/s10570-018-2006-x(0123456789().,-volV()0123456789().,-volV)

Cox WO, Merz EH (1958) Correlation of Dynamic and Steady Flow Viscosities. Polym Sci 28:619–622

Debiagi F, Faria-Tischer PCS, Mali S (2020) Nanofibrillated cellulose obtained from soybean hull using simple and eco-friendly processes based on reactive extrusion. Cellulose. doi: 10.1007/s10570-019-02893-0

Dimic-Misic K, Vanhatalo K, Dahl O, Gane P (2018) Rheological Properties Comparison of Aqueous Dispersed Nanocellulose Derived from a Novel Pathway-produced Microcrystalline Cellulose or by Conventional Methods. Appl Rheol 28:64474

Diop CIK, Lavoie J-M (2017) Isolation of Nanocrystalline Cellulose: A Technological Route for Valorizing Recycled Tetra Pak Aseptic Multilayered Food Packaging Wastes. Waste and Biomass Valorization 8:. doi: 10.1007/s12649-016-9585-2

Diop CIK, Tajvidi M, Bilodeau MA, et al (2017) Isolation of lignocellulose nanofibrils (LCNF) and application as adhesive replacement in wood composites: example of fiberboard. Cellulose 24:3037–3050. doi: 10.1007/s10570-017-1320-z

Dufresne A (2019) Nanocellulose Processing Properties and Potential Applications. Curr For Reports 5:. doi: 10.1007/s40725-019-00088-1

Eberle APR, Baird DG, Wapperom P, Vélez-García GM (2009) Obtaining reliable transient rheological data on concentrated short fiber suspensions using a rotational rheometer. J Rheol (N Y N Y) 53:. doi: 10.1122/1.3177348

Eberle APR, Ortman K, Baird DG (2011) Structure and Rheology of fiber suspensions. In: John Wiley & Sons

Espinosa E, Bascón-Villegas I, Rosal A, et al (2019) PVA/(ligno)nanocellulose biocomposite films. Effect of residual lignin content on structural, mechanical, barrier and antioxidant properties. Int J Biol Macromol 141:197–206. doi: 10.1016/J.IJBIOMAC.2019.08.262

Espinosa E, Tarrés Q, Delgado-Aguilar M, et al (2016) Suitability of wheat straw semichemical pulp for the fabrication of lignocellulosic nanofibres and their application to papermaking slurries. Cellulose 23:837–852. doi: 10.1007/s10570-015-0807-8

Fu H, Li Y, Wang B, et al (2021) Structural change and redispersion characteristic of dried lignin-containing cellulose nanofibril and its reinforcement in PVA nanocomposite film. Cellulose 28:7749–7764. doi: 10.1007/s10570-021-04041-z

Gleissle W, Hochstein B (2003) Validity of the Cox–Merz rule for concentrated suspensions. J Rheol (N Y N Y) 47:. doi: 10.1122/1.1574020

Guan Gong (2014) Rheological properties of nanocellulose material. In: Kristiina Oksman, Aji P Mathew, Pia Qvintus, et al. (eds) Handbook of green material. World Scientific, Singapore,

p vi: 139-157

Herrera M, Thitiwutthisakul K, Yang X, et al (2018) Preparation and evaluation of high-lignin content cellulose nanofibrils from eucalyptus pulp. Cellulose 25:3121–3133. doi: 10.1007/s10570-018-1764-9

Hubbe M (2021) When Defects Dominate: Rheology of Nanofibrillated Cellulose Suspensions. BioResources 16:16–18

Iglesias MC, Hamade F, Aksoy B, et al (2021a) Correlations between Rheological Behavior and Intrinsic Properties of Nanofibrillated Cellulose from Wood and Soybean Hulls with Varying Lignin Content. BioResources 16:4831–4845. doi: 10.15376/biores.16.3.4831-4845

Iglesias MC, McMichael PS, Asafu-Adjaye O, et al (2021b) Interfacial interactions between urea formaldehyde and cellulose nanofibrils (CNFs) of varying chemical composition and their impact on particle board (PB) manufacture. Cellulose 28:7969–7979. doi: 10.1007/s10570-021-04007-1

Iglesias MC, Shivyari N, Norris A, et al (2020) The effect of residual lignin on the rheological properties of cellulose nanofibril suspensions. J Wood Chem Technol 40:1–13. doi: 10.1080/02773813.2020.1828472

Isogai A, Saito T, Fukuzumi H (2011) TEMPO-oxidized cellulose nanofibers. Nanoscale 3:71–85. doi: 10.1039/c0nr00583e

Jiang J, Carrillo-Enríquez NC, Oguzlu H, et al (2020) Acidic deep eutectic solvent assisted isolation of lignin containing nanocellulose from thermomechanical pulp. Carbohydr Polym 247:116727. doi: 10.1016/J.CARBPOL.2020.116727

Kimura K, Kikuchi S, Yamasaki S (1999) Accurate root length measurement by image analysis. Plant Soil 216:117–127. doi: 10.1016/j.agwat.2007.03.002

Klemm D, Kramer F, Moritz S, et al (2011) Nanocelluloses: A new family of nature-based materials. Angew Chemie - Int Ed 50:5438–5466. doi: 10.1002/anie.201001273

Larkin PJ (2011) Chapter 9: Unknown IR and raman spectra. In: IR and Raman Spectroscopy - Principles and Spectral Interpretation. Elsevier, United States, pp 177–212

Lê HQ, Dimic-Misic K, Johansson LSL, et al (2018) Effect of lignin on the morphology and rheological properties of nanofibrillated cellulose produced from γ-valerolactone/water fractionation process. Cellulose 25:179–194. doi: 10.1007/s10570-017-1602-5

Macosko CW (1994) Rheology: Principle, measurements, and applications. WILEY-VCH Verlag GmbH &Co., Canada

Mezger TG (2014) Applied Rheology with Joe Flow on Rheology Road, 4th edition. Anton Paar GmbH, Austria

Moberg T, Sahlin K, Yao K, et al (2017) Rheological properties of nanocellulose suspensions: effects of fibril/particle dimensions and surface characteristics. Cellulose 24:. doi: 10.1007/s10570-017-1283-0

Moon RJ, Martini A, Nairn J, et al (2011) Cellulose nanomaterials review: structure, properties and nanocomposites. Chem Soc Rev Chem Soc Rev 40:3941–3994. doi: 10.1039/c0cs00108b

Nazari B, Kumar V, Bousfield DW, Toivakka M (2016) Rheology of cellulose nanofibers suspensions: boundary driven flow. J Rheol (N Y N Y) 60:1151–1159. doi: 10.1122/1.4960336

Popescu CM, Tibirna CM, Raschip IE, et al (2008) Bulk and Surface Characterization of Unbleached and Bleached Softwood Kraft Pulp Fibres. Cellul Chem Technol 42:525–547

Rojo E, Peresin MS, Sampson WW, et al (2015) Comprehensive elucidation of the effect of residual lignin on the physical, barrier, mechanical and surface properties of nanocellulose

films. Green Chem 17:1853–1866. doi: 10.1039/C4GC02398F

Segal L, Creely JJ, Martin AE, Conrad CM (1959) An Empirical Method for Estimating the Degree of Crystallinity of Native Cellulose Using the X-Ray Diffractometer. Text Res J 29:786–794. doi: 10.1177/004051755902901003

Shafiei-Sabet S, Y. Hamad W, G. Hatzikiriakos S (2012) Rheology of Nanocrystalline Cellulose Aqueous Suspensions. Langmuir 28:17124–17133. doi: 10.1021/la303380v

Solala I (2011) Mechanochemical reactions in lignocelluloseic materials. Dissertation, Aalto Universty

Solala I, Iglesias MC, Peresin MS (2019) On the potential of lignin-containing cellulose nanofibrils (LCNFs): a review on properties and applications. Cellulose 27:1853-1877. doi: 10.1007/s10570-019-02899-8)

Yang H, Yan R, Chen H, et al (2007) Characteristics of hemicellulose, cellulose and lignin pyrolysis. Fuel 86:1781–1788. doi: 10.1016/j.fuel.2006.12.013

Yuan T, Zeng J, Wang B, et al (2021) Lignin containing cellulose nanofibers (LCNFs): Lignin content-morphology-rheology relationships. Carbohydr Polym 254:117441. doi: 10.1016/J.CARBPOL.2020.117441

5. Interfacial interactions between urea formaldehyde and cellulose nanofibrils (CNFs) of varying chemical composition and their impact on particle boards (PBs) manufacture

This chapter has been published in "Iglesias, M. C., McMichael, P. S., Asafu-Adjaye, O., Via, B. K., & Peresin, M. S. (2021). Interfacial interactions between urea formaldehyde and cellulose nanofibrils (CNFs) of varying chemical composition and their impact on particle board (PB) manufacture. *Cellulose*, 1-11."

5.1. Abstract

Wood-based panels are commonly used as building materials for interior and exterior purposes. Their production and utilization have increased in recent decades due to the useful properties that they posess. Adhesive-bonded products comprise up to 80% of the wood alternatives on the global market, and of that, urea-formaldehyde (UF) makes up approximately 81% of the resins used. To improve UF performance, the utilization of microfibrillated cellulose has been demonstrated to be effective. However, further understanding of the mechanisms of the interactions is of relevant importance.

In this work, we studied interfacial interactions between UF with bleached (BCNFs) and unbleached (LCNFs) cellulose nanofibrils using quartz crystal microbalance with dissipation monitoring (QCM-D) technique, observing the superior performance of lignin-containing CNF. Additionally, the surface free energies were investigated using contact angle Measurements (CA), showing a decrease of the values mainly when utilizing LCNF, which was later correlated with the wettability properties of the PBs. PBs with different adhesive/CNF formulations were produced, showing larger improvements when adding LCNF in terms of modulus of elasticity (MOE), modulus of rupture (MOR), and internal bonding (IB).

To gain a better understanding of the interactions between CNF and UF, both CNFs were fully characterized in terms of morphology, chemical composition, charge density, as well as thermal and colloidal stability.

5.1.1. Index words

Cellulose nanofibrils, LCNF, urea formaldehyde, QCM-D, interfacial interactions, cellulosic nanofibers, wood adhesives, particleboard, lignin-containing cellulose nanofibrils.

5.1.2. Project partners

This work was supported by the Wood-Based Composites Center, a National Science Foundation Industry/ University Cooperative Research Center (Award 1624536-IIP). Additional support from the USDA National Institute of Food and Agriculture, Hatch program (ALA013-384 17003), McIntire-Stennis program (1022526), and the School of Forestry and Wildlife Sciences at Auburn University is much appreciated.

5.2. Introduction

Wood-based panels are commonly used as building materials both for interior and exterior purposes. Their production and utilization has been increasing over the past few decades due to their versatility, effectiveness, and the environmental benefits they present (Hansted et al. 2019). Among the wood-panel alternatives, particle board, fiber board, and oriented strand board (OSB) are some of the most frequently used (Ayrilmis et al. 2016; Hansted et al. 2019). Specifically, for particle board manufacturing, three layers are normally formed where larger particles are used for the core layer, improving the mechanical properties. Thinner particles are used for the two outer layers in order to obtain a smooth surface (Hansted et al. 2019).

Adhesive-bonded products make up 80% of the wood products on the global market, and of that, urea-formaldehyde (UF) makes up more than 81% of the resins used (Lei et al. 2008).

It was reported by the Food and Agriculture Organization Corporate Statistical Database (FAOSTAT) that in 2019, the United States produced 4,346,542 m^3 of particles boards, being the main producer in North America (FAOSTAT 2019).

UF is a commonly used resin that holds together the particles and confers the required mechanical properties to the panel for its final application. Along with UF, other formaldehyde-based resins are primarily used due to the combination of their effectiveness and relatively low cost (Amini et al. 2017), as well as their ease of application and lack of color (Salari et al. 2013). One of the most notable disadvantages of UF when used for interior particle board is that this adhesive is well known as a carcinogen and its use poses a human health issue during both wood composite manufacturing and use (Diop et al. 2017). The emission of formaldehyde is most often caused by unreacted formaldehyde trapped as a gas in the structure, as well as formaldehyde dissolving in water that enters the panel (Salari et al. 2013). Despite the high toxicologic risks when using this adhesive, the global formaldehyde business is expected to reach 36.6 million tons at the end of 2026, due to the construction market being the biggest consumer of these resins (Transparency Market Research 2018).

Other than adjusting the urea to formaldehyde ratio, various fillers can be utilized to reduce the amount of resin needed. Common fillers must be insoluble in UF, these include cellulose, silica, talc, and chalk (Claub et al. 2011; İstek et al. 2020). Traditional fillers are made of larger particles, limiting mobility and making homogenization difficult (Dukarska and Czarnecki 2016). Thus, smaller particles, i.e. nano-sized, can induce such properties as improved mechanical strength and thermal resistance (Dukarska and Czarnecki 2016), as well as lower resin consumption, thus

substantially reducing costs. (Lei et al. 2008). Regarding nanoparticles used as filler for wood adhesives, nanoclay and nanosilica are among those reported in the literature (Lei et al. 2010; Zahedsheijani et al. 2012; Salari et al. 2013; Dukarska and Czarnecki 2016).

As the most abundant natural polymer in the world (Klemm et al. 2005), and due to the continuous improvement of technology designed to isolate materials at the nanoscale, cellulose has been positioned to be used in a number of high-performance applications. When reducing its size into the nanoscale, cellulose fibers can be separated into small particles generally known as nanocellulose (Klemm et al. 2011; Moon et al. 2011; Lavoine et al. 2012). These nanoparticles can be obtained by different approaches; the most commonly used are chemical and mechanical treatments to obtain cellulose nanocrystals (CNCs) and cellulose nanofibrils (CNFs), respectively. In recent years, nanocellulose has been increasingly studied for its many intriguing properties and immense potential. For example, micro and nano fibrillated cellulose have been recently investigated as fillers for wood adhesives in particle boards (Mahrdt et al. 2016; Hansted et al. 2019; Morais Júnior et al. 2020), OSB (Veigel et al. 2011, 2012), and plywood (Kawalerczyk et al. 2020). Veigel et al. (2011) studied the effect of the addition of CNF fibers into UF for wood beams and they determined that by adding 2 wt.% of CNF, the adhesive toughness increased up to 45 %. Following the same approach, Veigel et al. (2012) reported the effect of nanocellulose reinforced UF and melamine urea formaldehyde (MUF) adhesives for particle boards and OSB manufacture. They demonstrated that by adding 1 wt.% of CNF, the fracture energy and fracture toughness can be improved for both wood panels. In addition, Mahrdt et al. (2016) described the addition of microfibrillated cellulose (MFC) to UF for particle boards resulting in better mechanical performance. These results were determined to be due to the larger particle size when adding MFC, improving the adhesive availability for bonding with other particles. Recently,

Kawalerczyk et al. 2020, studied the effect of CNC addition on plywood panels to react with phenol formaldehyde (PF) resins. They found that 3 g of CNC to 100 g dry mass of resin was the optimum ratio to assist in the effective transference of stress along the bond line, and they observed improved mechanical properties of the panels at that ratio.

In attempts to reduce the adhesive consumption, some research groups have worked on the production of wood panels using nanocellulose as a complete replacement for commercial adhesives. Diop et al. (2017) demonstrated that using 20% unbleached CNF at 3 wt.% of consistency on fiber board panels improved the internal bonding and modulus of rupture when compared with 15 and 25 % CNF addition. Recently, Kojima et al. (2018) did similar work on particle boards, showing that the higher the amount of CNF added to the panel, the better the properties. As a negative aspect, when comparing particles boards made only with UF or PF, they concluded that the properties of the board with 20 wt.% CNF corresponded to those of the boards with 1 wt.% UF or PF.

Although several groups have studied the addition of CNFs or MFC to wood panels showing how the properties can be improved, the actual interactions between UF and CNF, which may help to improve the final properties of the boards, are unknown. The objective of this work was to demonstrate how UF resins and CNF from bleached and unbleached cellulose pulps interact in real time by using quartz crystal microbalance with dissipation monitoring (QCM-D).

5.3. Experimental

5.3.1. Materials

5.3.1.1. Chemicals

Commercial UF containing 65 % solid content was provided by Hexion. Ammonium sulfate [$(NH_4)_2SO_4$] with a molecular weight of 132.14 g/mol was purchased from MilliporeSigma Lot: AM1256517 846, hydrochloric acid (HCl) was purchased from Macron® batch number: 0000162657, and sodium hydroxide (NaOH) (50 % w/w) from J.T. Baker Lot: 642022 CAS 3727-03. The water used was deionized and purified with a Thermo Scientific Barnstead Nanopure (18.2 MΩ cm).

For charge density measurements, cationic polymer polydimethyl diallyl ammonium chloride (p-DADMAC) 0.001 N, sample number 920, and anionic polymer polyvinyl sulfuric acid potassium salt (PVSK) 0.001 N, sample number 919, were purchased from BTG.

5.3.1.2. Cellulose pulps

For the purposes of this work, two never dried samples from softwood, bleached and unbleached, were used as raw material for nanocellulose production. Cellulose pulps were kindly provided by a US kraft mill.

5.3.1.3. Cellulose nanofibrils (CNFs) production

Cellulose nanofibrils were produced at the Forest Products Development Center of Auburn University. For this purpose, celluloses pulps were washed using HCl until they reached pH=3 and left for 30 min at that pH in order to eliminate possible metallic particles. Then, pulps were washed using DI water until a pH of 5 was reached. Afterwards, the pH was adjusted to 9 using NaOH and

left for 30 min to convert the fibers into their sodium form (Horvath et al. 2006). Finally, cellulose pulps were washed using DI water until the conductivity of the filtrate reached < 5µS/cm.

Once the pulps were properly washed, a suspension at 2 wt.% of consistency was prepared. The suspensions were then fibrillated until reaching the nanoscale using the Masuko Supermasscolloider (MKZA-10-15J), allowing the materials to defibrillate. After the mechanical process, a gel-like consistency was obtained. Sodium azide was incorporated into the samples to avoid microorganism growth. Samples were stored in the cold room at 5 ºC until further use.

5.3.2. Methods

5.3.2.1. Characterization of CNF suspensions

i. Zeta-potential and charge density

The colloidal stability of the suspensions was assessed by measuring charge density and zeta potential. pH was measured using a SympHony Benchtop Multi Parameter Meter B30PCI (VWR®) equipped with pH and conductivity electrodes. Measurements were repeated 15 times and averaged. Zeta potential was measured using an Anton Paar Litesizer 500 (Graz, Austria). Samples were diluted at 0.01 %wt. and sonicated for 2 min with a cold bath to avoid heating of the samples. A Vibra Cell sonicator (Newtown, CA) was utilized with 20 KW and 20 % of amplitude to promote a better dispersion of the colloidal suspension. Charge density of the fibers was measured following the method described in Iglesias et al. 2020. Both zeta potential and charge density were measured six times, with the pH of suspensions at 6.5. A statistical analysis ANOVA was performed and reported.

ii. Thermal stability

The thermal behavior of the samples was measured by Thermogravimetric Analysis (TGA). Dry samples were tested in aluminum pans in a TGA-50 from Shimadzu (Kyoto, Japan). Samples were heated from room temperature to 600 °C at a rate of 10 °C/min under a nitrogen atmosphere. Data was processed with ta60 software, version 2.11 from Shimadzu. The sample weight was approximately 15 mg for all CNFs. Measurements were performed in duplicate.

iii. Chemical composition

Chemical and structural composition of the samples was analyzed by Fourier-transform infrared spectroscopy with attenuated total reflectance accessory (FTIR-ATR) using a PerkinElmer Spotlight 400 FT-IR Imaging System (Massachusetts, US) with an ATR accessory. Before the measurements, a background spectrum was recorded for each unique sample. Afterwards, all spectra were collected from 400 to 4000 cm^{-1} with a 4 cm^{-1} wavenumber resolution after 64 continuous scans. The baseline was corrected, and the data was processed with Spectrum 6 Spectroscopy Software (PerkinElmer, Massachusetts, US). Measurements were performed by duplicate.

iv. Morphology

The morphology of the samples was studied utilizing atomic force microscopy (AFM). For AFM imaging, silicon surfaces were cleaned using UV ozone for 30 min and submerged for 15 min into 0.1 wt. % polyethylenimine (PEI), which was used as an anchoring solution. CNF suspensions were diluted at 0.2 wt.% and sonicated for 2 min using a Vibra Cell sonicator (Newtown, CA) with 20 KW and 20 % of amplitude to promote delamination and prevent their agglomeration, with a cold bath to avoid heating of the samples. Suspensions were deposited onto a silica surface by spin coating technique. Images were obtained in tapping mode using an Anton

Paar TOSCATM 400 (Graz, Austria) with a silicon cantilever. Image size was 5 μm x 5 μm. Images were processed with Gwyddion software 2.49 (SourceForge).

v. Rheological behavior

Rheological properties of the cellulose nanofibrils were measured using a strain-controlled rotational rheometer (Physica MCR302, Anton Paar). Rheological measurements were performed on a 25 mm diameter parallel plate fixture geometry. The sample was loaded on the rheometer and allowed to equilibrate for 10 min before investigation of rheological properties. Tests were performed with a solvent trap of deionized water to prevent water loss due to extensive testing. A preliminary shear protocol was performed at a shear rate of 0.001 s^{-1} for 20 min to prevent structure change before measuring oscillatory dynamics. The dispersion microstructure was investigated with amplitude sweeps to determine the linear viscoelastic region (LVR) without severe structure deformation and frequency sweeps at 0.1 % strain within LVR to measure storage (G') and loss (G") moduli across a range of angular frequencies. Finally, flow curves to investigate structure deformation under shear across a range of shear rates were measured. Measurements were performed at a constant temperature of 25 ºC.

5.3.2.2. Interactions between UF and cellulose nanofibrils

i. Surface contact angle measurements (SCA)

Surface free energy was determined by contact angle measurements using a Dataphysics OCA50 optical goniometer with DDE/3 (Filderstadt, Germany). Measurements were performed using three liquids with different polarities, namely ethylene glycol, diiodomethane, and water. The dispense drop was 2 μL in volume, at a fast speed. Contact angle results were utilized for surface free energy calculations utilizing the acid-base model.

ii. Quartz Crystal Microbalance with Dissipation Monitoring (QCM-D)

Interactions between UF, bleached and unbleached CNFs were studied with a QSense Analyzer from Biolin Scientific (Västra Frölunda, Sweden). The basic principle of the QCM-D is the measurement of the changes in frequency (Hz) of a piezoelectric sensor that has a base resonance of 5 MHz and has overtones of 15, 25, 35, 45, 55 and 75 MHz; changes in the frequency resonance are proportional to a change in mass on the sensor, as only the surface is interacting with a flow of matter, and those changes are likewise correlated to the mass adsorption on the sensors surface (Example 1991; KSV Instruments Ltd 2002; Voinova et al. 2002).

All measurements were performed at 25 °C with a constant flow of 100 µL/min. Gold crystals were previously coated with the different types of nanocelluloses utilizing the same method explained in Section 2.4.4. Once the sensors were coated, in situ experiments were performed inside the QCM-D chambers.

In the particle board industry, a hardener is commonly used to improve the properties of the final product. For this purpose, ammonium sulfate [$(NH_4)_2SO_4$] is commonly mixed with water and the adhesive for an effective wood particle impregnation. In our study, we prepared a solution of adhesive and hardener and analyzed the interactions between this mixture and the different nanofibers. Only the changes of the third overtone are presented.

5.3.2.3. Particle boards production and characterization

i. Particles board (PB) manufacturing

Particle boards with 8.4% of adhesive loading, with respect to the total dry wood particle weight, were manufactured. Only 1% of UF was replaced using BCNF or LCNF, the two different types of nanocelluloses previously characterized. Additionally, 0.6% of wax and 3% of hardener were used based on the wood particles and adhesive weights, respectively. The components

comprising the liquid phase of the PBs production were all mixed together and then sprayed on the wood particles. The initial moisture content (MC) of the wood particles was 3%, while at the end of the spraying process and before pressing, the MC was ~8.9±0.6% for all the samples. The target density was 0.6 g/cm^3, in order to produce high density panels.

Wood particles were placed inside a concrete mixer and covered with a vinyl plastic to avoid losing material while mixing. Then, the liquid phase was sprayed using a spray gun while the wood particles were continuously rotated in the concrete mixer.

After the mixing process, wood panels were hand-formed using a mold with dimensions 40 cm x 40 cm on top of a metal sheet. After forming the wood mat, a second metal sheet was placed on top of the mat. Two metallic stoppers with 1.1 cm of thickness were used during the pressing at each side of the wood mat, ensuring that the thickness of the panels remained constant. Finally, wood mats were pressed using a Wabash hydraulic press (model 50-24-2TM) for 3 min at 2.5 MPa and 200 ºC. Wood panels were stored in a conditioning room at a temperature of 22.5 ºC and 55.2 % of relative humidity, until characterization. For practical purposes, panels were denoted as (i) UF, for PB containing only UF, (ii) UF/BCNF for PB containing 1% of bleached CNF, and (iii) UF/LCNF for PB containing 1% of unbleached CNF.

ii. PBs characterization

For water absorption (WA), thickness swelling (TS), modulus of elasticity (MOE) and modulus of rupture (MOR) samples of 30.5 cm of length and 8 cm of width were used. WA and TS were measured following Standard ASTM D1037-12. Samples were pre-labeled in eight points which were equally spaced at the edge of each side and 2.5 cm from the edge to the center of the panel. Samples were fully submerged into tap water and properly secured using extra weight to keep them always underwater. After 2 hours, the samples were removed, and the excess water was

drained. Additionally, a paper towel was used to carefully eliminate the remaining water on the surface of the panels. PBs were weighted and the thickness was measured in the same eight points as at the beginning.

WA was calculated using the weight of the panels before and after being submerged in water (equation 5.1). TS was calculated utilizing the thickness before and after the panels were introduced into the water (equation 5.2).

$$\%\mathrm{WA} = \frac{\mathrm{Weight_{final}}\text{-}\mathrm{Weight_{initial}}}{\mathrm{Weight_{initial}}} \text{ x } 100 \quad (5.1)$$

$$\%\mathrm{TS} = \frac{\mathrm{thickness_{final}}\text{-}\mathrm{thickness_{final}}}{\mathrm{thickness_{final}}} \text{ x } 100 \quad (5.2)$$

To measure the mechanical performance of the panels, a Zwick/Roell Z010 equipped with different heads was utilized to measure MOE, MOR, and internal bonding (IB). Samples with dimensions of 5 cm x 5 cm were utilized for IB measurements. Tests were performed by quadruplicate for MOE, MOR TS, and WA, and eight times for IB; the average and standard deviations were calculated and reported.

5.4. Results and discussion

5.4.1. CNF characterization

5.4.1.1. Zeta-potential and charge density

Table 5.1 summarizes solid content, pH, zeta potential, and charge density of the two different CNFs. For samples containing lignin, the charge density value was larger than for the bleached CNF. This could be explained due to the presence of lignin, where more carboxylic and

OH groups are present within the surface of the fibers (Crestini et al. 2017). Regarding zeta potential, BCNF present a slightly higher value than LCNF. Zeta potential is related not only to the solid particles but also to the liquid of the media, describing the charging behavior at the solid-liquid interface. Two main mechanisms affect the charge between electrochemical double layer charges; (i) acid-base reactions between the liquid media and the functional groups present on the solid, and (ii) the absorption of water ions. Although samples containing lignin present higher numbers of functional groups, this excess can inhibit the complete dissociation of acid-based groups or their protonation, thus, reducing their zeta potential, as we observed in Table 5.1. This inhibition occurs due to the repulsions between the functional charged groups on the surface of the fibers (Thomas Luxbacher 2014). Statistical analysis ANOVA (α=0.05) reveals a significant difference between zeta potential and charge density of bleached and unbleached sample.

Table 5.1. Dry content, pH, Zeta potential, and charge density for bleached and unbleached CNFs.

Property	**Unit**	**BCNF**	**LCNF**
Dry Content	wt.%	2.00±0.01	2.00±0.10
pH		6.50±0.01	6.51±0.10
Zeta Potential	mV	-30.3±0.80	-27.1±1.11
Charge density	µeq/g	258.9±14.9	302.2±15.0

5.4.1.2. Thermogravimetric Analysis (TGA)

The thermal decomposition and the derivative of the CNFs are presented in Figure 5.1. Similar behavior can be observed for both samples. T_{max} can be related with the velocity at which the sample decomposed, which can be observed as the maximum temperature value of the derivative (dm/dT). In this study, $T_{max\ (BCNF)}$ = 340.5 ºC and $T_{max\ (LCNF)}$ = 334.1 ºC. Additionally, T_{onset} of both samples was similar: this is considered as the temperature at which the mass loss of the sample becomes more apparent (Nair and Yan 2015).Specifically, $T_{onset\ (BCNF)}$ = 291.4 ºC and

$T_{onset\ (LCNF)}$ = 293.5 ºC. These results are in agreement with those reported in the literature for samples containing different amount of lignin (Herrera et al. 2018; Iglesias et al. 2020). Observing the derivatives curves, LCNF shows a small jump at 270 °C. It has been described in the literature that lignin has a broad range of decomposition temperature due to the presence of different groups in its structure (Yang et al. 2007; Brebu and Vasile 2010). Thus, this small peak may correspond to the presence of lignin.

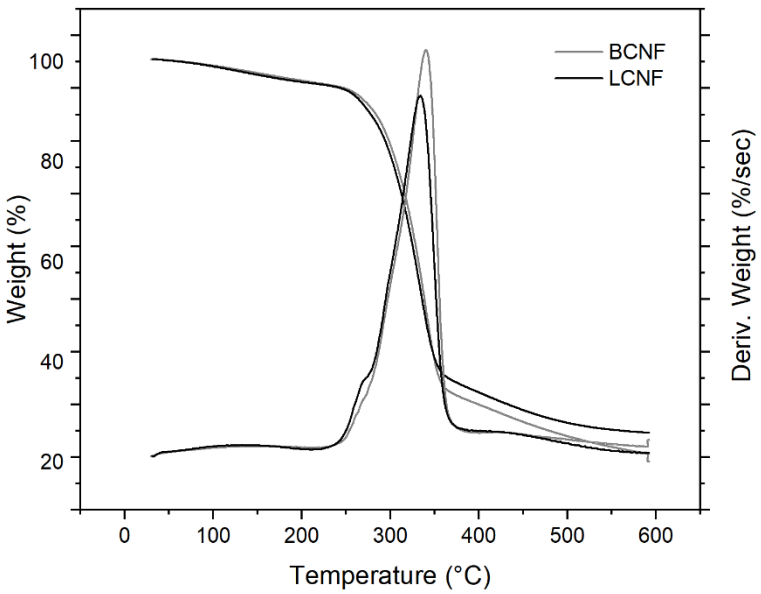

Figure 5.1. TGA spectra and weight derivative of BCNF (grey) and LCNF (black) measured in nitrogen atmosphere.

5.4.1.3. Fourier-transform infrared spectroscopy with attenuated total reflectance accessory (ATR-FTIR)

Figure 5.2 shows the FT-IR spectra for BCNF and LCNF nanofibers in the range of 400 - 4000 cm^{-1}. The peak at 1029 cm^{-1} was utilized as a parameter to normalize the spectra. Such a peak corresponds to the C-O stretching vibrations of lignin and polysaccharides (Huang et al. 2016) and showed a higher intensity for the bleached sample, which could be attributed to better

mobility of the C-O due to the absence of lignin. As can be observed when comparing the graphs, both samples present a FT-IR spectrum that is very similar, since no chemical treatment was used. Similar results are reported in the literature for samples with different lignin contents (Iglesias et al. 2020).

In the fingerprint region the main differences between the samples can be observed at 1160 cm^{-1} due to the C-O-C stretching of the pyranose ring, corresponding to the cellulose structure, showing a larger intensity for the BCNF samples. Additionally, at 1104 and 897 cm^{-1} there are stretching vibrations corresponding to C-OH and C-C, respectively (Yang et al. 2007).

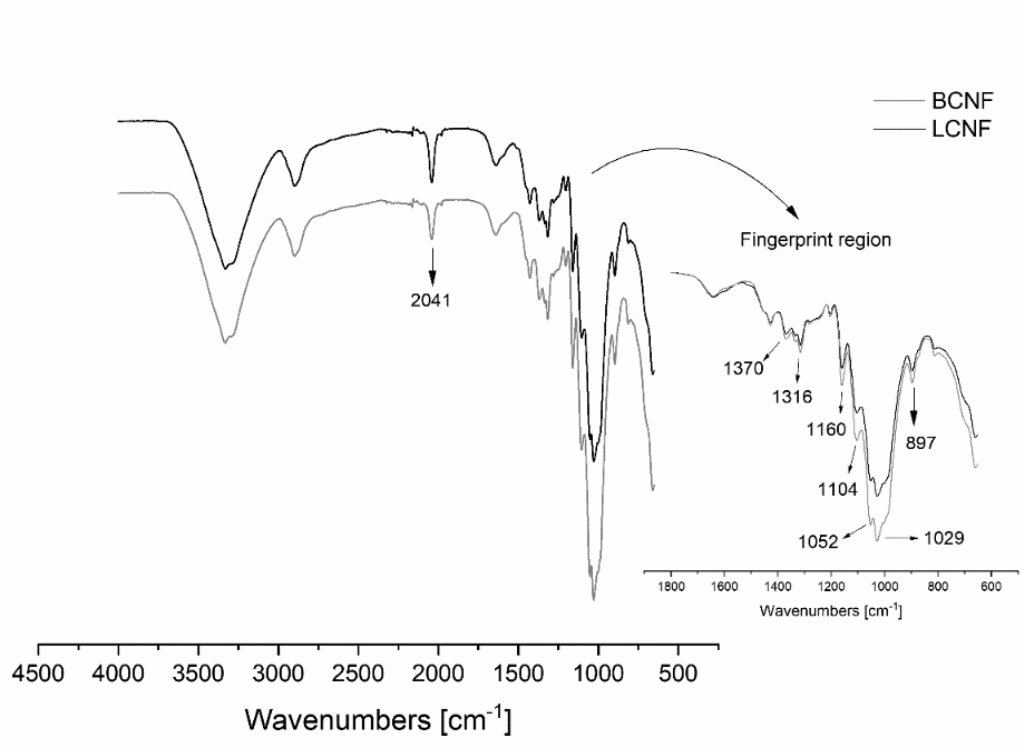

Figure 5.2. FT-IR spectra for BCNF (grey) and LCNF (black).

5.4.1.4 Microscopy

The morphology of the fibers observed in Figure 5.3 was measured by atomic force microscopy (AFM). It can be observed that the defibrillation of the samples; in general, are long

fibers with only a few nanometers present in the diameter dimension. Both samples present an entangled structure.

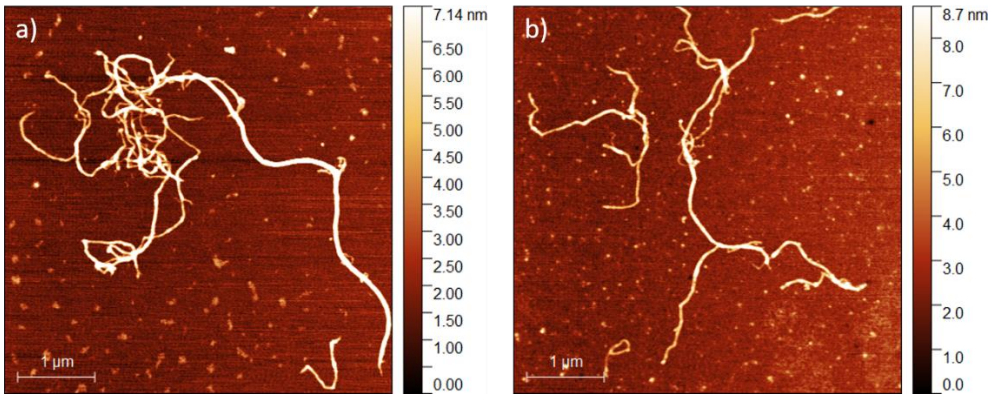

Figure. 5.3. AFM topography images of a) BCNF and b) LCNF.

5.4.1.5. Rheology

Rheological measurements assessed the viscous behavior of the samples. Figure 5.4 shows the flow curves for each sample. At lower shear rates, LCNF containing lignin shows a viscosity almost four orders of magnitude larger than BCNF. This could be due to the presence of lignin, which inhibits the movement of the fibers, and thus, increases viscosity. At high shear rates, both samples show similar viscous behavior, which may be due to the alignment of the fibers as the shear rate increases. Similar rheological behaviors have been reported in the literature for samples with different lignin contents (Iglesias et al. 2020). The reduction of the viscosity as the shear rate increase is particularly beneficial when spraying the samples into the wood particles during the PBs manufacturing process.

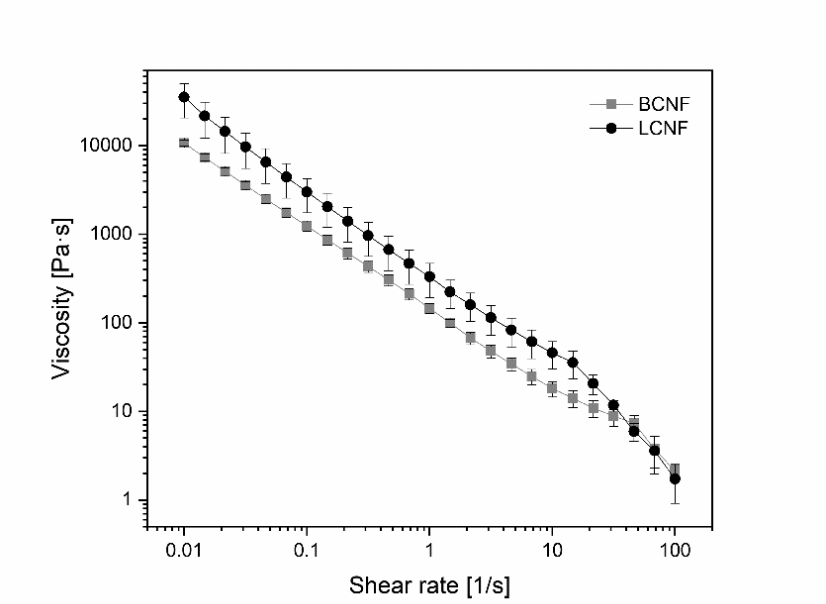

Figure 5.4. Flow curve of BCNF (grey square), and LCNF (black circles).

5.4.2. Interactions studies between UF and cellulose nanofibrils

5.4.2.1. Surface contact angle measurements (CAM)

Initially, the surface free energy of the UF and the two different nanocelluloses, BCNF and LCNF, was measured showing values of 43.4, 44.7, and 42.3 mN/m, respectively. In order to observe how the interaction between UF/BCNF and UF/LCNF affects the surface free energy, silicon surfaces were coated with layers of both components and measured. The obtained data showed that there is a decrease of the surface free energy when incorporating CNF to the UF. Surface free energy of UF/BCNF and UF/LCNF were 43.2 and 42.8 mN/m, respectively. LCNF shows a greater decrease of the surface free energy of the adhesive compared with the BCNF sample. This could be related to the hydrophobic characteristics of lignin (Solala et al. 2019) present in the LCNF sample.

5.4.2.2. Quartz Crystal Microbalance with Dissipation Monitoring (QCM-D)

Figures 5.5 a) and b) show the interaction between BCNF and LCNF and a mixture of UF with hardener, respectively. We can observe in both graphs the irreversible mass absorption on the surface after rinsing the system with water.

BCNF and LCNF surfaces prepared by spin coating were first stabilized in Milli-Q water, allowing the surface to hydrate. Once the systems were stable, a solution of UF, hardener, and water was flowed through the equipment channels and an apparent decrease of the frequency was observed. To model the surfaces, Broadfit mathematical model was applied, and the mass absorbed onto the surface was calculated.

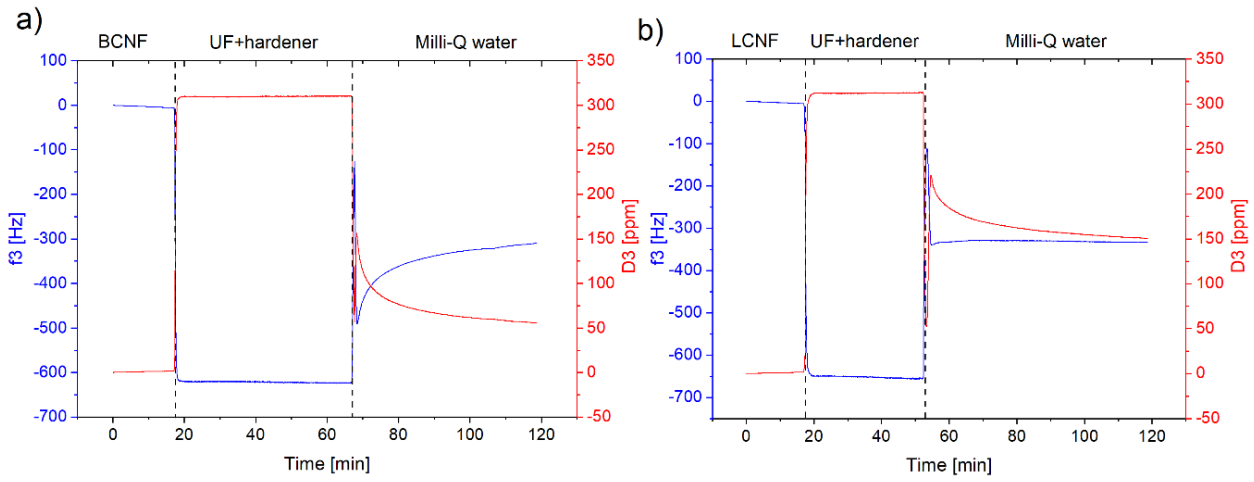

Figure 5.5. QCM-D spectra interactions between model surfaces of a) BCNF and b) LCNF, with a mixture of UF and hardener both irreversibly absorbed after rinsing with Milli-Q water.

For BCNF, the change in frequency was $\Delta f = -311.1$ Hz which was converted to 5.6 µg/cm^2. Additionally, after rinsing with water, LCNF presented a $\Delta f = -332.2$ Hz, meaning that 5.9 µg/cm^2 of mass remained irreversibly absorbed on the surface of the sensor.

As we can observe, LCNF showed a slightly higher interaction with the adhesive solution, compared with the BCNF sample. By analyzing the chemical groups present on each type of fiber,

LCNF is composed of not only cellulose and hemicelluloses, but also lignin. It is well known that the structure of kraft lignin possesses hydroxyl, carboxyl, and epoxy groups (Crestini et al. 2017) which may have strong interactions with the amide, carbonyl and OH groups present in the UF resin (Akinterinwa et al. 2020).

5.4.3. PBs characterization

Mechanical and physical testing of PBs were measured in quadruplicate, and the results were averaged. The averaged mechanical and physical properties were analyzed by one-way analysis of variance respectively, followed by a Tukey test for mean separation. Particleboard properties improved with the addition of 1% CNF (Table 5.2) and the mean differences were significant ($p < 0.05$). Principally, the utilization of LCNF shows the best properties of the panels. TS and WA for LCNF-containing PBs was lower at both 2 and 24 hours. This could be explained due to the hydrophobic nature of the lignin present in the LCNF fibers. In agreement with these results, we observed a decrease of the UF's surface free energy with the addition of LCNF, which could be related to a reduction of the sample's wettability as probed with WA and TS results.

Regarding the mechanical properties of the panels, both MOE and MOR improved with the addition of LCNF by 18 and 25%, respectively. In addition, IB also increased by 33% when adding LCNF. As we observed in the QCM-D analysis, the interactions between the nanofibers and the adhesive mixture are favored due to the higher charge density and functional groups present in the lignin.

Table 5.2. Experimental data for mechanical and physical properties of PBs with CNFs addition.

	Thickness swelling		Water absorption		IB	MOE	MOR
	2 hours	24 hours	2 hours	24 hours			
PBs	%	%	%	%	N/mm^2	MPa	MPa
UF	37.4 ± 1.5^{a}	45.8 ± 1.4^{d}	72.9 ± 2.3^{g}	91.2 ± 2.4^{j}	0.3 ± 0.1^{m}	752.2 ± 75.0^{o}	4.1 ± 0.4^{r}
UF/BCNF	41.5 ± 1.5^{b}	47.0 ± 1.4^{e}	64.7 ± 2.3^{h}	86.0 ± 2.3^{k}	0.3 ± 0.0^{m}	842.2 ± 70.4^{p}	4.5 ± 0.4^{r}
UF/LCNF	33.6 ± 1.4^{c}	43.3 ± 1.3^{f}	46.5 ± 2.4^{i}	77.3 ± 2.3^{l}	0.4 ± 0.0^{n}	889.0 ± 73.8^{q}	5.1 ± 0.4^{s}

* Different superscript letter means are significantly different ($p<0.05$).

5.5. Conclusions

In this work we have extensively analyzed the interactions between UF and cellulose nanofibrils with different chemical compositions. As a general effect, we observed an improvement of the properties of the wood panels by replacing 1% of UF with BCNF and LCNF. The enhanced properties when adding nanocellulose can be attributed to the ability of the nanoparticles to transfer the stress through the bond line, thus enhancing the bonding between the wood particles.

The larger interactions at the interfaces between LCNF and UF obtained by QCM-D analysis were confirmed when measuring the properties of the final particle boards. Additionally, the larger reduction of the surface free energy when using lignin-containing CNF was also observed through the wettability properties of the panels, increasing their hydrophobicity, and allowing lower thickness swelling and water absorption after 2 and 24 hours. The improved performance of the PBs when using LCNF could be also attributed to the higher charge density of this sample, which may allow for better interactions between the adhesive, nanocellulose, and wood particles.

5.6. Literature cited

Akinterinwa A, Ismaila A, Aliyu B (2020) Concise Chemistry of Urea Formaldehyde Resins and Formaldehyde Emission. Insights Chem Biochem 1–6

Amini E, Tajvidi M, Gardner DJ, Bousfield DW (2017) Utilization of cellulose nanofibrils as a binder for particleboard manufacture. BioResources 12:4093–4110. doi: 10.15376/biores.12.2.4093-4110

Ayrilmis N, Lee YK, Kwon JH, et al (2016) Formaldehyde emission and VOCs from LVLs produced with three grades of urea-formaldehyde resin modified with nanocellulose. Build Environ 97:82–87. doi: 10.1016/j.buildenv.2015.12.009

Brebu M, Vasile C (2010) Thermal degradation of lignin—a review. Cellul Chem Technol 44:353–363

Claub S, Allenspach K, Gabriel J, Niemz P (2011) Improving the thermal stability of one-component polyurethane adhesives by adding filler material. Wood Sci Technol 45:383–388. doi: 10.1007/s00226-010-0321-y

Crestini C, Lange H, Sette M, Argyropoulos DS (2017) On the structure of softwood kraft lignin. Green Chem 19:4104. doi: 10.1039/c7gc01812f

Diop CIK, Tajvidi M, Bilodeau MA, et al (2017) Evaluation of the incorporation of lignocellulose nanofibrils as sustainable adhesive replacement in medium density fiberboards. Ind Crops Prod 24:3037–3050. doi: 10.1016/j.indcrop.2017.08.004

Dukarska D, Czarnecki R (2016) Fumed silica as a filler for MUPF resin in the process of manufacturing water-resistant plywood. Eur J Wood Wood Prod 74:5–14. doi: 10.1007/s00107-015-0955-4

Example A (1991) Dissipative QCM. Langmuir 1–3

FAOSTAT 2019 http://www.fao.org/faostat/en/#data/QC

Hansted FA, Hansted AL, Durango Padilla ER, et al (2019) The use of nanocellulose in the production of medium density Particleboard panels and the modification of its physical properties. BioResource 14:5071–5079. doi: 10.15376/biores.14.3.5071-5079

Herrera M, Thitiwutthisakul K, Yang X, et al (2018) Preparation and evaluation of high-lignin content cellulose nanofibrils from eucalyptus pulp. Cellulose 25:3121–3133. doi: 10.1007/s10570-018-1764-9

Horvath EA, Lindström T, Laine J (2006) On the indirect polyelectrolyte titration of cellulosic fibers. Conditions for charge stoichiometry and comparison with ESCA. Langmuir 22:824–830. doi: 10.1021/la052217i

Huang Y, Wang Z, Wang L, et al (2016) Analysis of lignin aromatic structure in wood fractions based on IR spectroscopy. J Wood Chem Technol 36:377–382. doi: 10.1080/02773813.2016.1179325

Iglesias MC, Shivyari N, Norris A, et al (2020) The effect of residual lignin on the rheological properties of cellulose nanofibril suspensions. J Wood Chem Technol 40:370–381. doi: 10.1080/02773813.2020.1828472

İstek A, Biçer A, Özlüsoylu İ (2020) Effect of sodium carboxymethyl cellulose (Na-CMC) added to urea-formaldehyde resin on particleboard properties. TURKISH J Agric For 44:526–532. doi: 10.3906/tar-1905-87

Kawalerczyk J, Dziurka D, Mirski R, et al (2020) The effect of nanocellulose addition to phenol-formaldehyde adhesive in water-resistant plywood manufacturing. BioResources 15:5388–5401. doi: 10.15376/biores.15.3.5388-5401

Klemm D, Heublein B, Fink HP, Bohn A (2005) Cellulose: Fascinating biopolymer and

sustainable raw material. Angew Chemie - Int Ed 44:3358–3393. doi: 10.1002/anie.200460587

Klemm D, Kramer F, Moritz S, et al (2011) Nanocelluloses: A new family of nature-based materials. Angew Chemie - Int Ed 50:5438–5466. doi: 10.1002/anie.201001273

Kojima Y, Kato N, Ota K, et al (2018) Cellulose Nanofiber as a Complete Natural Binder for Particleboard. For Prod J 68:203–210. doi: 10.13073/FPJ-D-18-00034

KSV Instruments Ltd (2002) What Is a Quartz Crystal Microbalance – Qcm. 1–10

Lavoine N, Desloges I, Dufresne A, Bras J (2012) Microfibrillated cellulose - Its barrier properties and applications in cellulosic materials: A review. Carbohydr Polym 90:735–764. doi: 10.1016/j.carbpol.2012.05.026

Lei H, Du G, Pizzi A, et al (2010) Influence of nanoclay on phenol-formaldehyde and phenol-urea-formaldehyde resins for wood adhesives. J Adhes Sci Technol 24:1567–1576. doi: 10.1163/016942410X500945

Lei H, Du G, Pizzi A, Celzard A (2008) Influence of nanoclay on urea-formaldehyde resins for wood adhesives and its model. J Appl Polym Sci 109:2442–2451. doi: 10.1002/app.28359

Mahrdt E, Pinkl S, Schmidberger C, et al (2016) Effect of addition of microfibrillated cellulose to urea-formaldehyde on selected adhesive characteristics and distribution in particle board. Cellulose 23:571–580. doi: 10.1007/s10570-015-0818-5

Moon RJ, Martini A, Nairn J, et al (2011) Cellulose nanomaterials review: structure, properties and nanocomposites. Chem Soc Rev Chem Soc Rev 40:3941–3994. doi: 10.1039/c0cs00108b

Morais Júnior RR, Cardoso G V., Ferreira ES, Costa HL (2020) Surface characterization, mechanical and abrasion resistance of nanocellulose-reinforced wood panels. Surf Topogr Metrol Prop 8:025011. doi: 10.1088/2051-672X/ab8aa5

Nair SS, Yan N (2015) Effect of high residual lignin on the thermal stability of nanofibrils and its enhanced mechanical performance in aqueous environments. Cellulose 22:3137–3150. doi: 10.1007/s10570-015-0737-5

Salari A, Tabarsa T, Khazaeian A, Saraeian A (2013) Improving some of applied properties of oriented strand board (OSB) made from underutilized low quality paulownia (Paulownia fortunie) wood employing nano-SiO2. Ind Crops Prod 42:1–9. doi: 10.1016/j.indcrop.2012.05.010

Solala I, Iglesias MC, Peresin MS (2019) On the potential of lignin-containing cellulose nanofibrils (LCNFs): a review on properties and applications. Cellulose 27:1853-1877. doi: 10.1007/s10570-019-02899-8)

Thomas Luxbacher (2014) The ZETA guide - Principles of the streaming potential technique, First. Anton Paar GmbH., Graz, Autria

Transparency Market Research (2018) https://www.globenewswire.com/news-release/2018/01/03/1281428/0/en/Global-Formaldehyde-Market-is-expected-to-reach-36-6-million-tons-towards-the-end-of-2026-Transparency-Market-Research.html

Veigel S, Müller U, Keckes J, et al (2011) Cellulose nanofibrils as filler for adhesives: Effect on specific fracture energy of solid wood-adhesive bonds. Cellulose 18:1227–1237. doi: 10.1007/s10570-011-9576-1

Veigel S, Rathke J, Weigl M, Gindl-Altmutter W (2012) Particle board and oriented strand board prepared with nanocellulose- reinforced adhesive. J Nanomater 2012:1–8. doi: 10.1155/2012/158503

Voinova M V., Jonson M, Kasemo B (2002) “Missing mass” effect in biosensor’s QCM applications. Biosens Bioelectron 17:835–841. doi: 10.1016/S0956-5663(02)00050-7

Yang H, Yan R, Chen H, et al (2007) Characteristics of hemicellulose, cellulose and lignin

pyrolysis. Fuel 86:1781–1788. doi: 10.1016/j.fuel.2006.12.013

Zahedsheijani R, Faezipour M, Tarmian A, et al (2012) The effect of Na + montmorillonite (NaMMT) nanoclay on thermal properties of medium density fiberboard (MDF). Eur J Wood Wood Prod 70:565–571. doi: 10.1007/s00107-011-0583-6

6. Analyzing the effect of lignin on the defibrillation process during the obtention of cellulose nanofibrils suspensions

6.1. Abstract

When lignocellulosic biomass is chemically treated to obtain cellulose pulps, lignin structure, which is well known for its interconnected arrangement based on aromatic units, changes when compared with its native counterpart. Analyzing residual kraft lignin remaining on cellulose pulps, free phenolic hydroxyl groups are generated during the pulping process, which increases the hydrophilicity of lignin, and as a result, its solubility, resulting in the separation of the cellulose fibers from the lignin matrix. It has been proposed that during the mechanical production of lignin-containing cellulose nanofibrils (LCNFs), free radicals are stabilized due to the aromatic resonant structures of lignin, enabling better repulsion between the fibrils, leading to better defibrillation of the nanocellulose suspensions. Additionally, the chemical composition of the starting material, in terms of lignin and hemicelluloses content, as well as the degree of polymerization (DP) of the samples, play an important role in their rheological behavior, which is of relevance as they affect handling and processing. In this work, we focused on the effects of lignin during the production of LCNF from kraft softwood cellulose pulps containing different amounts of residual lignin. Mechanoradical formation has been measured by electron paramagnetic resonance (EPR) at different stages of the nanocellulose production. Additionally, the effects of lignin on the morphology, chemical composition, surface chemistry, as well as colloidal stability, thermal stability, and interfacial free energy values were analyzed.

6.1.1. Index words

Lignin-containing cellulose nanofibrils, LCNF, antioxidant, lignin free radicals, mechanoradicals, nanocellulose suspensions, lignocellulosic suspensions.

6.1. Introduction

Over the years, research has been primarily focused on using purely bleached cellulose pulp to produce nanocellulosic materials, allowing for the production of system with well-defined chemical composition and a more standardized understanding of their properties. This has resulted in the development of a larger spectrum of applications, such as food packaging (Aulin et al. 2010), biomedical applications due to its good biocompatibility (Pitkänen et al. 2014), and even the production of aerogels microspheres as cell culture scaffolds (Cai et al. 2014). When working with lignocellulosic biomass, the presence of components such as hemicelluloses and lignin add an extra challenge to the nanocellulose suspensions when trying to explain their behavior and properties. Although cellulose structure is independent of the tree species, lignin and hemicelluloses are characteristic of each species due to their primary precursors and the linkages between them (Jiang 1997; Naimi et al. 2016). In addition to this, it is well known that the chemical process utilized to produce cellulose pulp out of wood chips directly impacts the chemical structure of the remaining lignin on the fibers (Wang et al. 2016). For example, regarding the surface charge of the fibers, sulfide pulps have a higher impact on the surface properties of the fibers related to the higher content of carboxyl and carbonyl groups (Strunk et al. 2012). Besides, the cleavage of ether groups form lignin gives rise to lignosulfonate compounds, increasing the repulsion between the fibers (Chakar and Ragauskas 2004). As a result, the uncertainty of how lignin is affected introduces an extra challenge when intending to modify the surface chemistry of cellulose fibrils

in order to improve their compatibility in nanocomposites for improved performance such as wood composites, adsorbents, among other. However, some applications may take advantage of the presence of the additional polyphenolic groups and polysaccharides present in the cell wall, allowing for the utilization of lignin-containing cellulose nanofibrils (LCNFs) on their systems (Solala et al. 2020).

Among the known advantages of the presence of lignin in the production of LCNFs are: i) its ability to retain free radicals easily due to its chemical structure, allowing for improved defibrillation of the cell wall (Solala 2011); ii) the reduced energy consumption and iii) production costs (Spence et al. 2011). When producing nanocellulose out of cellulose pulp by mechanical treatments, activation energy is generated on the cellulose fibers, allowing the polymeric chain to break (Hon 1979) and enabling the formation of radicals (more commonly known as mechanoradicals). A representation of this is shown in Figure 6.1. This process can be even more significant in the presence of lignin. Other than being abundantly present in wood, lignin is also considered a natural antioxidant due to the scavenging action of its phenolic structures, which are oxygen-containing reactive free radicals (Dizhbite et al. 2004).

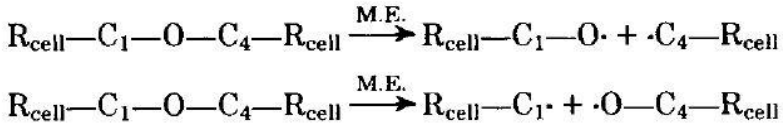

Figure 6.1. Proposed paths for glucosidic bond rupture during mechanical process of cellulose fibers (Hon 1979). Reprinted with permission of John Wiley & Sons, Inc.

Electron paramagnetic resonance (EPR) is an approach commonly utilized to study the presence of free radicals in different materials. It is a spectroscopic technique that depends on the absorption of electromagnetic radiation on the specimen. Different molecules and atoms have their

electrons at different energy levels, which can be measured and interpreted using this method (Duin 2011). Precisely, EPR can measure the interactions, in terms of energy, between unpaired electrons in a material and a magnetic field generated by the equipment (Duin 2011) while following their relaxation time, similarly to the nuclear magnetic resonance. One of the first wood-related works utilizing this technique was published by Rex (1960). He analyzed wood, lignins, tannins, and humic acid-free radicals, showing that free radicals depend on the type of source and treatment the material was subjected to. In the earliest 2000s, Iller et al. (2002) analyzed the relative free radical concentration for three different textile bleached cellulose pulps to compare the stability of the formed mechanoradicals after 3 hours and after ten days since the irradiation process. Results show that free radicals mainly decay during the first 12 hours after the irradiation and remain unchanged over time.

In recent years, it has been proposed in the scientific literature that LCNFs present an improved defibrillation level than fully bleached samples, resulting in smaller fibers diameters, attributing this to the scavenging ability of lignin that reduces the ability of the fibrils to recombine. Spence et al. (2010) studied the effect of chemical composition on microfibrillar cellulose (MFC) films from wood species. When characterizing the fibers, it was concluded that MFCs containing lignin present a higher surface area than their bleached counterpart, meaning that as the lignin content increased, the diameter of the nanofibrils was reduced. These results were attributed to the possible reduction of hydrogen bonds due to the presence of lignin, which makes fibers more individualized. Following the same trend and gaining a better insight into the effect of lignin during a mechanical process, Solala et al. (2012) studied the formation of mechanoradicals in detail using EPR on birch pulps containing 2.2, 1.5, and <1% lignin while producing LCNFs by mechanical grinding. Measurements were performed one week after the refining process to allow the decay of

unstable free radicals. Results show that the higher the lignin content and the more passes through the grinder, the more significant was the number of free radicals present on the suspensions. This was attributed to the scavenging ability of lignin, which can stabilize the cellulosic mechanoradicals formed during the mechanical process, avoiding the crosslinking of the cellulose fibers and thus, favoring a better deconstruction of the fibers as the lignin content increase (Solala et al. 2012).

Rojo et al. (2015) reported similar correlation between lignin content and fibrils diameter on LCNFs, attributing this behavior to the antioxidant property of lignin. Furthermore, Espinosa et al. (2019) reported the production of LCNF fibers from wheat straw, where lignin favored fibrillation, compared with the lignin-free samples. Although they did not specify the amount of lignin remaining on the samples, they attributed this behavior to the lignin mechanoradicals presence during the fibrillation of the samples.

Gaps in the knowledge of materials with higher lignin contents, different raw materials, and different stages of the defibrillation process still remain. In an attempt to bridge this gap, we studied the scavenging ability of lignin during LCNF production from softwood cellulose pulps containing higher lignin contents (16.8, 6.9, 2.8, and <1.0 %) by pure mechanical treatment of the samples. Aliquots were taken during the nanocellulose production after 0, 1, 5, 8, and 14 passes through the Masuko Supermasscolloider immediately after the manufacturing and at 5 and 10 days after the day of production and stored for EPR analysis.

6.2. Materials and methods

6.2.1. Materials

For the purpose of this work, four cellulose pulps were produced as described in Chapter 5, varying the processing conditions allowed obtaining samples with different chemical compositions, mainly different lignin content, and labelled as 16.8, 6.9, 2.8, and <1.0% lignin. The complete characterization of the cellulose pulps can be found in the Appendix of this dissertation.

6.2.2. Methods

6.2.2.1. Cellulose nanofibrils (CNFs) production

Cellulose nanofibrils were produced at the Forest Products Development Center of Auburn University. For this purpose, suspensions at 2 wt.% of consistency were prepared using DI water. The suspensions were fibrillated using the Masuko Supermasscolloider (MKZA-10-15J, Japan). A total of 14 passes through the equipment were used, controlling the gap between the disks at each step. Additionally, different disks combinations were used to improve the defibrillation of the sample. After the mechanical process, a gel-like consistency was obtained. During the nanocellulose production, aliquots were taken for EPR measurements, as explained in the following section. The complete characterization of the resulting nanofibrillated cellulose suspensions is presented in Chapter 4.

6.2.2.2. Electron paramagnetic resonance spectroscopy (EPR)

EPR spectra at X-band frequency (9 GHz) were obtained with a Bruker EMX spectrometer fitted with the ER-4119-HS high sensitivity perpendicular-mode cavity or the ER-4116-DM dual-

mode cavity. The sample was cooled with a liquid nitrogen finger Dewar (77 K) an Oxford Instruments ESR 900 flow cryostat with an ITC4 temperature controller (4.2 – 200 K).

For the spectroscopic measurements, during the nanocellulose production, aliquots were taken at 0, 1, 5, 8, and 14 passes immediately after processing and after 1, 5, and 10 days from the production day. When producing the LCNFs, aliquots were taken and placed inside the EPR glass tubes, as shown in Figure 6.2. Then, tubes were carefully immersed into liquid nitrogen to prevent free radical recombination reactions and avoid the most unstable radicals disappearing. Then, tubes were stored in liquid nitrogen until the analysis was performed. Measurements were performed in triplicate.

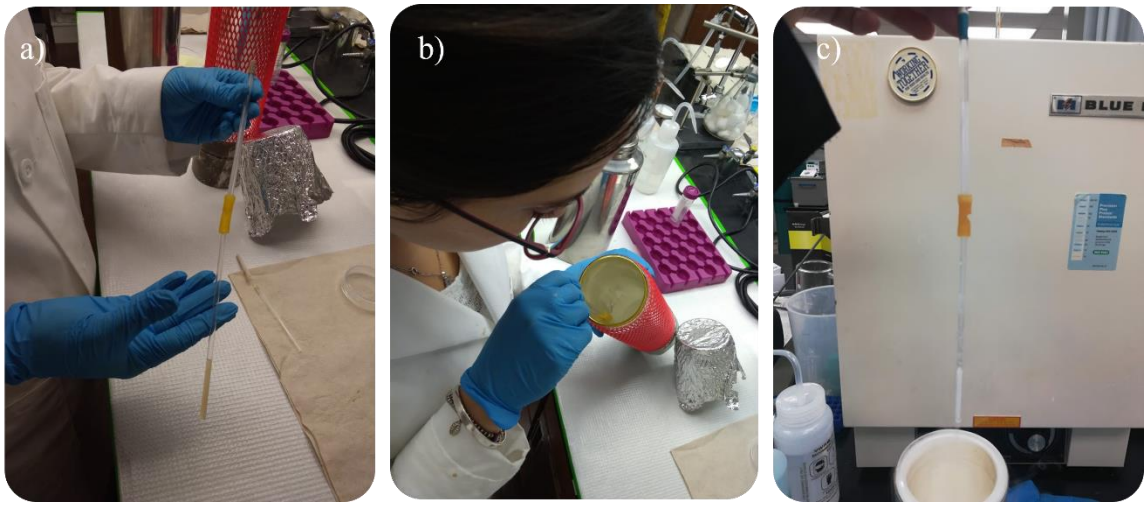

Figure 6.2. EPR sample preparation, a) LCNF suspensions inside the EPR tubes, b) freezing samples with liquid nitrogen, and c) sample ready to store in liquid nitrogen until measurement.

6.3. Preliminary EPR data results

EPR spectra were collected for 16.8, 6.9, 2.8, and <1.0 % samples, as shown in Figures 6.3. Before any mechanical treatment, due to the lack of intrinsic free radicals on the samples, EPR

signals should not be apparent on the spectra (Hon 1979). However, as shown in Figure 6.2, all of the measured samples present multiple signals, which were more intense after 0, 1, and 5 passes, which could be an indication of contamination in the samples.

For samples containing 16.8 and <1.0 % lignin, a significant amount of Cu^{2+} complex was detected. The presence of copper isotopes generates a split on the signal, which can be observed as the four different peaks in the spectra. The Cu signal is intense for samples 0, 1, and 5 and has a smaller intensity for samples 8 and 14 passes.

For the sample containing 16.8 % lignin, the radical content was calculated by comparing the double integrals of the samples with that of a 10 mM copper standard. The concentration (expressed in mM) for samples after 0, 1, 5, 8, and 14 passes were calculated as 27, 20, 19, 1.1 and 1.3 mM, respectively.

A different spectrum was observed regarding the sample containing 6.9 and 2.8 % lignin. In these cases, a significant amount of Mn^{2+} complex was detected. Unpaired electrons with different magnetic nuclei can make the signal split into two or more different signals, which is why the spectra become more complex (Duin 2011). For sample containing 6.9 % lignin, the concentration of free radicals (expressed in mM) after 0, 1, 5, 8, and 14 was calculated as 15.4, 13.9, 11.1, 3.4, and 1.7 mM, respectively.

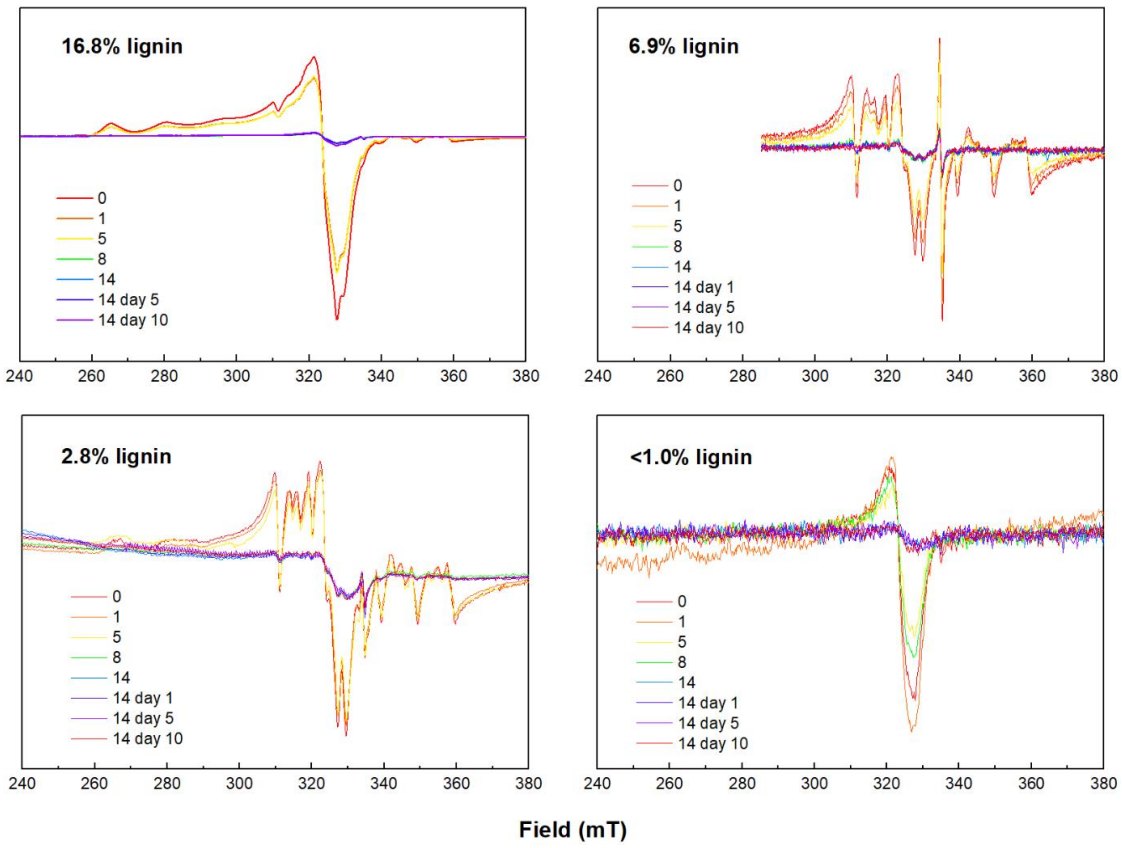

Figure 6.3. EPR Spectra for LCNF samples with different lignin content.

Based on the obtained data, we believe that samples contamination with metallic particles occurred while washing the cellulose fibers using tap water during the screening of the cellulose pulp. We assume this because all the process stages, from pulp production to nanocellulose production and sample collection, were carefully performed, taking care of every condition to avoid any possible contamination. As a result, due to the presence of metallic components mentioned above, it was not possible to determine which free radicals corresponded to the presence of lignin and which ones corresponded to the presence of Cu^{2+} and Mn^{2+}.

6.4. Conclusions

The EPR measurements did not provide expected results due to the presence of metal traces that entirely affect the measurements, making it not viable to quantify the free radicals corresponding to the presence of lignin on the samples.

6.5. Future work

As previously mentioned, there is still a knowledge gap in understanding the generation of free radicals in samples with more significant lignin content and from different raw materials. Additionally, the presence of more unstable radicals generated during the mechanical process of nanofibrillated cellulose is also of interest since this will affect the recombination reactions and, thus, the interactions between the fibrils.

Future work will involve producing a new set of cellulose pulps from different lignocellulosic materials and studying by EPR the generation of free radicals during the production of LCNFs. We will take special care during the washing process of the cellulose pulps using DI water.

Finally, the objective will be to correlate the intrinsic properties of those materials with their ability to generate free radicals during the production of the suspension. We will also include studying the morphology and surface properties of the fibers during the different grinding steps to have a deeper understanding of the properties of the fibers through the obtention process. Furthermore, we will perform nuclear magnetic resonance spectroscopy (NMR) on the samples to study the differences in chemical composition.

6.7. Literature cited

Aulin C, Netrval J, Wågberg L, Lindström T (2010) Aerogels from nanofibrillated cellulose with tunable oleophobicity. Soft Matter 6:3298. doi: 10.1039/c001939a

Cai H, Sharma S, Liu W, et al (2014) Aerogel Microspheres from Natural Cellulose Nanofibrils and Their Application as Cell Culture Scaffold. Biomacromolecules 15:. doi: 10.1021/bm5003976

Chakar FS, Ragauskas AJ (2004) Review of current and future softwood kraft lignin process chemistry. Ind Crops Prod 20:131–141. doi: 10.1016/j.indcrop.2004.04.016

Dizhbite T, Telysheva G, Jurkjane V, Viesturs U (2004) Characterization of the radical scavenging activity of lignins - Natural antioxidants. Bioresour Technol 95:309–317. doi: 10.1016/j.biortech.2004.02.024

Duin E (2011) Electron Paramagnetic Resonance Theory - EPR manual

Espinosa E, Bascón-Villegas I, Rosal A, et al (2019) PVA/(ligno)nanocellulose biocomposite films. Effect of residual lignin content on structural, mechanical, barrier and antioxidant properties. Int J Biol Macromol 141:197–206. doi: 10.1016/J.IJBIOMAC.2019.08.262

Hon DNS (1979) Formation and behavior of mechanoradicals in pulp cellulose. J Appl Polym Sci 23:1487–1499. doi: 10.1002/app.1979.070230519

Iller E, Kukielka A, Stupińska H, Mikolajczyk W (2002) Electron-beam stimulation of the reactivity of cellulose pulps for production of derivatives. Radiat Phys Chem 63:253–257. doi: 10.1016/S0969-806X(01)00646-6

Jiang Z-H (1997) Advances and applications of quantitative 31P NMR for the structural elucidation of lignin. McGill University

Naimi LJ, Sokhansanj S, Bi X, Lim CJ (2016) Development of a Size Reduction Equation

for Woody Biomass: The Influence of Branch Wood Properties on Rittinger's Constant. Am Soc Agric Biol Eng 59:1475–1484. doi: 10.13031/trans.59.11347

Pitkänen M, Kangas H, Laitinen O, et al (2014) Characteristics and safety of nano-sized cellulose fibrils. Cellulose 21:. doi: 10.1007/s10570-014-0397-x

Rex R (1960) Electron Paramagnetic Resonance Studies of Stable Free Radicals in Lignins and Humic Acids. Nature 188:1185–1186

Rojo E, Peresin MS, Sampson WW, et al (2015) Comprehensive elucidation of the effect of residual lignin on the physical, barrier, mechanical and surface properties of nanocellulose films. Green Chem 17:1853–1866. doi: 10.1039/C4GC02398F

Solala I (2011) Mechanochemical reactions in lignocelluloseic materials. Dissertation, Aalto Universty

Solala I, Iglesias MC, Peresin MS (2020) On the potential of lignin-containing cellulose nanofibrils (LCNFs): a review on properties and applications. Cellulose 27:1853–1877. doi: 10.1007/s10570-019-02899-8

Solala I, Volperts A, Andersone A, et al (2012) Mechanoradical formation and its effects on birch kraft pulp during the preparation of nanofibrillated cellulose with Masuko refining. Holzforschung 66:477–483. doi: 10.1515/HF.2011.183

Spence KL, Venditti RA, Rojas OJ, et al (2011) A comparative study of energy consumption and physical properties of microfibrillated cellulose produced by different processing methods. Cellulose 18:1097–1111. doi: 10.1007/s10570-011-9533-z

Spence KL, Venditti RA, Rojas OJ, et al (2010) The effect of chemical composition on microfibrillar cellulose films from wood pulps: Water interactions and physical properties for packaging applications. Cellulose 17:835–848. doi: 10.1007/s10570-010-9424-8

Strunk P, Lindgren Å, Agnemo R, Eliasson B (2012) Properties of cellulose pulps and their influence on the production of a cellulose ether. Nord Pulp Pap Res J 27:24–34. doi: 10.3183/NPPRJ-2012-27-01-p024-034

Wang C, Kelley SS, Venditti RA (2016) Lignin-based thermoplastic materials. ChemSusChem 9:770–783. doi: 10.1002/cssc.201501531

7. General conclusions

Population growth and the economic development of our society have led to the increased consumption of products mainly derived from fossil-based sources. The increased utilization of these materials and the absence of technologies that allow us to recycle or reutilize them is calling for biobased alternatives to mitigate the pollution in our environment and ecosystems.

This dissertation presents an extensive analysis to elucidate the interfacial interactions among the different chemical components present on cellulose nanofibrils suspensions (CNFs). Emphasis was made on the importance of understanding and considering the interactions occurring in colloidal systems specifically to explain the behavior of those systems and their intrinsic and viscoelastic properties. Specifically, the relevance of studying the rheological behavior of suspensions relies on elucidating the response of the samples during handling and processing for specific target applications.

As alternative technologies are developed for more sustainable biobased products, the biorefinery concept opens the possibility of utilizing various natural resources that can be converted to produce biobased materials to introduce into the market and provide an alternative to the current non-renewable products situation. Indeed, the use of by-products such as sawdust, soybean hulls, cotton linters, linen, and even hemp residues enable a variety of alternatives to produce cellulose nanofibrils (CNFs) that can be further used utilized. This work demonstrated how different biomass alternatives can be utilized to produce CNF suspensions, supporting the biorefinery model in which different lignocellulosic materials provided the necessary prototype to produce these colloidal suspensions.

During the past years, many of the studies involving CNFs have focused on utilizing fully bleached cellulose nanofibrils (BCNFs) due to the simplicity and well-known structure of their

components. Performing a bleaching stage after the pulping process eliminates additional components such as hemicelluloses, lignin, pectin, extractives, among others, depending on the utilized biomass. This has allowed using BCNFs for several applications. Nevertheless, this work demonstrated how the presence of additional chemical components on the fibrils could deliver different properties to the colloidal suspensions. Consequently, intrinsic properties such as thermal stability, crystallinity, and chemical functionalities can be altered based on the source and processing conditions, opening the possibility of selecting them based on the desired applications. In addition, it was proved that producing BCNF might not be necessary for specific applications since different characteristics can be achieved by utilizing lignin-containing cellulose nanofibrils (LCNFs).

As mentioned above, a variety of components might remain on the fibrous material by producing LCNFs from different lignocellulosic biomass and even from the same source applying different extraction conditions. In this work, the production of LCNFs suspension from softwood cellulose pulps with varying chemical compositions was achieved. Within the same raw material, additional components such as lignin and hemicellulose conferred different functional groups to the nanofibrils. The chemistry of those chemical groups and the amount in which they are present directly affected the properties of the suspensions, such as the intrinsic and viscoelastic properties.

When selecting a target application, studying the interactions at the interfaces between CNFs and the desired materials can offer a better insight into the final performance they will have when applied. Thus, in this work, the interfacial interactions between CNFs with different chemical compositions and wood adhesive were assessed and correlated with the final properties of the wood panels made thereof.

Appendix

Cellulose pulps characterization

A1. Introduction

In order to have a complete understanding about the raw material utilized to produce the LCNF samples from Chapter 4, the cellulose pulps mentioned in the mentoned chapter were fully characterized and the results are presented in this Appendix.

A2. Characterization of cellulose pulps

A2.1. Lignin content

For an accurate lignin content assessment, TAPPI Standard T222 Acid insoluble lignin in wood and pulp (Reaffirmation of T 222 om-02) (Standard 2002). Briefly, 1.1 g of oven dried sample were grinded to pass 80-mesh screen. Then, 10 mL of H_2SO_4 at 72 % were added and leave to react for 2 hours. During this time, samples were mixed every 15 min to improve the process. Once the time was completed, samples were diluted at 4 % using DI water and placed in a 20 L standard autoclave for 1 hour at 121 ºC. After the autoclave, samples were filtrated, and the remaining solids dried in the oven at 105 ºC for 4 hours after which the weights were recorded, and the insoluble lignin was calculated. Measurements were performed by duplicate.

A2.2. Intrinsic viscosity

Intrinsic viscosity was measured by following the standard ISO 5351:2012 “Pulps-Determination of limiting viscosity number in cupri-ethylenediamine (CED) solutions”. To determine the intrinsic viscosity of the samples, it is necessary to perform a bleaching step without

degrading the samples. Once the bleaching process is done, the cellulose pulps were washed with abundant DI water to remove all the excess of chemicals. Afterwards, a 1 g paper sheet was produced.

A2.3. Degree of polymerization (DP)

The degree of polymerization was calculated using the equation (A.1) developed by Staundiger, Mark, and Howink.

$$\eta = K_{DP} * DP^{a} \quad (A.1)$$

Where K_{DP} is a variable dependent on the polymer and the solvent and depends on the DP range as indicated in Table A.1.

Table A.1. parameters used for DP values (Marx–Figini 1987).

Range DP	**Range (ŋ)**	**K_{DP}**	**a**
<950	<420	0,42	1,00
>950	>420	2,29	0,76

A2.4. Thermogravimetric Analysis (TGA)

Thermal stability of the samples was assessed with a TGA-50 from Shimadzu (Kyoto, Japan) using nitrogen at a flow rate of 20 mL/min. The samples were heated from 10 °C to 600 °C, at a heating rate of 10 °C/min. About 15 mg of sample were analyzed in each case, with measurements performed in duplicate using aluminum pans. The data was processed with Shimadzu TA60 software (version 2.11).

A2.5. Fourier-transform infrared spectroscopy with attenuated total reflectance accessory (ATR-FTIR)

The chemical composition of the cellulose pulps was analyzed by FT-IR spectroscopy, using a Perkin Elmer Spotlight 400 FT-IR imaging system equipped with deuterated triglycine sulfate DTGS detector and built in ATR module with diamond/Zn crystal. All spectra were recorded over the spectral range from 4000 to 400 cm-1 at room temperature and after 64 scans.

A2.6. X-Ray powder diffraction (XRD)

XRD analyzes were performed using a RIGAKU Smartlab SE model equipped with Cu Kα irradiation (λ= 1.541 Å) at 40 kV and 50 mA. Measurements were performed at a scan speed of 0.1 second/step from 10° to 60° θ/2θ, at 10°/min. The crystalline index (CI) was calculated using Segal's method (Segal et al. 1959) defined in equation A.2 as:

$$\mathrm{CI} = \frac{\mathrm{I_{200}\text{-}I_{Am}}}{\mathrm{I_{200}}} \times 100\% \qquad \text{(A.2)}$$

where $I200$ is the maximum intensity of the 200-lattice diffraction peak, and I_{Am} is the intensity scattered by the amorphous fraction of the sample.

A3. Results and discussion

A3.1. Cellulose pulps characterization

A3.1.1. Lignin content, intrinsic viscosity, and degree of polymerization

The chemical composition of the samples, intrinsic viscosity, and degree of polymerization are presented in Table A.2.

Table A.2. shows the compilation results of lignin content, intrinsic viscosity, and DPv.

Sample	**Lignin content**	**Intrinsic viscosity**	**DPv**
	(%)	(mL/g)	
P1	16.8 ± 0.1	1182 ± 10	3711
P2	6.9 ± 0.1	1070 ± 10	3255
P3	2.8 ± 0.0	788 ± 10	2176
P4	<1.0	804 ± 10	2235

Based on the lignin content results, we confirmed the effectiveness of the pulping process to remove lignin in different rates. Regarding the intrinsic viscosity and the degree of polymerization, their values are larger as the lignin content on the samples increase. As can be observed in table 5, pulp 4 with <1% lignin content presents slightly higher values of viscosity and DPv than the sample containing 2.8% lignin. Nevertheless, the variation coefficient between the DPv of these samples is 1.89%, meaning that they are comparable, and the increase is not significative. Additionally, it is well known that a chlorine-based bleaching is more selective that a traditional oxygen delignification process, preserving as a result, the viscosity and DP of the sample (Sixta et al. 2006). Thus, the obtained variation could be attribute due to experimental error. Using the obtained lignin content values, , samples were labelled based on the amount of lignin as 16.8%, 6.9%, 2.8%, and <1.0% along the chapter.

A3.1.2. Thermal decomposition

Figure A.1 shows the thermal stability spectra of all four cellulose pulps and Table A.3 summarizes the different temperatures values of the samples. T_{onset} is defined as the temperature where the thermal decomposition of the sample begins, while T_{max} is the maximum temperature of the derivative peak (Nair et al. 2017).

Table A.3. T_{onset} and T_{max} of LCNF samples.

Pulp (% lignin)	**T_{onset} (ºC)**	**T_{max} (ºC)**
16.8	277	371
6.9	296	365
2.8	303	363
<1.0	303	362

Analyzing Table A.3., samples containing <1.0 and 2.8% lignin present a T_{onset} of 303 ºC. As the lignin content increase to 6.9 and 16.8%, the hemicelluloses content also increases, and the thermal decomposition begins at lower temperatures of 296 and 277 ºC, respectively. This decrease on the T_{onset}, can be attribute due to the different chemical composition of the samples. It is well known that cellulose starts decomposing at approximately 300 ºC. Meanwhile, hemicelluloses and lignin beginning to decay at temperatures of 220 and 200 ºC, respectively (Yang et al. 2007).

Differences were also observed in the solid residues remaining after the pyrolysis. As the lignin content on the samples increase, the residue is higher. This could be related with the difficulties of lignin to decompose (Herrera et al. 2018) which can also be observed on the derivative curve where, as the lignin content on the samples increases, the mass loss rate is reduced.

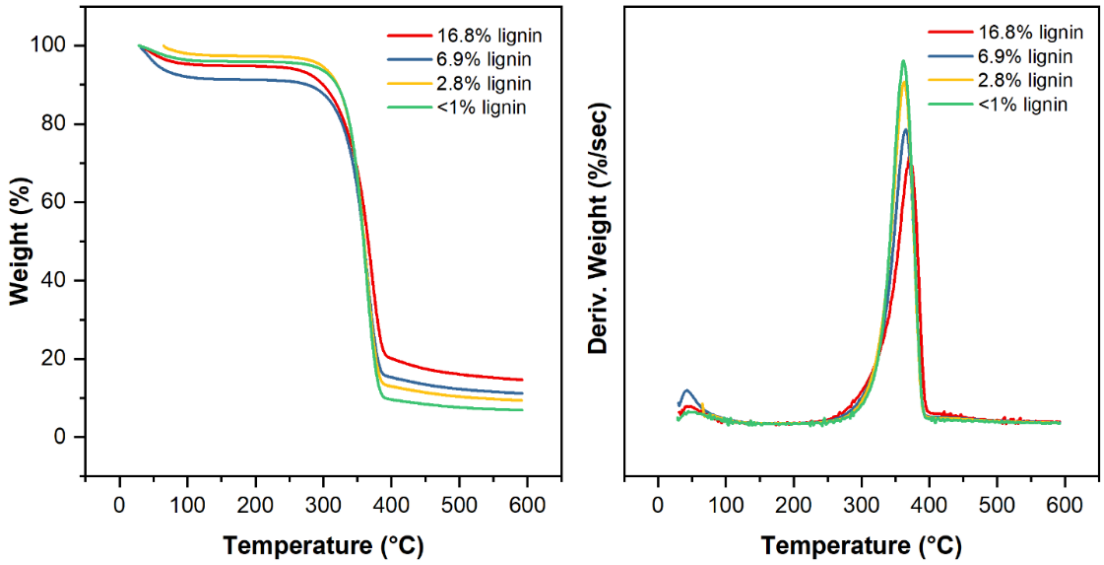

Figure A.1. Thermal stability of cellulose pulps containing; a) <1.0, b) 2.8, c) 6.9, and d) 16.8% lignin

A3.1.3. Chemical composition

A qualitative analysis on the chemical composition of the samples is presented in Figure A.2. The FT-IR spectra shows the most characteristic bands for cellulosic samples, together with typical signals for the functional groups present in lignin. As a general classification, lignocellulosic samples containing cellulose, hemicelluloses, and lignin on their composition, possess organic groups such as aldehydes, ketones, alcohols, aromatic compounds, esters, and alkenes (Yang et al. 2007). Most of these components are formed by oxygen-containing groups and alkyl/aliphatic groups as denoted in Figure A.2.

The presence of lignin can be corroborated in the fingerprint region of the spectra, by the shoulder formed at 1591 cm^{-1} which is attribute due to the aromatic skeletal vibrations present in lignin, as well as the C=O stretching vibrations (Huang et al. 2016). Additionally, the signal at 1267 cm^{-1} which appear in samples 16.8 and 6.9 %, can be related with OH deformation caused by the phenolic groups present in lignin (Diop et al. 2017).

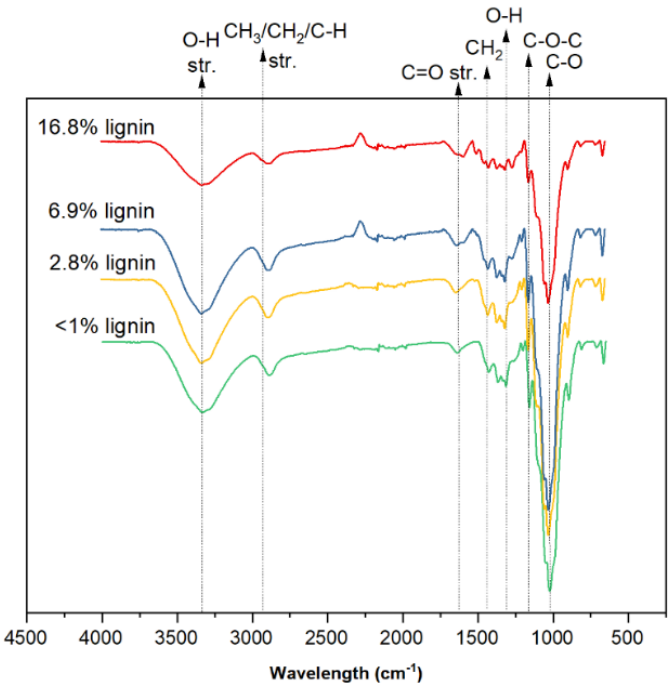

Figure A.2. FT-IR spectra of cellulose pulps containing; a) <1.0, b) 2.8, c) 6.9, and d) 16.8% lignin.

A3.1.4. Crystallinity

The crystallinity index of the samples is presented in Figure A.3. As can be observed, as lignin and hemicelluloses are removed from the samples, their crystallinity increases since these two components contribute to the amorphous material in cellulose pulps (Espinosa et al. 2017). As can be noticed, bleached cellulose fibers containing <1.0 % lignin did not follow the same trend given that its crystallinity decreases compare with the sample containing 2.8 % lignin. It is well known that bleaching can damage the crystallinity of the fibers and a similar trend for wood samples has been reported in the literature (Debiagi et al. 2020; Iglesias et al. 2021). Additionally, as an increase in crystallinity is explained by the reduction in the non-crystalline components of the lignocellulosic fibers, its increment can be related with the decrease on the degree of polymerization (DPv) (Puri 1984) as we observed in Table A.2, where sample containing <1.0 %

lignin shows a slightly higher DPv than sample containing 2.8 % lignin. Nevertheless, we observed no significant difference between the values presented here, after performing an ANOVA statistical analysis.

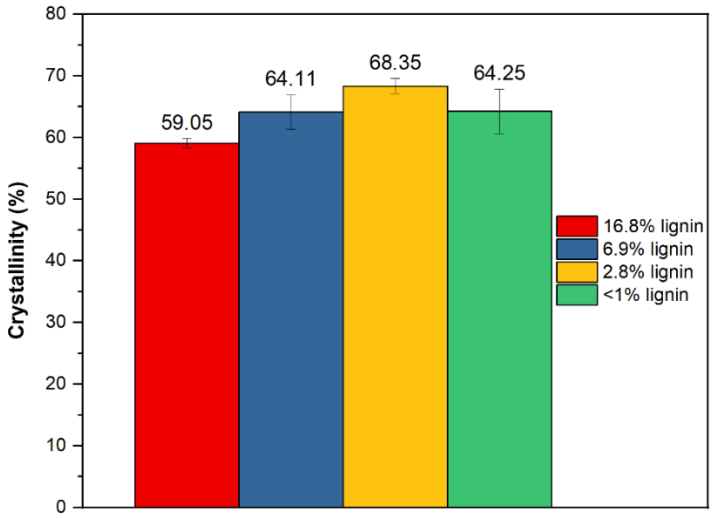

Figure A.3. Crystallinity index of softwood and cellulose pulps containing <1.0, 2.8, 6.9, and 16.8 % of lignin.

A4. Conclusions

Four different cellulose pulps were produced, utilizing a traditional Kraft pulping process. Among samples, we modified the pulping time to obtain different delignification results. One of the samples was fully bleached for comparison purposes.

The celluloses pulps were fully characterized in terms of lignin content, viscosity, degree of polymerization, crystallinity, chemical composition, and thermal stability. It was observed that as the lignin content of the samples increases, their thermal stability decreases due to the presence of lignin and hemicelluloses. Additionally, the crystallinity of the samples is reduced since these components are amorphous when compared with the pure crystalline structure of cellulose.

A6. Literature cited

Debiagi F, Faria-Tischer PCS, Mali S (2020) Nanofibrillated cellulose obtained from soybean hull using simple and eco-friendly processes based on reactive extrusion. Cellulose. doi: 10.1007/s10570-019-02893-0

Diop CIK, Tajvidi M, Bilodeau MA, et al (2017) Isolation of lignocellulose nanofibrils (LCNF) and application as adhesive replacement in wood composites: example of fiberboard. Cellulose 24:3037–3050. doi: 10.1007/s10570-017-1320-z

Espinosa E, Domínguez-Robles J, Sánchez R, et al (2017) The effect of pre-treatment on the production of lignocellulosic nanofibers and their application as a reinforcing agent in paper. Cellulose 24:2605–2618. doi: 10.1007/s10570-017-1281-2

Herrera M, Thitiwutthisakul K, Yang X, et al (2018) Preparation and evaluation of high-lignin content cellulose nanofibrils from eucalyptus pulp. Cellulose 25:3121–3133. doi: 10.1007/s10570-018-1764-9

Huang Y, Wang Z, Wang L, et al (2016) Analysis of lignin aromatic structure in wood fractions based on IR spectroscopy. J Wood Chem Technol 36:377–382. doi: 10.1080/02773813.2016.1179325

Iglesias MC, Hamade F, Aksoy B, et al (2021) Correlations between Rheological Behavior and Intrinsic Properties of Nanofibrillated Cellulose from Wood and Soybean Hulls with Varying Lignin Content. BioResources 16:4831–4845. doi: 10.15376/biores.16.3.4831-4845

Marx–Figini M (1987) The acid-catalized degradation of cellulose linters in distinct ranges of degree of polymerization. Appl Polym Sci 33:2097–2105

Nair SS, Kuo P-YY, Chen H, Yan N (2017) Investigating the effect of lignin on the mechanical, thermal, and barrier properties of cellulose nanofibril reinforced epoxy composite. Ind

Crops Prod 100:208–217. doi: 10.1016/j.indcrop.2017.02.032

Puri VP (1984) "Effect of crystallinity and degree of polymerization of cellulose on enzymatic saccharification. Biotechnol Bioeng 26:1219–1222

Segal L, Creely JJ, Martin AE, Conrad CM (1959) An Empirical Method for Estimating the Degree of Crystallinity of Native Cellulose Using the X-Ray Diffractometer. Text Res J 29:786–794. doi: 10.1177/004051755902901003

Sixta H, Süss H-U, Potthast A, et al (2006) Pulp bleaching. In: Sixta H (ed) Handbook of Pulp. WILEY-VCH Verlag GmbH &Co., Weinheim, pp 609–708

Standard T (2002) Acid-insoluble lignin in wood and pulp. T222 om-02

Yang H, Yan R, Chen H, et al (2007) Characteristics of hemicellulose, cellulose and lignin pyrolysis. Fuel 86:1781–1788. doi: 10.1016/j.fuel.2006.12.013